ISSN 0038-531X

Russian Original Vol. 58, No. 2, February, 1985

August, 1985

SATEAZ 58(2) 85–176 (1985)

SOVIET ATOMIC ENERGY

АТОМНАЯ ЭНЕРГИЯ
(ATOMNAYA ÉNERGIYA)

TRANSLATED FROM RUSSIAN

c/b CONSULTANTS BUREAU, NEW YORK

SOVIET ATOMIC ENERGY

Soviet Atomic Energy is abstracted or indexed in *Chemical Abstracts, Chemical Titles, Pollution Abstracts, Science Research Abstracts, Parts A and B, Safety Science Abstracts Journal, Current Contents, Energy Research Abstracts,* and *Engineering Index.*

Mailed in the USA by Publications Expediting, Inc., 200 Meacham Avenue, Elmont, NY 11003.

POSTMASTER: Send address changes to *Soviet Atomic Energy,* Plenum Publishing Corporation, 233 Spring Street, New York, NY 10013.

Soviet Atomic Energy is a translation of *Atomnaya Énergiya,* a publication of the Academy of Sciences of the USSR.

An agreement with the Copyright Agency of the USSR (VAAP) makes available both advance copies of the Russian journal and original glossy photographs and artwork. This serves to decrease the necessary time lag between publication of the original and publication of the translation and helps to improve the quality of the latter. The translation began with the first issue of the Russian journal.

Consultants Bureau journals appear about six months after the publication of the original Russian issue. For bibliographic accuracy, the English issue published by Consultants Bureau carries the same number and date as the original Russian from which it was translated. For example, a Russian issue published in December will appear in a Consultants Bureau English translation about the following June, but the translation issue will carry the December date. When ordering any volume or particular issue of a Consultants Bureau journal, please specify the date and, where applicable, the volume and issue numbers of the original Russian. The material you will receive will be a translation of that Russian volume or issue.

Subscription (2 volumes per year)
Vols. 56 & 57: $560 (domestic), $621 (foreign)
Vols. 58 & 59: $645 (domestic), $715 (foreign)
Single Issue: $100
Single Article: $9.50

CONSULTANTS BUREAU, NEW YORK AND LONDON

c/b
233 Spring Street
New York, New York 10013

Published monthly. Second-class postage paid at Jamaica, New York 11431.

SOVIET ATOMIC ENERGY

A translation of *Atomnaya Énergiya*

August, 1985

Volume 58, Number 2 February, 1985

CONTENTS

Engl./Russ.

ARTICLES

Method of Calculating the Physical Characteristics of Heterogeneous-Reactor Cells — A. Yu. Kvaratskheli and B. P. Kochurov 85 83

Study of the Influence of Inhomogeneities in the Energy Distribution on the Readings of Extrareactor Ionization Chambers — A. N. Kamyshan, Yu. A. Krainov, A. M. Luzhnov, V. V. Lysenko, V. V. Morozov, A. I. Musorin, N. R. Nigmatulin, and S. G. Tsypin 97 91

Calculating Neutron-Flux Functionals by the Monte Carlo Method in Breeder Systems with Leakage Specified by a Geometric Paramter — L. V. Maiorov 100 93

Facility for the Irradiation of Fuel Elements in the SM-2 and MIR Reactors with Variable Operating Regimes — V. A. Tsykanov, A. F. Grachev, E. P. Klochkov, V. A. Kuprienko, and V. K. Shamardin. 105 97

Mathematical Model of the Behavior of Oxide Microfuel-Elements in a High-Temperature Gas-Cooled Reactor — S. A. Balankin and E. A. Rybakova 111 101

Radiation Erosion of Welded Joints in Steels Promising for Fusion Systems — B. A. Kalin, V. I. Pol'skii, D. M. Skorov, E. E. Goncharov, I. L. Artemenkov, and A. P. Morozov 116 104

Leakage of Tritium in a Thermonuclear Reactor — Yu. V. Martynenko, and Yu. N. Yavlinskii. 124 111

Providing Radiation Safety in Handling Radioactive Wastes from Nuclear Power Stations — E. I. Vorob'ev, L. A. Il'in, A. S. Belitskii, O. A. Pavlovskii, and V. D. Stepanova 127 113

Measurement of the Cross Sections of the Reaction $^{237}Np(n, 2n)^{236}Np(22.5\ h)$ for Neutron Energies in the Range 7-10 MeV — N. V. Kornilov, V. Ya. Baryba, A. V. Balitskii, A. P. Rudenko, B. D. Kuz'minov, O. A. Sal'nikov, E. A. Gromova, S. S. Kovalenko, L. D. Preobrazhenskaya, A. V. Stepanov, Yu. A. Nemilov, Yu. A. Selitskii, B. I. Tarler, V. B. Funshtein, V. A. Yakovlev, Sh. Darotsi, P. Raich, and I. Chikai 131 117

Calculation of the Neutron Yield from Thick Targets Bombarded by Electrons with Energies up to 500 MeV — N. L. Emets, B. A. Shilyaev, and V. A. Yamnitskii 136 120

Evaluation of the Characteristics of the Emission of Secondary Electrons from a Metal Bombarded by Photons with Energies in the Range 0.05-1.0 MeV — M. L. Gol'din and V. D. Tkachenko. . . . 141 124

CONTENTS

(continued)

Engl./Russ.

LETTERS TO THE EDITOR

Cross Section of the ^{58}Ni(n, p) Reaction for Neutron Energies of 7-10 MeV — N. V. Kornilov, V. Ya. Baryba, A. V. Balitskii, A. N. Rudenko, S. Daroci, P. Raics, and Z. Papp. 147 128

Gaseous Saturation of the Primary Circuit Coolant in Nuclear Steam Supply Systems of Water-Moderated Water-Cooled Power Reactors — Yu. A. Kalaida, A. P. Lastochkin, V. I. Esin, V. S. Sysoev, Yu. D. Katkov, M. G. Khor'kov, G. E. Perfil'ev, and V. A. Dobrogorskii 149 129

Differential Cross Sections for the Inelastic Scattering of 14-MeV Neutrons by Niobium — A. A. Lychagin, G. V. Kotel'nikova, B. V. Devkin, V. A. Vinogradov, A. N. Mironov, and O. A. Sal'nikov . 152 131

Influence of Activator Concentration on the Dosimetric Properties of Radiophotoluminescent Glasses — N. Z. Andreeva, N. N. Vil'chinskaya, A. V. Dmitryuk, A. S. Perminov, G. T. Petrovskii, and O. Ch. Savvina 155 132

Influence of the Anisotropy of Elastic Scattering on Neutron Moderating Parameters — V. V. Kulik 160 135

Measurement of the Ratio of the Cross Sections for Fissioning of ^{237}Np and ^{235}U by Neutrons with Energies in the Range 4-11 MeV — A. A. Goverdovskii, A. K. Gordyushin, B. D. Kuz'minov, V. F. Mitrofanov, A. I. Sergachev, S. M. Solov'ev, and G. M. Stepchenkova 163 137

Yields of Long-Lived Radionuclides in the Irradiation of Be, C, Mg, Si, and Sc by Charged Particles — I. O. Konstantinov, P. P. Dmitriev, and V. I. Bolotskikh 167 140

Energy Dependences of the Scattering Cross Sections of Fast Neutrons by ^{50}Cr and ^{54}Cr Nuclei — I. A. Korzh, V. A. Mishchenko, M. V. Pasechnik, and N. M. Pravdivyi 171 143

Neutron Yield in High-Energy Deuteron-Nuclear Reactions — V. S. Barashenkov, L. G. Levchuk, Zh. Zh. Musul'manbekov, A. N. Sosnin, and S. Yu. Shmakov 174 145

The Russian press date (podpisano k pechati) of this issue was 1/28/1985. Publication therefore did not occur prior to this date, but must be assumed to have taken place reasonably soon thereafter.

ARTICLES

METHOD OF CALCULATING THE PHYSICAL CHARACTERISTICS OF HETEROGENEOUS-REACTOR CELLS

A. Yu. Kvaratskheli and B. P. Kochurov

UDC 621.039.51.13

As is known, in heterogeneous theory [1-3], reactor calculation involves calculating the characteristics of the units and calculating the reactor with specified characteristics of the units. The second stage has undergone considerable development in recent years, with the elimination of long-range effects and the formulation of the equations in difference form [4, 5], allowing reactors with a large number of units to be calculated by methods similar to those for homogeneous diffusional equations.

There is also considerable interest in the solution of the first part of the problem. For several years, we have been working with computer programs based on the methods of calculating the unit characteristics outlined below, which are widely used in the theoretical investigation of reactors. Individual problems were discussed in [6-10], which have not been widely distributed; see also [11, 12].

In the present work, a sufficiently complete account is given of methods of solving the first part of the problem of heterogeneous calculation of a reactor.

In the initial formulation of the heterogeneous method [1, 2], each unit was characterized by a constant breeding factor η, equal to the number of fast neutrons produced in the unit on absorbing one thermal neutron, and the thermal constant γ, equal to the ratio of the number of neutrons absorbed in the unit in unit time (or the total current in the unit) to the (asymptotic) neutron density at its surface. With modern requirements on the accuracy of calculations, the inadequacy of this description is obvious: two parameters cannot possibly provide a correct representation of all the diverse processes occurring in the cell (neutron retardation, breeding and absorption of neutrons in the superthermal region). The systematic description of neutron migration requires expansion of the theory to a dipole formulation; see [3], for example. In the present work, consideration is limited to methods of calculating "monopole" and axial "dipole" characteristics of the units. In a small-group representation of heterogeneous equations (in practice, G groups are used; G = 2-6), the properties of the unit may be specified by a matrix Λ including $G \times G$ parameters* relating the G vector flux Φ and the vector current J_0 in the direction of the unit at the boundary of a cylindrical surface of radius ρ:

$$J = \Lambda N;\ J \equiv J_0/2\pi D;\ N_g \equiv \frac{D_g}{D}\Phi_g;\quad g = 1, \ldots, G-1, \tag{1}$$

where D_g is the diffusion coefficient in the moderator; D is its value for the thermal group. Equation (1) is a natural generalization of the analogous relation of single-velocity theory determining the thermal constant γ.

An alternative characteristic of the unit, which is formally completely equivalent to the Λ matrix, is the $G \times G$ matrix of the "response" U, specifying the relation between the regular and singular parts of the solution in the modulator [11, 13, 14]:

$$N(r) = CI_0C^{-1}A + CK_0C^{-1}B;\quad B = UA, \tag{2}$$

where $I_0 = \operatorname{diag}_g \{I_0(xr)\}$; $K_0 = \operatorname{diag}_g \{K_0(\varkappa_g r)\}$; the parameters $\varkappa_g$ and the parameters of the triangular matrix C are related to the moderator properties [11]; A is an arbitrary G vector.

Note the difference between Eqs. (1) and (2). If Eq. (2) is intimately related to the formulation of the heterogeneous theory of the reactor presuming the specified form of the

*Later, greater detailing of the Λ-matrix parameters is required.

Translated from Atomnaya Énergiya, Vol. 58, No. 2, pp. 83-91, February, 1985. Original article submitted June 1, 1984.

0038-531X/85/5802-0085$09.50

solution in the moderator, the relation between the current and neutron flux at the surface of the cylindrical volume is specified in Eq. (1) regardless of the method of reactor calculation subsequently employed. In this sense, the matrix Λ is a more general characteristic.

In using the complete $G \times G$ matrix Λ instead of the two constants η and γ, as noted above, taking account of such processes as deceleration of neutrons in the unit ceases to be a limitation on the theory, and therefore the unit may be understood to be any cylindrical volume including a considerable layer of moderator, of size up to the dimensions of the equivalent cell (and more, provided that the centers of other units do not fall within the chosen surfaces in the further calculation of the reactor). Formally, this does not lead to any contradiction: for different radii, $\Lambda(\rho)$ which are uniquely related (through the matrix U) and mutually equivalent may be determined. The inclusion of a considerable layer of moderator in the volume of the unit is also favorable in a number of other respects. In this case, N becomes a true and not asymptotic flux; the neutron current is determined by the derivative of the neutron flux, since diffusional theory holds in the vicinity of a surface of radius ρ. To perform exemplary calculations, modern universal multigroup programs must be used, with convolution of the results in a small-group representation, and the above choice of the unit allows intragroup spectral effects to be effectively included in the Λ matrix; the energy microstructure of the flux associated with the resonant absorption of neutrons is considerably smoothed at the surface of such a unit. In addition, it is possible to isolate the part of the matrix Λ associated with the neutrons arising in fission in sufficiently simple form: this allows the effective breeder coefficient of the neutrons to be included as an eigenvalue in the form of a linear factor in the equation of the heterogeneous reactor.

As usual in the heterogeneous method, the basic hypothesis of the theory is assumed to hold: regions in which the diffusional approximation is valid — i.e., either the inhomogeneity is small or the distance between the surfaces of the unit R in comparison with the neutron path length in the moderator l is such that $\exp(-R/l) \ll 1$ — must exist in the moderator.

Note that in recent attempts to solve the equations of neutron transfer in a reactor in the nonheterogeneous case there has been a definite trend away from the representation of the cell characteristics by rigorously specified mean cross sections over the cell volume. The cell characteristics are determined in some way by parameters relating the values of the fluxes and neutron currents at the surface. Thus, in the refined homogenization method [15, 16], a set of test functions with single neutron currents in each group, ordered according to the degree of symmetry of the specified functions at the cell surface, is constructed. Some analogous approaches were discussed in [17]. In [18, 19], a method associated with specifying unidirectional neutron fluxes at the surface was discussed. The cell characteristics in this case are the transmission and reflection functions. These theories have much in common. The concept of a γ constant, necessarily generalized, is currently taking on broader significance, and has been used in other approaches differing from the sink–source method. Thus, there is a definite trend to convergence in the heterogeneous approach and modern modifications of the homogeneous method, the formulations of which are based on short-range effects from the very beginning.

It is appropriate to single out [13, 14, 18, 20, 21] here. The method outlined below for obtaining the Λ matrix has a number of important differences from the methods in [13, 14, 18, 20, 21]. The most general case is considered, taking account of neutron-physics processes over the whole energy range. The theory is based on detailed multigroup solutions: the transition to a small-group representation is made at the stage of Λ-matrix formation. The superposition principle is used, thereby offering the possibility of using linear combinations of solutions, which may be naturally formed with only slight modification of the basic scheme of cell calculation. The superposition principle allows the solution associated with specifying the fission density (and not with the complete sources, including the moderation energy currents) to be completely isolated. Under the very credible hypothesis that the dependence of the solution on the chosen distribution function of the fission density is weak, the part of the Λ matrix associated with the breeding coefficient of the neutrons, which is very simply constructed, may be rigorously isolated. It is sufficient here simply to construct the solution with a fixed source in the cell rather than to solve the eigenvalue problem (as suggested in [18], for example). At the same time, the specific features of constructing the solution when using the method here proposed for the probability of the first collision are such that the series of $G + 1$ variants of cell calculation necessary for the calculation of the Λ matrix may be reduced, in terms of computational demands, to two variants of this calculation. In addition to the monopole component of the Λ matrix, a method of calculating

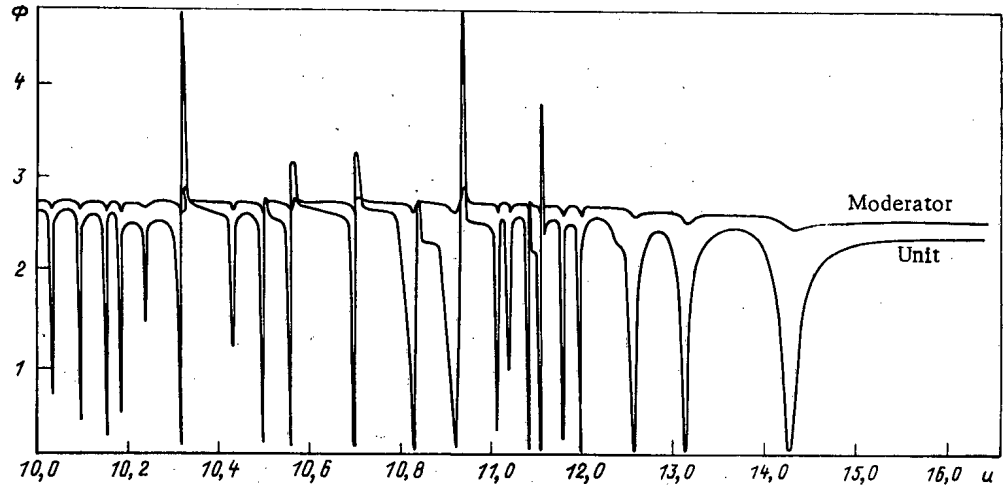

Fig. 1. Distribution of the mean neutron fluxes over the unit and the moderator in the region of strong resonances as a function of the lethargy u, calculated by the TRIFON program [6] (natural-uranium unit of radius 2 cm; layer of heavy-water moderator of thickness 6 cm).

the axial "dipole" component on the basis of expanding all the quantities in terms of the parameter $\alpha^2 = \pi^2/H^2$ is proposed (H is the effective reactor height).

After solving the equations of a heterogeneous reactor with Λ matrices as the input parameters, it is then necessary to determine the energy liberation in the units, the number of neutrons absorbed in the cell elements, the activation of the detectors, etc. For reaction x, this is accomplished using the activation matrix $\mathcal{P}_x$, so that the intensity vector X in the G groups is specified by the quantity

$$X = \mathcal{P}_x N, \tag{3}$$

and the total intensity is obtained by summing the components X. The method of calculating $\mathcal{P}_x$ is considered below.*

Calculation of the Spatial–Energy Distribution of Neutrons in a Cylindrical Cell of a Reactor. The Λ matrix is calculated on the basis of the TRIFON program [6], permitting accurate calculation of the spatial–energy distribution of neutrons in the cell. Using this program in a multizone cylindrical cell, the multigroup system of integral equations of neutron transfer is solved (by the collision-probability method)†

$$\Phi^i(r) = \int K^i(r, r')\,(\Sigma_s^i \Phi^i + Q^i)(r')\,dr', \tag{4}$$

where i is the number of the energy interval; K^i is the kernel of the neutron-transfer operator; Σ^i_s is the cross section of elastic and inelastic scattering in group i. The source

$$Q^i = Q_l^i + Q_f^i \tag{5}$$

is related to the neutrons scattered from the above-lying groups

$$Q_l^i = \sum_{j<i} \Sigma^{ij}\Phi^j, \tag{6}$$

and the neutrons arising from fission over the whole energy range

$$Q_f^i = \sum_j \vartheta^i \nu^j \Sigma_f^j \Phi^j. \tag{7}$$

In solving Eq. (4), the source Q^i_f is assumed to be specified: its energy distribution corresponds to the spectrum of fission neutrons and the spatial distribution is represented by the function S(r) (for example, in accordance with the distribution of fission density for thermal neutrons), i.e.,

*To date, experimental investigations have shown a tendency to measure the fluxes, the hardness of the neutron spectra, etc. In fact, the activations of the detectors or their ratio is measured, which should be reflected in the theory, and these quantities must be represented in the experimental results.

†Modifications to take account of the axial leakage of neutrons are introduced below.

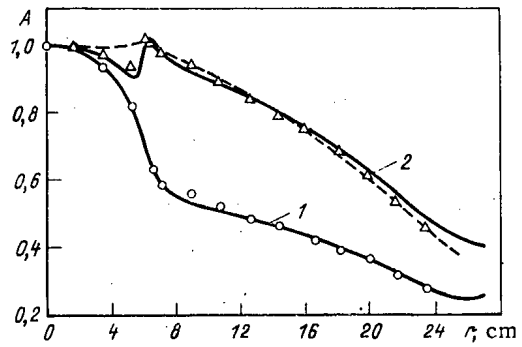

Fig. 2. Distribution of the activation A over the radius of a uranium pile [26]: 1) ^{235}U detectors (fission); 2) ^{238}U detectors (fission); the continuous curves correspond to heterogeneous calculation, the dashed curves to the fast-neutron flux of the first group, and the points to experimental data.

$$Q_j^i(r) = \vartheta^i S(r) \tag{8}$$

with the normalization condition

$$\sum_i \vartheta^i = 1; \quad \int S(r)\, dV = 1. \tag{9}$$

In other words, one neutron with a fission spectrum and distribution S(r) appears as a result of all the fissions in the cell.

The energy distribution is based on the multigroup representation using the system of constants of [22]. In the thermal group, the calculation is performed using the TERMIT thermalization program [7]. In the region where resonant effects exist, the cross section for the specified set of isotopes is calculated from the parameters of the resonance levels, and the initial group scale in the specified limits (j_1, j_2) is divided into smaller energy intervals. Suppose that in the corresponding interval of lethargies (u_0, u_n) $\mathcal{F}(u)$ is a function associated with the elementary estimates of the blocked resonant absorption of neutrons by all isotopes. Then the choice of the division (u_0, ..., u_k, ..., u_n) is determined from the relation (uniform scale over the region of values of $\mathcal{F}$)

$$\mathcal{F}(u_{k+1}) = \mathcal{F}(u_k) + \Delta\mathcal{F}; \quad \Delta\mathcal{F} = \frac{\mathcal{F}(u_n)}{n}; \qquad \mathcal{F}(u_0) = 0, \tag{10}$$

ensuring automatic closing-up of the points towards the center of the resonances. The function used as $\mathcal{F}(u)$ is

$$\mathcal{F}(u) = \sum_{ij} \sqrt{z_{ij}} \sqrt{\frac{\Gamma_{ij}}{2E_{ij}}} (\operatorname{arctg} x_{ij}^{\max} - \operatorname{arctg} x_{ij});$$

$$z_{ij} = y_{ij}/\sqrt{1+y_{ij}}; \quad y_{ij} = c_i \sigma_r^{ij} l_i; \quad x_{ij} = \frac{2(E-E_{ij})}{\Gamma_{ij} z_{ij}}; \tag{11}$$

$$u = \ln \frac{E_0}{E},$$

where l_i is the estimated mean chord; c_i is the concentration; σ_r^{ij} is the cross section at the center of the j-th resonance for isotope i; E_{ij} is the energy of the center of the resonance level; Γ_{ij} is the width of the resonance line. The calculations show that on average 5-7 intervals must be chosen in the division in order to obtain an acceptable accuracy in each resonance. If at least one of the energy intervals corresponds to the division, the transition cross section for all the isotopes is determined on the basis of the model of scattering at free atoms.

For each isotope k in each zone l, the integrals of radiational absorption, fission, and breeding are calculated up to the current group:

$$C_{kl}^{i}=V_kC_{kl}\sum_{j=1}^{i}\Phi_k^j\sigma_{c,\,l}^j;\quad F_{kl}^{i}=V_kC_{kl}\sum_{j=1}^{i}\Phi_k^j\sigma_{f,\,l}^j;$$

$$\nu F_{kl}^{i}=V_kC_{kl}\sum_{j=1}^{i}\Phi_k^j\nu\sigma_{f,\,l}^j; \tag{12}$$

as well as the neutron current along the energy axis:

$$\varepsilon_k^i=V_k\sum_{1\leqslant j\leqslant i}\sum_{m>i}\Sigma_k^{j\to m}\Phi_k^j, \tag{13}$$

their total values in the cell C^i, F^i, νF^i, ε^i, and in addition the integral (to the given energy) neutron current from the cell through its outer surface $\bar{J}_0^i$. For all groups with numbers below the boundary of the neutron-fission spectrum, the balance equation

$$C^i+F^i+\varepsilon^i+\bar{J}_0^i=1 \tag{14}$$

is satisfied; the contribution of the reaction (n, 2n) — usually very small — may lead to slight deviation of the sum on the left from unity. If there are no neutron currents from the cell, the number of absorbed neutrons is equal to the number of neutrons produced in fission:

$$C+F=1, \tag{15}$$

and the breeding coefficient, by definition, is

$$k_\infty=\nu F. \tag{16}$$

Thus, the TRIFON program is based almost entirely on the use of universal microconstants. Where necessary (for example, for ^{238}U in the region of unresolved or high-energy resonances), the cross section may be artifically blocked on the basis of the equivalence relation. In that case, it is possible to use resonant self-screening factors [22], which are functions of the effective dilution cross section

$$\sigma_0=\frac{A}{4\cdot0{,}6022}\,\frac{S_{ef}}{M};\quad \frac{S_{ef}}{M}=\frac{SD}{\gamma V}+\frac{4\cdot0{,}6022}{A}\,\sigma^s_{ef}, \tag{17}$$

where A is the atomic mass of the resonant absorber; M is its mass; γ is the density, g/cm^3; S is the surface; V is the volume of the unit; D is the Dankoff correction [23]; σ^s_{ef} is the effective scattering cross section of the moderator in the unit, referred to a single atom of resonant absorber in the unit.

Calculation of the Λ Matrix. Suppose, as mentioned above, that a cylindrical volume with a boundary of radius ρ is isolated, and a source Q_f normalized to unity with the energy distribution of the fission-neutron spectrum and some specified spatial distribution is fixed; see Eqs. (8) and (9). Let $N_0 \equiv N^{(1)}$ be the G vector flux* at the surface ρ obtained as a result of convolution of the multigroup solution with the source Q_f and the zero currents at the boundary ρ: $J^{(1)} = 0$. Suppose that $N^{(g)}$, $J^{(g)}$, $g = 2, \ldots, G + 1$ are the corresponding quantities obtained in solving G multigroup problems with the same source Q_f and nonzero linearly independent vectors $J(g)$. For the triangular matrix Λ_2 related to processes of neutron retardation and absorption, in accordance with Eq. (1), the following system of equations is valid:

$$\Lambda_2^{-1}J^{(g)}+N_0=N^{(g)},\quad g=2,\ldots,G+1. \tag{18}$$

Suppose that

$$\mathcal{K}_i^{(g)}=\int_{\Delta u_i}\nu\Sigma_f\Phi^{(g)}\,du\,dV \tag{19}$$

is the number of neutrons arising as a result of fission in the group $1 \leqslant i \leqslant G$ in solving the problem g. Analogously to Eq. (18), the following system of equations is valid:

$$QJ^{(g)}+\mathcal{K}_0=\mathcal{K}^{(g)};\quad g=2,\ldots,G+1;$$
$$\mathcal{K}_0\equiv\mathcal{K}^{(1)}. \tag{20}$$

*Below, for the sake of brevity, N and J defined in Eq. (1) will be called the neutron flux and current.

TABLE 1. Geometry and Composition of Equivalent Cylindrical TRX Cells; $v \equiv V_{mod}/V_{fu}$ [24]

Zone	ΔR, cm	Element (nuclear concentration, 10^{24} cm^{-3})	v	$\sqrt{\frac{S_{ef}}{M}}$	σ_0, b*
Fuel	0,4915	^{235}U (0,0006253) ^{238}U (0,047205)			
Gap	0,0127				
Casing	0,0711	Al (0,06025)			
Moderator	0,181	H (0,06676) O (0,03338)	1,0	0,379	14,2
	0,373	The same	2,35	0,433	18,5
	0,566	" "	4,02	0,451	20,1
	0,938	" "	8,11	0,461	21,0

*1 b = 10^{-28} m^2.

The matrix Q determines the contribution of the currents J in the integral of the form in Eq. (19). Adding the vector components in Eq. (20) gives a relation valid for any J (qJ is the scalar product of the vectors q and J)

$$qJ/(k-k_0)=1; \quad q=\{q_j\};$$
$$q_j=\sum_{i=1}^{G} Q_{ij}; \quad k=\sum_{i=1}^{G} \mathcal{K}_i. \tag{21}$$

For a critical reactor (with k = 1), Eq. (21) may be interpreted as a balance relation: the combination of currents J at the boundary is such that the resulting fission neutrons compensate the difference $k_0 - 1$.

Substituting Eq. (21) as the multiplier of N_0 into Eq. (18) gives the relation between N and J ($N_0 \otimes q \equiv \{N_{0i}q_j\}$)

$$N=[\Lambda_2^{-1}+N_0\otimes q/(k-k_0)]J. \tag{22}$$

In other words, the matrix Λ, taking account of the fission processes, is determined by the relation

$$\Lambda^{-1}=\Lambda_2^{-1}+N_0\otimes q/(k-k_0) \tag{23}$$

(in a critical reactor, k = 1).

It is possible to transform Eq. (23) so as to eliminate the possible singularity (analogously to the method of [15]). Multiplication of Eq. (18) by Λ_2 and scalar multiplication by q gives

$$qJ=q\Lambda_2 N/[1+q\Lambda_2 N_0/(k-k_0)]. \tag{24}$$

Substituting qJ in Eq. (22) on the right-hand side of Eq. (24), a relation between N and J determining Λ is obtained:

$$\Lambda=\Lambda_1+\Lambda_2; \quad \Lambda_1=-\Lambda_2 N_0\otimes q\Lambda_2/(k-v);$$
$$v\equiv k_0-q\Lambda_2 N_0. \tag{25}$$

In reactor calculation, k serves as an eigenvalue, which may be understood to be the neutron breeding coefficient. It follows from Eq. (25) that, when $k \equiv k_0$, N_0 is an eigenvector of the matrix Λ.

Calculating the Response Matrix U. Equivalence of the Characteristics of U and Λ. In determining the characteristics of the unit, the representation in Eq. (2) may be taken as the starting point and the matrix U calculated. In general form, in the small-group diffusional representation, the solution in the moderator of the cell takes the form [11]

$$N=IA+KB; \quad I\equiv CI_0C^{-1}; \quad K\equiv CK_0C^{-1}, \tag{26}$$

TABLE 2. Comparison of the Numbers of Reactions for TRX Cells by the TRIFON (T) Program and the Monte Carlo (MC) Method [24] with Normalization of the Total Number of Reactions to Unity and Zero Neutron Leakage*

Isotope	Process	Method	ν			
			1,0	2,35	4,02	8,11
^{238}U	$f-e$	T	0,05862	0,03863	0,02836	0,01893
		MC	0,05908 (0,3)	0,03896 (0,5)	0,02873 (0,5)	0,01907 (0,5)
	$c-e$	T	0,3436	0,1969	0,1290	0,07030
		MC	0,3477 (0,3)	0,1962 (0,5)	0,1294 (0,6)	0,07035 (0,8)
	$c-t$	T	0,11295	0,1492	0,15575	0,1424
		MC	0,1125 (0,2)	0,1488 (0,1)	0,1548 (0,1)	0,1409 (0,1)
^{235}U	$f-e$	T	0,07093	0,03898	0,02511	0,01354
		MC	0,07044 (0,3)	0,03865 (0,4)	0, 2501 (0,5)	0,01357 (0,5)
	$f-t$	T	0,29543	0,39920	0,42017	0,38626
		MC	0,29541 (0,2)	0,40075 (0,1)	0,42032 (0,1)	0,38508 (0,1)
	$c-e$	T	0,03540	0,01950	0,01251	0,00666
		MC	0,03151 (0,4)	0,01764 (0,4)	0,01135 (0,5)	0,00601 (0,5)
	$c-t$	T	0,05126	0,06841	0,07166	0,06564
		MC	0,05187 (0,2)	0,06919 (0,1)	0,07209 (0,1)	0,06573 (0,1)
k_∞		T	1,0502	1,1676	1,1559	1,0194
		MC	1,0517	1,1732	1,1587	1,0185

*f, fission; c, radiational capture; e, superthermal processes (above 0.625 eV); t, processes in thermal region; k_∞, breeding coefficient. The error of the Monte Carlo method, %, is shown in parentheses.

and the vector J is

$$J = \alpha IA - \beta KB; \quad \alpha \equiv CyII_0^{-1}C^{-1};$$
$$\beta = CyK_1K_0^{-1}C^{-1}; \quad y = \operatorname{diag}_g \{\varkappa_g \rho\}. \tag{27}$$

Suppose that

$$N_0 = (I + KP)W; \quad P = CI_1K_1^{-1}C^{-1} \tag{28}$$

is the solution due to the above-defined single source with zero currents through the surface ρ; W is a constant G vector. In Eq. (1), A and B are redefined, replacing N by the difference

$$n = N - N_0. \tag{29}$$

It follows from Eqs. (26) and (27) that

$$A = K(J + \beta n); \quad B = -I(J - \alpha n). \tag{30}$$

It follows from Eq. (2) that

$$U_2A = B \tag{31}$$

or

$$(I + U_2K)J = (I\alpha - U_2K\beta)n. \tag{32}$$

Equation (32), which follows from Eq. (31), is nothing but Eq. (1) if U_2 and Λ_2 are related as follows:

$$\Lambda_2 = (I\alpha - K\beta U_2)(I + KU_2)^{-1}. \tag{33}$$

A linear relation analogous to Eq. (20) is valid for the amplitude A; from this relation, the elements of the triangular matrix $\mathcal{P}$ characterizing the linear relation between the number of fissions and the amplitude A may be determined:

$$\mathcal{P}A^{(g)} + \mathcal{K}_0 = \mathcal{K}^{(g)}; \quad g = 2, \ldots, G+1. \tag{34}$$

In particular, it follows from Eq. (34) that

$$pA/(k - k_0) = 1; \quad p_i = \sum_{j=1}^{i} \mathcal{P}_{ji}. \tag{35}$$

TABLE 3. Composition of Equivalent Uranium–Water Cells [26]

Type	Zone	ΔR, cm	Element (nuclear concentration, 10^{24} cm^{-3})
1	Fuel	0,486	^{235}U (0,000305), ^{238}U (0,0232), O (0,047)
	Casing	0,071	Al (0,0602)
	Moderator	0,391	H (0,0666), O (0,0333)
2	Fuel	0,490	^{235}U (0,000615), ^{238}U (0,0474)
	Casing	0,071	Al (0,0602)
	Moderator	0,387	H (0,0666), O (0,0333)

Rewriting Eq. (31) in the form

$$U_2 A + B_0 = B, \quad B_0 = I\alpha N_0 \tag{36}$$

and using Eq. (35), it is found that

$$[U_2 + B_0 \otimes p/(k-k_0)]\, A = B, \tag{37}$$

i.e., the total "response" matrix U is

$$U = U_1 + U_2; \quad U_1 = B_0 \otimes p\,/\,(k-k_0), \tag{38}$$

while the matrices Λ and U are related by Eq. (33), like Λ_2 and U_2.

It is readily evident that in view of Eq. (30)

$$A = K(1+\beta\Lambda^{-1})\, J \tag{39}$$

and Eq. (34) transforms to Eqs. (20); the relation between Q and $\mathcal{P}$ is specified by the equation

$$Q = \mathcal{P}K(1+\beta\Lambda_2^{-1}). \tag{40}$$

Thus, the equivalence of the two methods of calculating the characteristics of the unit has been shown, and a unique relation between U and Λ has been established.

Calculating the Activation Coefficients. Suppose that

$$H_i^{(g)} = \int\limits_{\Delta u_i V_x} \Sigma_x \Phi^{(g)}\, du\, dV \tag{41}$$

is the intensity of the specified reaction x defined by the cross section Σ_X in the specified volume V_X for group i (i = 1, ..., G) in calculation g. If $\mathcal{P}_X$ is the matrix determining the contribution of currents in the specified reaction, a system of equations analogous to Eq. (20) is valid:

$$\mathcal{P}_{x,2} J^{(g)} + H_0 = H^{(g)}; \quad H_0 \equiv H^{(1)}; \quad g = 2, \ldots, G+1, \tag{42}$$

and for the total matrix $\mathcal{P}_X$ including the contribution from fission the expression obtained is

$$\mathcal{P}_x = \mathcal{P}_{x,2} + H_0 \otimes q\Lambda_2/(k-v). \tag{43}$$

By constructing the individual components of the vector $\mathcal{P}_X N$, the number of reactions in the energy intervals of the specified group division is determined, together with their sum—the total number of reactions. As $k \to k_0$ and $N \to N_0$, the activation is determined by the vector H_0 ($\Lambda N_0 = 0$!):

$$\mathcal{P}_x N \to \mathcal{P}_x N_0 = H_0. \tag{44}$$

Calculating the Axial Component Λ^Z of the Matrix. Axial leakage of neutrons is taken into account by terms proportional to

$$\alpha^2 = \pi^2/H^2. \tag{45}$$

The calculations are performed with an accuracy of up to first order of the expansion in terms of α^2:

$$\Lambda \to \Lambda + \alpha^2\Lambda^z;\ \Lambda_2 \to \Lambda_2 + \alpha^2\Lambda_2^z;$$
$$N_0 \to N_0 + \alpha^2 N^z;\ k_0 \to k_0 + \alpha^2 k^z;\ q \to q + \alpha^2 q^z. \tag{46}$$

It is assumed that finally over the height of the reactor (in any of the groups of the multigroup system of equations)

$$\Phi = \Phi(r)\, e^{i\alpha z};\ Q = Q(r)\, e^{i\alpha z};\ r \equiv (x, y). \tag{47}$$

If, dividing the cell into M layers of volumes V_m (in an infinite layer, beyond the limits of the cell, it is assumed that $\Sigma_{M+1} = \Sigma_{sM+1} = \Sigma_M$), the collision-probability method is applied to Eq. (4), integrating it over the volumes V_m, the following system of equations is obtained:

$$V\Phi = \mathcal{L}(\alpha^2)\,(\Sigma_s\Phi + Q);\quad V \equiv \operatorname{diag}_m \{V_m\} \tag{48}$$

with the matrix elements

$$\mathcal{L}_{mn} = T_{mn} - T_{m-1n} - T_{mn-1} + T_{m-1n-1}\,(m > n);\ \mathcal{L}_{mn} = \mathcal{L}_{nm};$$
$$\mathcal{L}_{nn} = T_{nn} - 2T_{n-1n} + T_{n-1n-1} + (V_n/\alpha)\ \operatorname{arctg}(\alpha/\Sigma_n);\ T_{mn} = R^-_{mn} + R^+_{mn};$$
$$R^{\pm}_{mn} = 2\int_0^{r_m} dt \int_0^{\pi/2} d\vartheta \exp[-(s_m \pm s_n)\sin\vartheta] \times (\alpha^2\cos^2\vartheta + \Sigma_m^2)^{-1}(\alpha^2\cos^2\vartheta + \Sigma_n^2)^{-1} \times$$
$$\times \{\cos[B(x_m \pm x_n)](\Sigma_m\Sigma_n - \alpha^2\cos^2\vartheta) - \sin[B(x_m \pm x_n)]\,\alpha(\Sigma_m + \Sigma_n)\}, \tag{49}$$

where

$$x_m = \sqrt{r_m^2 + t^2};\ B = \alpha\operatorname{ctg}\vartheta;\quad S_m = \sum_{k(r_k > t)} \Sigma_k\left(\sqrt{r_k^2 - t^2} - \sqrt{r_{k-1}^2 - t^2}\right).$$

If the expansion is limited to first order in α^2

$$\Phi = \Phi_0 + \alpha^2\Phi^z;\ Q = Q_0 + \alpha^2 Q^z;\ \mathcal{L} = \mathcal{L}_0 + \alpha^2\mathcal{L}^z, \tag{50}$$

two equations may be obtained of the form

$$V\Phi_0 = \mathcal{L}_0(\Sigma_s\Phi_0 + Q_0);\ V\Phi^z = \mathcal{L}_0(\Sigma_s\Phi^z + Q^z) + \mathcal{L}^z(\Sigma_s\Phi_0 + Q_0) \tag{51}$$

where the matrix elements $\mathcal{L}_0$ and $\mathcal{L}^z$ are given by Eqs. (14.19), (14.20), and (16.83)-(16.39) of [8].

Together with the known boundary conditions for Φ_0 (see [8], for example), the boundary conditions for Φ^z are formulated. Leakage of neutrons in the axial direction created in layer n with the emission density

$$\Psi_{0n} = \Sigma_{sn}\Phi_{0n} + Q_{0n} \tag{52}$$

may be represented in the form [8]

$$J^z_{0,n} = \alpha^2 \sum_{m=1}^{M+1} \mathcal{L}^z_{mn}\Sigma_m\Psi_{0n}, \tag{53}$$

in accordance with which a compensating source of density $Q^z_{M+1} = J^2_0,\ _{M+1}/V_{M+1}$ is placed in layer M + 1. Taking account of the normalization

$$V_n = \sum_{m=1}^{M+1} \Sigma_m\mathcal{L}_{0,mn} \tag{54}$$

an equation is obtained for the vector fluxes of dimensionality M:

$$V\Psi_0 = \Sigma_s\mathcal{L}_0^{(\theta)}\Psi_0 + Q_0;\quad V\Psi^z = \Sigma_s\mathcal{L}_0^{(\theta)}\Psi^z + \Sigma_s\mathcal{L}^{z(\theta)}\Psi_0 + Q^z. \tag{55}$$

The operators

$$\mathcal{L}_0^{(\theta)} = \mathcal{L}_0 + \theta\mathcal{L}_0';\ \mathcal{L}^{z(\theta)} = \mathcal{L}^z + \theta\mathcal{L}^{z'};$$
$$\mathcal{L}'_{0,mn} = \mathcal{L}_{0,Nn}\mathcal{L}_{0,mN}/S_0;$$
$$\mathcal{L}^{z'}_{mn} = (\mathcal{L}_{0,mN}\mathcal{L}^z_{Nn} + \mathcal{L}_{0,Nn}\mathcal{L}^z_{mN} - S^z/S_0)/S_0; \tag{56}$$

TABLE 4. Heterogeneous Characteristics of Cells at a Surface of Radius ρ = 0.948 cm

Type	Λ_2	N_0	q	p_{235}	p_{238}
1	0,0284 — — — —0,0360 0,1910 — — 0,0105—0,2400 0,1842 — —0,0027 0,0614—0,1741 0,1915 $k_0 = 1{,}109,\ v = 0{,}032$	59,1 7,14 7,14 4,74	0,991 0,995 1,066 1,133	0,000 0,021 —0,005 1,171	0,052 0,011 0,002 0,615
2	0,0299 —0,0370 0,1991 0,0103—0,2310 0,1871 —0,0025 0,0565—0,1687 0,2997 $k_0 = 1{,}166,\ v = 0{,}059$	55,5 6,87 6,52 2,67	1,026 1,037 1,139 1,245	0,000 0,015 0,008 1,000	0,047 0,015 0,008 1,000

*Energy interval divided into groups with boundaries of 10.5 MeV, 10 keV, 100 eV, 0.465 eV, 0. The diffusion coefficients in water are 1.416, 0.594, 0.584, 0.145 cm, respectively; $p_{x,j} = \sum_{i=1}^{4} \mathcal{P}_{x,ij}$.

$$S = \sum_{n=1}^{M} \Sigma_n \mathcal{L}_{nN}; \quad N \equiv M + 1$$

may be obtained as a result of expansion (to terms of order α^2) of the following equation in terms of the M vectors of the flux:

$$\begin{gathered} V\Psi(\alpha^2) = \Sigma_s \mathcal{L}^{(\theta)}(\alpha^2)\Psi + Q(\alpha^2); \\ \mathcal{L}_{mn}(\alpha^2) = \mathcal{L}_{mn}(\alpha^2) + \theta \mathcal{L}'_{mn}(\alpha^2); \\ \mathcal{L}'_{mn}(\alpha^2) = \mathcal{L}_{mN}(\alpha^2)\mathcal{L}_{Nn}(\alpha^2)/S(\alpha^2); \\ S(\alpha^2) = \sum_{m=1}^{M+1} \Sigma_m \mathcal{L}_{mN}(\alpha^2); \\ N \equiv M + 1. \end{gathered} \tag{57}$$

The current $\bar{J}_0$ due to the deviation of the parameter θ from unity and its axial component may be obtained as a sum of the form (the sum operator <I, •>)

$$\begin{gathered} \bar{J}_0 = \langle I,\ (E - \theta)\Sigma \mathcal{L}'_0 \Psi_0 \rangle; \\ \bar{J}^z_0 = \langle I,\ V\langle \Sigma - \Sigma_s \rangle \Phi^z - \Sigma \mid \mathcal{L}^z + (\theta - E)\mathcal{L}^{z'} \mid \Psi_0 \rangle. \end{gathered} \tag{58}$$

Equations analogous to Eqs. (18) and (20) but taking account of axial leakage may be written in the form

$$\begin{gathered} (\bar{\Lambda}^z_2)^{-1} J^{(g)} + \Lambda_2^{-1} J^{z(g)} + N^z_0 = N^{z(g)}; \\ (g = 2, \ldots, G + 1); \\ Q^z J^{(g)} + Q J^{z(g)} + \mathcal{K}^z_0 = \mathcal{K}^{z(g)}; \\ \mathcal{K}^{z(g)}_i = \int_{\Delta u_i} \nu \Sigma_f \Phi^{z(g)} du\, dV; \quad N^z_0 \equiv N^{z(1)}; \\ \mathcal{K}^z_0 \equiv \mathcal{K}^{z(1)}; \quad \bar{\Lambda}^z_2 = -\Lambda_2 (\Lambda^z_2)^{-1} \Lambda_2. \end{gathered} \tag{59}$$

After finding Λ^z_2 and Q^z from Eq. (59), the substitutions in Eq. (46) are used to construct the matrix Λ taking account of axial leakage.

The matrix elements of Eq. (56) in a series of G + 1 calculations are determined in terms of one set of elements $\mathcal{L}_{ij}$ calculated once and stored in the external memory of the computer (all that changes is the currents, i.e., the parameters θ in G groups); in addition, special

TABLE 5. Parameters Characterizing the Axial Leakage, cm^2

Type	Λ_2^z	N^z	q^z
1	0,637 −0,106 0,375 0,002 0,246 0,352 0,006 −0,222 0,188 0,565 $k^z = -49{,}8$	−2247 −270 −291 −213	−28,6 −9,12 −6,54 −3,56
2	0,604 −0,075 0,389 −0,007 0,223 0,362 0,008 −0,202 0,177 0,492 $k^z = -47{,}9$	−1973 −244 −251 −110	−26,9 −8,04 −5,41 −2,26

choice of θ — for example, in two groups $(1, 1)$, $(\theta_0, 1)$, $(1, \theta_0)$ — allows the bulk of the computations to be reduced by memorizing identical parts of the solution. Therefore, in terms of the computational demands, a series of G + 1 calculations is approximately equivalent to double complete calculation of the cell.

Numerical Examples. A fragment of the spatial—energy distribution of the neutrons in the region of strong resonances of ^{238}U for a two-zone cell is shown in Fig. 1. Table 1 shows the initial data for cells of TRX critical piles and Table 2 shows the results of their calculation in comparison with calculation by the Monte Carlo method [24]. The cross section of ^{238}U in groups 11-24 takes account of resonant self-screening [22], calculated using the parameter σ_0; see Eq. (17). Below 1 keV, detailed account is taken of the resonant cross sections with the parameters of the levels taken from [25] in performing the calculations.

Table 3 shows the geometry and composition of the cells of a uranium—water critical pile [26] (in the central zone, there are 37 units of type 1 and in the peripheral zone 936 units of type 2; hexagonal lattice with a step of 1.806 cm); Tables 4 and 5 show their heterogeneous characteristics. Calculation by the DISHER heterogeneous program [11] clearly reproduces the dip in the experimental distribution of detector activation (Fig. 2) from ^{238}U (according to the fission reaction), differing from the distribution of the fast-neutron flux.

LITERATURE CITED

1. A. D. Galanin, "Calculating the thermal-use coefficient in a heterogeneous reactor," in: Reactor Construction and Theory of Reactors. Papers of Soviet Delegation to the First Geneva Conference [in Russian], Vol. 5, Izd. Akad. Nauk SSSR, Moscow (1955), pp. 236-250.
2. S. M. Feinberg, "Heterogeneous methods of reactor calculation," in: Reactor Construction and Theory of Reactors. Papers of Soviet Delegation to the First Geneva Conference [in Russian], Vol. 5, Izd. Akad. Nauk SSSR, Moscow (1955), pp. 152-190.
3. A. D. Galanin, Theory of a Heterogeneous Reactor [in Russian], Atomizdat, Moscow (1971).
4. S. S. Gorodkov, "New method of calculating heterogeneous reactors," Preprint IAÉ-2251 [in Russian], I. V. Kurchatov Institute of Atomic Power, Moscow (1973); see also Preprints IAÉ-2296 (1973); IAÉ-2502 (1975); IAÉ-2728 (1976).
5. B. P. Kochurov and V. M. Malofeev, "Difference approach to solving heterogeneous-reactor equations," At. Energ., 42, No. 2, 87-90 (1977); Ann. Nucl. Energ., 4, 21-25 (1977).
6. A. Ya. Burmistrov and B. P. Kochurov, Spatial—Energy Distribution of Neutrons in a Cylindrical Cell of a Reactor (TRIFON Program). Preprint ITÉF-107 [in Russian], Institute of Theoretical and Experimental Physics, Moscow (1978).
7. V. M. Mikhailov, TERMIT — A Program for Solving the Multigroup Integral Neutron-Transfer Equation in the Thermal Region for a Cylindrical Cell. Preprint ITÉF-119 [in Russian], Institute of Theoretical and Experimental Physics, Moscow (1978).
8. B. P. Kochurov, Test Calculations of Physical Parameters of TRX, BETTIS, and MIT Critical Piles by the TRIFON Program. Preprint ITÉF-164 [in Russian], Institute of Theoretical and Experimental Physics, Moscow (1980).
9. B. P. Kochurov, Calculating the Matrix of Effective Boundary Conditions at the Surface of a Multizone Cylindrical Unit. Preprint ITÉF-94 [in Russian], Institute of Theoretical and Experimental Physics, Moscow (1980).

10. A. Yu. Kvaratskheli and B. P. Kochurov, Method of Calculating the Axial Component of the Matrix of Effective Boundary Conditions at the Surface of a Cylindrical Cell of a Reactor. Preprint ITÉF-98 [in Russian], Institute of Theoretical and Experimental Physics, Moscow (1983).
11. B. P. Kochurov, Numerical Methods in the Theory of a Heterogeneous Reactor [in Russian], Atomizdat, Moscow (1980).
12. B. P. Kochurov, "Development of numerical methods in the theory of a heterogeneous reactor," Candidate's Dissertation, Moscow (1981).
13. T. Auerbach, "Heterogeneous theory of finite lattice cells," EIR, Ber., No. 200 (1970).
14. Ph. Berna, "A consistent approach of heterogeneous theory leading to dipolar formulation. II. Calculation of heterogeneous parameters," J. Nucl. Energ., 26, 319-331 (1972).
15. N. I. Laletin and A. V. El'shin, "Refining the method of homogenization of a heterogeneous reactor," At. Energ., 43, No. 4, 247-253 (1977).
16. N. I. Laletin, "Equations of a heterogeneous reactor," Vopr. At. Nauki Tekh., Ser. Fiz. Tekh. Yad. Reakt., No. 5(18), 31-46 (1981).
17. L. V. Maiorov, "Calculating the constants of the diffusional finite-difference equations for heterogeneous reactors," Vopr. At. Nauki Tekh., Ser. Fiz. Tekh. Yad. Reakt., No. 5 (34), 3-18 (1983).
18. R. Bonalumi, "Rigorous homogenized diffusion theory parameters for neutrons," Nucl. Sci. Eng., 17, 219-265 (1981).
19. Z. Weiss and S. Zindahl, "High-order response matrix equations in two-dimensional geometry," Nucl. Sci. Eng., 58, 166-181 (1975).
20. R. Bonalumi, "Diffusion equations and cell homogenization made rigorous," Energ. Nucl., 21, No. 4, 231-244 (1974).
21. G. Pierini, "A consistent homogenization procedure to obtain few-group cell parameters," Trans. Am. Nucl. Soc., 30, 246-247 (1978).
22. L. P. Abagyan, N. O. Bazazyants, M. N. Nikolaev, and A. M. Tsibulya, Group Constants for Calculating Reactors and Shielding [in Russian], Énergoizdat, Moscow (1981).
23. A. Sauer, "Approximate escape probabilities," Nucl. Sci. Eng., 16, No. 3, 329-335 (1963).
24. J. Hardy, Monte Carlo Analysis of TRX Lattices with ENDF/B-3 Data. Seminar on ^{238}U Resonance Capture, BNL-NCS-50541 (1975).
25. J. Stehn et al., Neutron Cross Sections, BNL-325, Suppl. No. 2 (1965).
26. Kouts et al., "Physics of slightly enriched normal water lattices (theory and experiment)," in: Proceedings of Second UN International Conference on the Peaceful Uses of Atomic Energy, Vol. 12, Geneva (1958), pp. 446-482.

STUDY OF THE INFLUENCE OF INHOMOGENEITIES IN THE ENERGY DISTRIBUTION ON THE READINGS OF EXTRAREACTOR IONIZATION CHAMBERS

A. N. Kamyshan, Yu. A. Krainov,
A. M. Luzhnov, V. V. Lysenko,
V. V. Morozov, A. I. Musorin,
N. R. Nigmatulin, and S. G. Tsypin

UDC 621.039.512.44

As the size and power of reactors increase, the problem of monitoring and control of the energy distribution takes on increasing importance. In addition to the detailed differential characteristics of the energy distribution it is important also to know a number of its integrated characteristics. Thus, e.g., the main contribution to the deviation of the energy distribution from the given values is made by the fundamental and first height harmonics, whose amplitudes characterize the power and power imbalance between the upper and lower halves of the reactor core, respectively [1]. In this paper we consider problems associated with the possibility of obtaining the integrated characteristics of the energy distribution from the readings of detectors set up outside the reactor.

The readings D of an extrareactor detector can be represented as

$$D = \int_V F(\mathbf{r}) S(\mathbf{r}_0, \mathbf{r})\, d\mathbf{r}, \tag{1}$$

where $S(\mathbf{r}_0, \mathbf{r})$ is the space-dependent weighting function of a detector located at the point $\mathbf{r}_0$, $F(\mathbf{r})$ is the energy distribution, and V is the volume of the reactor core. Presenting the integral (1) in the form of the sum of two integrals, taken over the lower and upper halves of the reactor core, and taking into account the fact that the integral of $F(\mathbf{r})$ is proportional to the power of the region over which the integration is performed, by the mean-value theorem for a definite integral we get

$$D = S_1 W_1 + S_2 W_2. \tag{2}$$

Here W_1 and W_2 are the powers of the lower and upper halves of the reactor core, respectively, and S_1 and S_2 are the weighting coefficients that characterize the contribution to the detector reading from the energy release in the lower and upper halves of the reactor core, respectively. Next, using the definition of axial offset AO (the integrated characteristic of the power imbalance between the lower and upper halves of the reactor core)

$$\mathrm{AO} = (W_1 - W_2)/(W_1 + W_2) \tag{3}$$

($W_1 + W_2 = W$ is the reactor power), we transform Eq. (2) into

$$D = W(a_0 + a_1 \mathrm{AO}), \tag{4}$$

where $a_0 = (S_1 + S_2)/2$ and $a_1 = (S_1 - S_2)/2$.

In the general case the weighting coefficients S_1 and S_2 in Eq. (2) depend on the form of the energy distribution $F(\mathbf{r})$, although the weighting function $S(\mathbf{r}_0, \mathbf{r})$ of the detector does not depend on the energy distribution. It was assumed that on a real class of functions $F(\mathbf{r})$ the values of the weighting coefficients vary only slightly and, therefore, with some approximation these coefficients can be assumed to be constant.

To verify this assumption we used data obtained during the start-up of the first block with a VVÉR-1000 water-moderated water-cooled power reactor at the South Ukrainian Atomic Power Plant. A sample of size N = 48 taken from the experimental data was used to perform a regression analysis [2] for the model

$$\tilde{D} = a_0 + a_1 \mathrm{AO}. \tag{5}$$

Here $\tilde{D}$ is the reading of the extrareactor detector, divided by the thermal power of the reactor. The extrareactor detectors used were ionization chambers set up in twos in three verti-

Translated from Atomnaya Énergiya, Vol. 58, No. 2, pp. 91-93, February, 1985. Original article submitted May 30, 1984; revision submitted October 8, 1984.

0038-531X/85/5802-0097$09.50

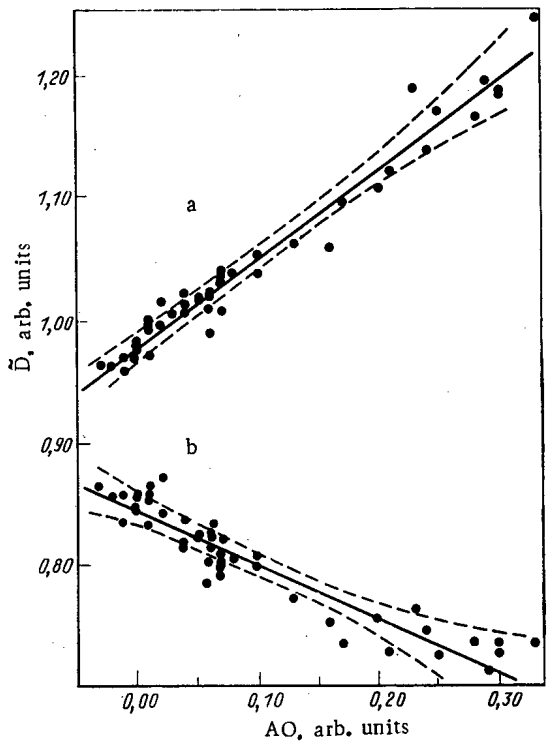

Fig. 1. Regression lines of $\tilde{D} = a_0 + a_1$ AO and a 99% confidence interval as a function of AO for the lower detector (a) for $a_0 = 0.974$, $a_1 = 0.754$ and the upper detector (b) for $a_0 = 0.843$ and $a_1 = -0.426$.

cal protection-system tubes which are arranged symmetrically around the reactor at equal distances from the central axis of the reactor [3]. As the signal from the upper detector we took the averaged reading of three chambers set up opposite the upper part of the reactor core, while as the signal of the lower detector we took the readings of three chambers set up opposite the lower part of the reactor core. The thermal power W of the reactor was determined from the heat balance.

Figure 1 shows the regression lines of $\tilde{D}$ as a function of AO.* The value of the sample linear correlation coefficient between D and AO is 0.98 for the lower dectector (see Fig. 1a) and 0.96 for the upper detector (Fig. 1b). Using the regression estimates obtained, we determined the weighting coefficients of the detectors: $S^l_1 = 1.73$ and $S^l_2 = 0.220$ for the lower detector and $S^u_1 = 0.417$ and $S^u_2 = 1.27$ for the upper detector, i.e., the contributions of energy release in the lower and upper halves of the reactor core to the readings of the lower and upper detectors are 89, 11 and 24, 76%, respectively. It is interesting to note that the values obtained for the relative weighting coefficients for the lower detector almost coincide with the corresponding values (87 and 13%) obtained for extrareactor detectors at the Indian Point-2 Atomic Power Plant [4]. The discrepancy between the values of the weighting coefficients for the upper detector can be attributed to the asymmetry of the properties of the radiation shielding and the nuclear reactor relative to the central plane of the reactor core.

The considerable difference between the weighting coefficients (functions) of the detectors located at different heights of the reactor core enables the average height of the energy distribution to be estimated [5]. Thus, having two detectors set up at different heights of the reactor core, we can consider the height distribution of the energy in the two-harmonics approximation. Indeed, when the system of equations (2), written for the readings D^l and D^u of the lower and upper detectors, respectively, is solved for W_1 and W_2 we find as estimate of the power $W = W_1 + W_2$ in the form of a linear combination of the readings of the detectors [6] and an estimate of the value of AO,

$$AO = (c_1 D^l - c_2 D^u)/(c_3 D^l + c_4 D^u), \tag{6}$$

*The values of AO were obtained from the readings of sensors of the in-reactor monitoring system.

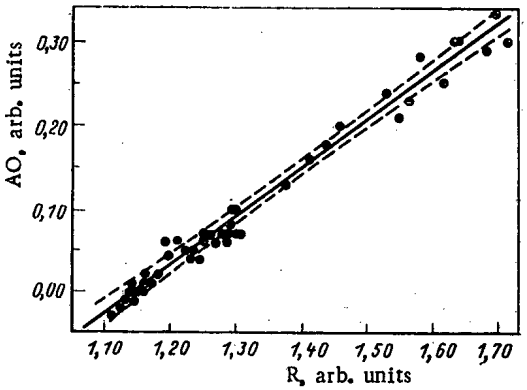

Fig. 2. Regression line of $AO = d_0 + d_1R$ and 99% confidence interval as a function of R for $d_0 = -0.663$ and $d_1 = 0.578$.

where $c_1 = S_2^u + S_1^u$, $c_2 = S_2^l + S_1^l$, $c_3 = S_2^u - S_1^u$, and $c_4 = S_1^l - S_2^l$. Next, expanding the right-hand side of Eq. (6) in powers of $R = D^l/D^u$ in the vicinity of the point R = 1 and taking into account only terms not higher than the first power, we get a simple linear relation between AO and the value of R,

$$AO = d_0 + d_1 R. \tag{7}$$

Figure 2 shows the regression line of AO as a function of R. (The value of the sample coefficient of the linear correlation between AO and R is 0.99.) The calculations were carried out on a sample that was also used to analyze the model (5).

Thus, in most cases the dependence of the readings of extrareactor detectors on the height of the energy distribution can be represented as a linear dependence on AO, while the estimate of the power can be represented as the linear combination of the detector readings. At the same time, from the readings of two detectors set up at different heights relative to the reactor core we can estimate the value of AO. The observed variances of the deviations of the experimental points from the regression lines (see Figs. 1 and 2) contain two components resulting from the errors of the experiment and the dependence of the weighting coefficients on the form of the energy distribution.

LITERATURE CITED

1. E. V. Filipchuk, V. A. Voznesenskii, V. G. Dunaev, et al., "Control of the energy distribution and safety of the VVÉR-1000 reactor during operation in a switching regime," At. Energ., 56, No. 1, 67 (1984).
2. J. Seber, Linear Regression Analysis, Wiley (1977).
3. I. S. Krasheninnikov and V. V. Matveev, "Design of data collecting instrumentation for power reactors and atomic power plants," At. Energ., 50, No. 2, 10 (1981).
4. M. Crump and J. Lee, "Calculation of spatial weighting functions for ex-core detectors," Trans. Am. Nucl. Soc., 23, 461 (1976).
5. A. M. Luzhnov, V. V. Morozov, N. S. Orekhova, and S. G. Tsypin, "Use of extrareactor detectors for monitoring the power and power distribution in a reactor," At. Tekh. Rubezhom, No. 8, 19 (1984).
6. A. N. Kamyshan, A. M. Luzhnov, A. S. Makhon'kov, et al., "On the application of extrareactor detectors for the determination of the reactor power and average energy distribution over the height of the reactor core," At. Energ., 57, No. 1, 18 (1984).

CALCULATING NEUTRON-FLUX FUNCTIONALS BY THE MONTE CARLO METHOD IN BREEDER SYSTEMS WITH LEAKAGE SPECIFIED BY A GEOMETRIC PARAMETER

L. V. Maiorov

UDC 621.039.51

An important role in reactor theory is played by the discussion of asymptotic neutron distribution functions established in homogeneous lattices far from the boundaries of the system. In the present work, algorithms for the calculation of the neutron-flux functionals by the Monte Carlo method in infinite homogeneous lattices with leakage specified by the geometric parameter B are considered [1, 2]. The use of a model problem concerning the neutron flux in an infinite lattice to describe systems of finite dimensions has been discussed repeatedly in the literature; therefore, questions of the interpretation of asymptotic solutions for real systems are not discussed here.

Formulation of the Problem

Consider an infinite heterogeneous lattice with central and translational symmetry. The latter means that the lattice coincides with itself after translation by a vector $\tau_n = n_1\tau_1 + n_2\tau_2 + n_3\tau_3$. Here $n = (n_1, n_2, n_3)$; n_1, n_2, n_3 are arbitrary integers; τ_1, τ_2, τ_3 are the directional vectors of the lattice.

The parallelepiped formed by the vectors τ_1, τ_2, τ_3 is said to be the elementary cell of the lattice (in contrast to a Wigner–Seitz cell). The internal part of the cell may have any complex structure. The lattice with central symmetry has a symmetry center and transforms to itself under inversion (the coordinate substitution $\mathbf{r} \to -\mathbf{r}$ relative to the symmetry center). For an infinite lattice, the criticality equation may be written in differential or integral form. The differential form of the equation for the neutron flux takes the form

$$\Omega \frac{\partial \Phi(\mathbf{r}, \Omega, E)}{\partial \mathbf{r}} + \Sigma_t(\mathbf{r}, E)\Phi(\mathbf{r}, \Omega, E) = \int \Sigma_S(\mathbf{r}, \Omega\Omega', E, E')\Phi(\mathbf{r}, \Omega', E')\,d\Omega'\,dE' + (1/\lambda)Q(\mathbf{r}, \Omega, E), \quad (1)$$

where the neutron-generation density $Q(\mathbf{r}, \Omega, E)$ is expressed in terms of the flux $\Phi(\mathbf{r}, \Omega, E)$ by the formula

$$Q(\mathbf{r}, \Omega, E) = 1/4\pi \int \chi(E, E')\Phi(\mathbf{r}, \Omega', E')\nu\Sigma_f(\mathbf{r}, E')\,dE'\,d\Omega'. \quad (2)$$

The integral form of the equation for the neutron-generation density per unit time is

$$Q(X) = 1/\lambda \int K(X, X')Q(X')\,dX', \quad (3)$$

where $K(X, X')$ is the Green's function for the lattice; $X = (\mathbf{r}, \Omega, E)$ is a point of phase space.

In operator form, the two equations are written as follows:

$$L\Phi = \lambda^{-1}H\Phi; \quad (4)$$

$$Q = \lambda^{-1}KQ; \quad (5)$$

$$K = HL^{-1}. \quad (6)$$

Consider the problem of determining the eigenvalues and eigenfunctions of Eqs. (1) and (3).

It follows from group theory that, on account of the translational symmetry, the eigenfunctions corresponding to a specified λ are linear combinations of the eigenfunctions of Eq. (1) or Eq. (3) satisfying the additional conditions

$$\Phi_\lambda(\mathbf{r}, \Omega, E) = e^{iBr}\varphi_\lambda(\mathbf{r}, \Omega, E), \quad (7)$$

Translated from Atomnaya Énergiya, Vol. 58, No. 2, pp. 93-96, February, 1985. Original article submitted July 18, 1983.

 0038-531X/85/5802-0100$09.50

where

$$\varphi_\lambda(\mathbf{r}+\mathbf{l}_n,\ \Omega,\ E)=\varphi_\lambda(\mathbf{r},\ \Omega,\ E) \tag{7a}$$

for any l_n, while

$$Q_\lambda(\mathbf{r},\ \Omega,\ E)=e^{iBr}q_\lambda(\mathbf{r},\ \Omega,\ E) \tag{8}$$

and

$$q_\lambda(\mathbf{r}+\mathbf{l}_n,\ \Omega,\ E)=q_\lambda(\mathbf{r},\ \Omega,\ E) \tag{8a}$$

also for any l_n.

The popular proofs of this assertion — see [3], Chaps. 9 and 10 — are based solely on the properties of translational symmetry of the operator of the eigenvalue problem.

Following [1, 2], the problem now considered is as follows. Suppose that the geometric parameter **B** is specified. It is required to find the maximum eigenvalue K_e (the neutron breeding coefficient in the lattice) of Eq. (1) or Eq. (3) with the additional condition in Eq. (7) or Eq. (8). The corresponding eigenfunctions will be called fundamental solutions of the criticality equations in a medium with leakage specified by the geometric parameter **B**. Fractionally linear functionals of the fundamental solutions (in particular, the neutron breeding coefficient) are of practical interest. Below, attention is confined to the description of calculations of linear functionals of the fundamental solutions by the Monte Carlo method, since the fractionally linear functionals and K_e are expressed in terms of these functionals in the usual manner [2].

Transformation of the Criticality Equation

The criticality equation is transformed to a form more convenient for calculation by the Monte Carlo method. The central cell of the infinite lattice is isolated and defined as the cell at the symmetry center of which the coordinate origin lies. It is obvious that the fundamental solution of the kinetic Eq. (1) for an infinite lattice satisfying the additional condition in Eq. (7a) with a specified geometric parameter **B** is simultaneously the solution of the same equation for the central cell with boundary conditions at its surface

$$\Phi_\alpha(\mathbf{r}+\mathbf{l}_\alpha,\ \Omega,\ E)=e^{i\mathbf{B}\mathbf{l}_\alpha}\Phi_\alpha(\mathbf{r},\ \Omega,\ E), \tag{9}$$

where $\alpha = 1, 2, 3$; Φ_α are the neutron fluxes at the opposite faces of the cell, coinciding when the cell as a whole is displaced by the vector l_α.

Determining the solution of the criticality equation for the central cell with the boundary conditions in Eq. (9) and using the periodicity conditions in Eq. (7a), the fundamental solution for the whole lattice is found.

The problem of solving the equations for a single cell with the boundary conditions in Eq. (9) has a simple interpretation. The neutron flux $\Phi(\mathbf{r},\ \Omega,\ E)$ arriving in the cell through the face at the point $\mathbf{r}$ ($\Omega\mathbf{p} > 0$, $\mathbf{p}$ is the internal normal to the face) is equal to the neutron flux arriving through the opposite face at the point $\mathbf{r} + \varepsilon l_\alpha$ multiplied by $e^{-i\varepsilon B l_\alpha}$, where $\alpha = 1, 2, 3$ and

$$\begin{aligned}&\varepsilon=+1 \quad \text{when} \quad \mathbf{l}_\alpha\mathbf{p}>0;\\ &\varepsilon=-1 \quad \text{when} \quad \mathbf{l}_\alpha\mathbf{p}<0.\end{aligned} \tag{10}$$

The integral equation for the neutron-generation density reduces to the equation for the central cell if its solution satisfying the conditions in Eqs. (8) and (8a) is sought.

Using the conditions in Eqs. (8) and (8a) and the translational symmetry of the Green's function

$$K(\mathbf{r},\ \mathbf{r}',\ \Omega\Omega',\ E,\ E')=K(\mathbf{r}+\mathbf{l}_n,\ \mathbf{r}'+\mathbf{l}_n,\ \Omega\Omega'E,\ E,\ E'), \tag{11}$$

it is found that

$$Q(\mathbf{r},\ \Omega,\ E)=\lambda\int_{V_0}^{-1}d\mathbf{r}'\int_0^\infty dE'\int_{4\pi}d\Omega'\tilde{K}\ (\mathbf{r},\ \mathbf{r}',\ \Omega\Omega',\ E,\ E')Q(\mathbf{r}',\ \Omega',\ E'), \tag{12}$$

where $\mathbf{r} \in V_0$, i.e., the point $\mathbf{r}$ belongs to the central cell, over the volume V_0 of which integration is taken, and

$$K(\mathbf{r}, \mathbf{r}', \Omega\Omega', E, E') = \sum_{n} e^{-i\mathbf{B}\mathbf{l}_n} K(\mathbf{r}+\mathbf{l}_n, \mathbf{r}', \Omega\Omega', E, E'). \tag{13}$$

The symbol V_∞ means that integration is taken over all of the infinite lattice.

It is obvious that Eq. (12) may be obtained from Eq. (1) with the boundary condition in Eq. (9). Its right-hand side is the sum of contributions to the solution from neutron fluxes which intersect 1, 2, 3, etc., times from division to division of the cell boundary. The equations are equivalent, but are useful in solving different problems.

The solution of Eqs. (1) and (9) or (12) may be written in the form of Eqs. (7) and (8). It follows from the inversional symmetry that the functions φ and q may always be orthonormalized so that their real parts are symmetric, and their imaginary parts are antisymmetric relative to the center of the cell, for example

$$\begin{aligned} \operatorname{Re}\varphi(\mathbf{r}, \Omega) &= \operatorname{Re}\varphi(-\mathbf{r}, -\Omega); \\ \operatorname{Im}\varphi(\mathbf{r}, \Omega) &= -\operatorname{Im}\varphi(-\mathbf{r}, -\Omega). \end{aligned} \tag{14}$$

Below, the solution will be sought in precisely this normalization. It is obvious that in precisely this case the functions Re Φ, Re Q are symmetric and Im Φ, Im Q are antisymmetric.

Some consequences and particular cases of Eqs. (1), (9), and (12) are now considered.

1. When $\mathbf{B} = 0$, the two equations are converted to the criticality equation for a cell of the lattice without leakage. The only difference is that, instead of a Wigner–Seitz cell, an elementary cell of the lattice with boundary conditions of periodicity at its faces is considered. It is obvious, however, that the solution of the two problems is identical.

2. The two equations may be solved by an iterative method using the solution in a lattice without leakage ($\mathbf{B} = 0$) as the zero approximation:

$$\Phi_n = \tilde{L}^{-1} H \Phi_{n-1}, \tag{15}$$

$$Q_n = K Q_{n-1}. \tag{16}$$

Here K is the notation for the integral operator of Eq. (12); $L^{-1}H$ is the inverse operator corresponding to Eq. (1) and the boundary condition in Eq. (9). The tilde over L indicates that the boundary conditions in Eq. (9) have been taken into account. The neutron flux and generation density when $\mathbf{B} = 0$ are described by the real symmetric functions

$$\begin{aligned} \Phi_0(\mathbf{r}, \Omega, E) &= \Phi_0(-\mathbf{r}, -\Omega, E); \\ Q_0(\mathbf{r}, \Omega, E) &= Q_0(-\mathbf{r}, -\Omega, E). \end{aligned} \tag{17}$$

Because of the inversional symmetry of the operators $\tilde{L}$, H, $\tilde{K}$, all the iterations of these functions are such that their real component is a symmetric function while their imaginary component is antisymmetric. For example,

$$\begin{aligned} \operatorname{Re}\Phi_n(\mathbf{r}, \Omega, E) &= \operatorname{Re}\Phi_n(-\mathbf{r}, -\Omega, E); \\ \operatorname{Im}\Phi_n(\mathbf{r}, \Omega, E) &= -\operatorname{Im}\Phi_n(-\mathbf{r}, -\Omega, E). \end{aligned} \tag{18}$$

3. If the functions Φ, Q are fundamental solutions of the criticality equations corresponding to a real eigenvalue, the complex conjugate functions Φ^*, Q* are solutions of the equations

$$\tilde{\lambda}\Phi^* = (\tilde{L}^{-1})^* H \Phi^*; \tag{19}$$

$$\lambda Q^* = \tilde{K}^* Q^*, \tag{20}$$

where the asterisk means that the operators $\tilde{L}^{-1}*$ and K* are complex-conjugate operators of Eqs. (15) and (16). In addition, if Eqs. (1) and (3) are considered for an infinite lattice, it is obvious that Φ and Φ^*, Q and Q* are pairs of solutions of the same equation. Their linear combinations are physically meaningful: $\Phi + \Phi^*$, $Q + Q^*$, $(\Phi - \Phi^*)/i$, $(Q - Q^*)/i$. It may readily be established that the neutron fluxes $1/2(\Phi + \Phi^*)$ and $1/2_i(\Phi - \Phi^*)$ may be brought as close together as is desired by shifting the coordinate origin. Therefore, below, it will be maintained that the functions $1/2(\Phi + \Phi^*)$ and $1/2(Q + Q^*)$ are physically meaningful. They

may be interpreted as the asymptotic distributions of the neutron flux and generation density in finite systems, where the curvature of the flux is characterized by the geometric parameter **B**.

4. The neutron-flux functionals in the central cell are expressed in terms of the neutron-generation density by relations of the form

$$(\gamma, \Phi)_0 \equiv \int_{V_0} \tilde{\gamma}(X)\, dX \int_{V_\infty} G(X, X') Q(X')\, dX', \tag{21}$$

where G(X, X') is the neutron flux at point X under the condition that the source is at point X'. It follows from the translational symmetry of the lattice and the periodicity of the function $q(X) = e^{-i\mathbf{B}\mathbf{r}}Q(X)$ that

$$(\gamma, \Phi)_0 = \int_{V_\infty} \tilde{\gamma}(X)\, dX \int_{V_0} G(X, X') Q(X')\, dX', \tag{22}$$

where $\gamma(X + l_n) = \gamma(X)$ and

$$\tilde{\gamma}(X) = \sum_{\mathbf{n}} \gamma(X) e^{i\mathbf{B}\mathbf{l}_n} \Delta_n(X). \tag{23}$$

Here the summation is taken over all cells of the lattice **n**.

The function $\Delta_n(X)$ is defined as follows:

$$\Delta_n(X) = \begin{cases} 1 & X \in V_n \\ 0 & X \bar{\in} V_n, \end{cases} \tag{24}$$

where V_n is the volume of phase space corresponding to the cell shifted relative to the central cell by the vector

$$\mathbf{l}_n = n_1\mathbf{l}_1 + n_2\mathbf{l}_2 + n_3\mathbf{l}_3.$$

The neutron flux in a lattice with leakage is the product of the functions $e^{i\mathbf{B}\mathbf{r}}\varphi(\mathbf{r})$ describing the macro- and microdistributions of the flux over the cell. The flux functionals φ (microdistributions) over the central (and hence, because of the periodicity of φ, in any) cell are

$$(\gamma, \varphi)_0 = \int_{V_\infty} \tilde{\tilde{\gamma}}\, dX \int_{V_0} G(X, X') Q(X')\, dX', \tag{25}$$

where

$$\tilde{\tilde{\gamma}}(X) = \gamma(X) e^{-i\mathbf{B}\mathbf{r}}. \tag{26}$$

Determining the Functionals of the Fundamental Solutions by the Monte Carlo Method

The neutron-flux functionals in a medium with specified leakage and a specified distribution of sources may be calculated by the Monte Carlo method using Eqs. (23) and (25). Neglecting the difference in neutron-generation density in lattices with and without leakage, all the functionals may be calculated from these formulas by a standard method on setting $Q(X) = Q_0(X)$ and replacing $\gamma(X)$ by $\tilde{\gamma}(X)$ or $\tilde{\tilde{\gamma}}(X)$. To do so, it is sufficient to model the neutron trajectories in an infinite lattice with a source $Q_0(X)$ in the central cell (see [6], for example, where the neutron-flux functionals in poles with an axial leakage $B_z \neq 0$ were calculated in this approximation).

In [2], it was proposed to calculate the neutron breeding coefficient using the formulas of perturbation theory, taking account of the importance function of the unperturbed problem or its approximation. Also in [2], a weighted algorithm for calculating the fission-density functionals in a medium with axial leakage was proposed, in the approximation where the fission spectrum is independent of the initial neutron energy and the type of fissile nucleus. In [5], this method was somewhat improved, eliminating the possibility, in principle, of unlimited increase in the dispersion with increase in accuracy of the calculation. Also in [5], using the uniformity of the solution along the z axis, the possiblity of calculating the neutron-flux functionals (and not only the fission-density functionals), taking account of the perturbation of the source distribution, was realized.

In the present work, a method of calculating arbitrary neutron-flux functionals in lattices with leakage in any direction is outlined, without any constraints on the model of neutron interaction with matter. The algorithm proposed is based on the weighted modeling of the iterative process in Eq. (15). The basis for weighted methods is well known (see [4, 7], for example); therefore, there is no need to dwell on it here.

In application to the given problem, the essence of the method reduces to the following. It is assumed that some small number N of iterations of Eq. (15) is sufficient for convergence with specified accuracy, if the neutron-generation density $Q_0(X)$ in the unperturbed problem without leakage is taken as the zero approximation. Then, to estimate any neutron-flux functionals (γ, Φ) in the perturbed problem $(\mathbf{B} \neq 0)$, it is sufficient to model the trajectory of neutrons of successive generations in an unperturbed medium (a cell with periodic boundary conditions).

In order to take account of the difference in the neutron distribution functions in the perturbed and unperturbed problems $(\mathbf{B} = 0, \mathbf{B} \neq 0)$, the contributions to the estimate of the functionals from neutrons of the given generation are taken with the weights accumulated in the preceding N and the present generation. The weight is determined by the formula

$$W = \exp\left[i \sum_{\alpha=1}^{3} (\mathbf{B}, \mathbf{l}_\alpha)(m_\alpha - m'_\alpha)\right],$$

where m'_α and m_α are the number of neutron flights in the course of the present and the preceding N generations through the face α in the positive and negative directions, respectively, with respect to the vector B (after which, because of the periodicity of the boundary conditions, the neutron returns to the cell through the opposite face). The physical meaning of the weight is obvious, since the perturbed problem $(\mathbf{B} \neq 0)$ is formulated as the problem of determining the neutron flux in the cell with a complex albedo e^{iBl_α} and the translational shift in Eq. (9). That all the usual estimates are undisturbed when they are used to calculate perturbation-theory problems with the perturbation described by weights was proved in [7], for example. Therefore, if estimates from the collision, for example, are used to estimate the flux functional (γ, Φ), the undisturbed estimate for the perturbed $(\mathbf{B} \neq 0)$ problem will take the form

$$1/2 \sum_j (X_j)\,|W(X_j) + W^*(X_j)|,$$

where X_j are the coordinates of collision point j; $W(X_j)$ is the weight at point X_j accumulated in the preceding N and the present generation. The other estimates (over the path length) are constructed in the same way.

The given algorithm was realized in the MCU program [8], which is a development of the MKPRT program [5]. The aim of the present work was to develop programs allowing the possible computational methodological errors to be eliminated in the analysis of critical benchmark experiments for uranium–water lattices of thermal reactors, which are used around the world to check nuclear-physics constants. The results of various researchers in calculating these piles (see [5], for example) by different programs with constants based on the estimates of the ENDF/B IV files lead to a systematic error of 1-1.5% for K_e. One possible explanation for this might be the methodological error in describing the leakage in plane XV. Calculations by the method proposed in the present work show that the difference in neutron breeding coefficient for lattices [5] with leakage that is identical in magnitude but opposite in direction $B_Z^2 = B_X^2 + B_Y^2$ is negligibly small in comparison with the discrepancy between the calculations and experiment.

The reasons for the discrepancy have now been established and attributed to the inaccuracy in the constants of the ENDF/B IV files. Calculations of the lattice considered in [5] by the ENDF/B V files agree with experiment. The corresponding changes in the constants were also made for the library of constants used in the MCU program [9].

The method developed in the present work may prove useful in calculating lattices with clearly expressed anisotropy of the migration length.

LITERATURE CITED

1. A. M. Weinberg and E. P. Wigner, Physical Theory of Neutron-Chain Reactors, University of Chicago Press (1958).

2. E. Gelbard and R. Lell, "Monte-Carlo treatment of fundamental neutron leakage in the presence of voids," Nucl. Sci. Eng., 63, 9 (1977).
3. E. Fermi, Notes on Quantum Mechanics, University of Chicago Press (1962).
4. S. M. Ermakov and G. A. Mikhailov, Course in Statistical Modeling [in Russian], Nauka, Moscow (1976).
5. A. S. Il'yashenko and L. V. Maiorov, "MKPRT program," Vopr. At. Nauki. Tekh., Ser. Fiz. Tekh. At. Reakt., No. 5(27), 77-82 (1982).
6. V. D. Kazaritskii, "Combined estimation of flux functionals using correlated sampling," At. Energ., 51, No. 3, 172-175 (1981).
7. J. Spanier and E. M. Gelbard, Monte Carlo Principles and Neutron-Transport Problems, Addison-Wesley, Reading, Mass. (1969).
8. V. G. Zolotukhin and L. V. Maiorov, Estimating the Critical Parameters of Reactors by the Monte Carlo Method [in Russian], Énergoatomizdat, Moscow (1984).
9. M. S. Yudkevich, "Analysis of experiments on critical piles with the aim of verifying constants for thermal-reactor calculation," in: Neutron Physics [in Russian], Vol. 1, TsNIIatominform, Moscow (1984), pp. 73-79.

FACILITY FOR THE IRRADIATION OF FUEL ELEMENTS IN THE SM-2 AND MIR REACTORS WITH VARIABLE OPERATING REGIMES

V. A. Tsykanov, A. F. Grachev,
E. P. Klochkov, V. A. Kuprienko,
and V. K. Shamardin

UDC 621.039.55

INTRODUCTION

Recently, in many countries, investigations of the behavior of fuel elements with variable power are being extended [1, 2]. These investigations have been promoted by the necessity of utilizing nuclear power stations in a controlled power system regime. The organization of fuel-element tests at variable power in individual cells of the core of a research reactor is accompanied by difficulties in maintaining stationary conditions in experiments being simultaneously conducted in other cells. Therefore, it is necessary to develop special procedures and the corresponding irradiation facilities with the means of autonomous power control, which would ensure that the fuel-element tests were carried out without affecting the reactor operation and other experiments being conducted in it. At the present time, systems are being used with a gaseous neutron absorber — ^{3}He [3] — for testing fuel elements in variable regimes. However, these systems are relatively expensive and complicated in servicing.

For fuel-element tests in the SM-2 and MIR reactors in variable regimes, compact irradiation facilities have been developed, which are simple and reliable in operation, and ensure a variation of power over a wide range. According to the physical operating principles and structural solutions, these facilities can be used in different types of research reactors.

Fuel-Element Testing Procedures in the SM-2 Reactor. The high-flux SM-2 reactor has cells arranged in the beryllium reflector, in which the different investigations on radiation material behavior are conducted [4]. The relative separation of the individual cells from the core allow the neutron physics characteristics in them to be varied without appreciable effect on the reactor operation. In addition, the SM-2 is well provided with supplementary systems, intended for the technical assurance of experiments to investigate the properties of structural materials and fuel elements directly during irradiation. All this has favored the conduct in this reactor of fuel-element tests in regimes of variations of heat release and also intrareactor investigations of instrumented fuel elements at variable power.

Testing of Fuel Elements with Sharp Changes of Heat Release. The procedure for testing fuel elements in conditions of sharp changes of heat release is based on the periodic rapid withdrawal of fuel-element assemblies from the irradiation zone, with subsequent return to this zone. These tests are designed to study the behavior of fuel elements with rapid changes

Translated from Atomnaya Énergiya, Vol. 58, No. 2, pp. 97-100, February, 1985. Original article submitted May 28, 1984.

0038-531X/85/5802-0105$09.50

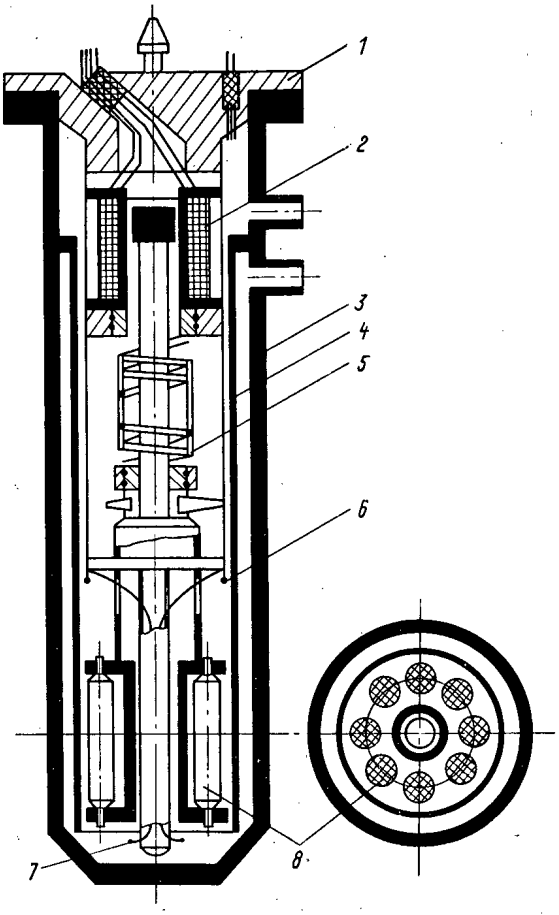

Fig. 1. "Élektropochta" irradiation facility. 1) Flange; 2) electromagnetic actuator; 3) casing; 4) flow separator; 5) compensating spring; 6, 7) thermoelectric transducers; 8) fuel element.

of reactor power, for example in the case of operation of the scram system, with a burst of reactivity. In addition, experiments conducted on specially manufactured fuel elements with a tight fit of the cladding on the fuel element, or fuel elements previously irradiated to a specified burnup, can be used for studying individual processes associated with the operation of the fuel elements at variable power. Sharp power fluctuations from 0 to 100% during 1-2 sec allow the appearance at an earlier stage of irradiation of certain effects, which are observed during slow changes of the heat release intensity in the fuel elements.

The "Élektropochta" irradiation facility for testing fuel elements in the SM-2 reactor during sharp changes of heat release is represented in Fig. 1. In this facility, the fuel-element assemblies are moved by means of an electromagnetic actuator, which has two power and two signal coils. The plunger of the actuator is connected to the fuel-element assembly. The stroke of the plunger to 500 mm provides complete withdrawal of the fuel-element assembly from the irradiation zone. The separable design of the fuel-element assembly allows remote control recharging of the fuel elements to be carried out in the conditions of a shielded chamber.

The change of the power release with movement of the assembly for different sections of the fuel element is shown in Fig. 2. By varying the path of the assembly during its movement, the range of variation of the power release in characteristic sections of the fuel element over the height can be controlled in a defined way. The time of complete withdrawal of a fuel-element assembly in the "Élektropochta" facility amounts to <2 sec.

Tests of Instrumented Fuel Elements during Variable Operating Regimes. Certain processes (deformation of the cladding, release of gaseous fission products from the fuel, etc.), determining the operating efficiency of the fuel elements, cannot be studied with sufficient

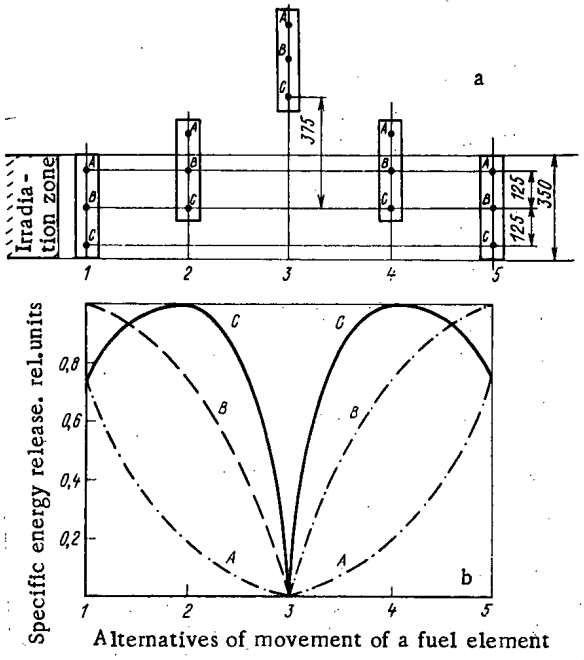

Fig. 2. Change of power release in different sections of a fuel element by movements of the assembly in the "Élektropochta" facility: a) alternatives of movement of the assembly; b) dependence of the power release on the position of the assembly; A, B, and C) characteristic sections in the fuel element; ——, ---, and -·-) changes of power release in these sections, respectively, during movement of the assembly.

reliability in conventional extrareactor investigations. They are studied indirectly during irradiation on instrumented fuel elements, i.e., equipped with measurement transducers. In order to conduct these investigations during variable regimes in the SM-2 reactor, a procedure was developed in which the control of the heat release in the fuel elements is based on a local change of the flux density of the thermal neutrons by means of a movable absorbing shield.

The TTs-SM irradiation facility for testing instrumented fuel elements is shown in Fig. 3. It consists of the channel casing, water pipe with absorbing shield, and a suspension bracket with the fuel element. The water pipe, serving for circulation of the coolant in the channel, consists of three descending and one ascending tube. The suspension bracket with the instrumented fuel element is installed in the ascending tube of the water pipe. The shield, consisting of several absorbing rods, can be rotated from outside of the water pipe from an electric motor installed in the head of the irradiation facility. The power of the fuel element depends on the position of the shield in the facility (Fig. 4). The number of absorbing rods in the shield and the distance between them are chosen from the results of previous investigations of the neutron-physics characteristics of the facility, taking account of the required range of variation of the thermal power of the fuel elements. The rate of change of power can be controlled by means of a stepwise rotation of the shield, with a choice of the necessary number of rods and of the holding time.

The modular grouping of the units of the TTs-SM facility allows it to be used repeatedly in reactor experiments with the replacement only of the suspension bracket with the fuel element. At the same time, depending on the problem to be solved, the construction and equipping of the fuel elements can be varied. Therefore, the TTs-SM facility is versatile and suitable for different intrareactor investigations of the behavior of fuel elements at different power.

Procedure for Loop Tests in the MIR Reactor. The MIR research reactor is equipped with several loop installations for testing fuel-element assemblies of power reactors in stationary

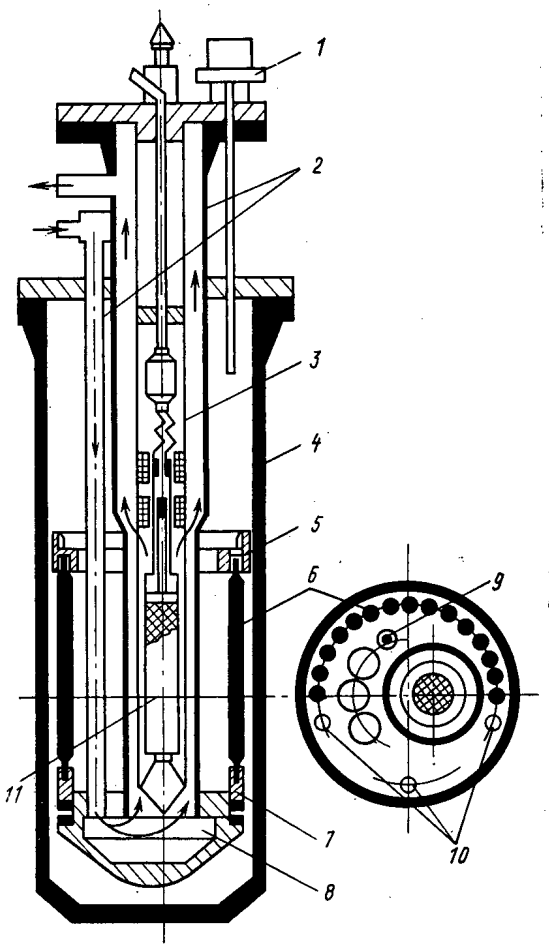

Fig. 3. TTs-SM irradiation facility: 1) electric motor; 2) water pipe; 3) suspension bracket; 4) casing; 5, 7) upper and lower yokes; 6) breeder fuel element; 8) collector; 9) direct load pickup; 10) drawbars; 11) fuel element.

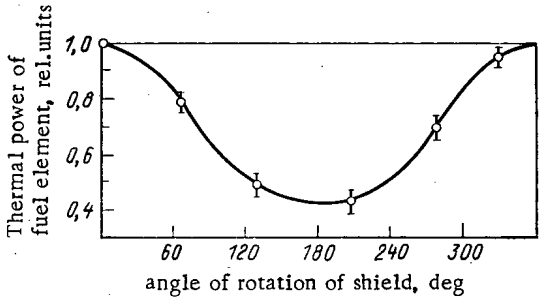

Fig. 4. Dependence of the change of thermal power of the fuel element on the position of the shield in the TTs-SM facility: o) experimental points, obtained directly by measurement of the fuel-element power in the reactor; ——) results of processing the activation measurements of the fission density in the fuel element for different positions of the shield.

conditions. All the irradiation cells (loop channels) are disposed directly in the core [5]. The large number of control and safety rods, located in different regions of the core, allow the power of the assemblies to be controlled in certain loop channels in the range from 80 to 100% of the nominal value, without detriment to experiments simultaneously being conducted in other channels. For a change of thermal power of the fuel element in a wider range during loop tests in the MIR reactor, a procedure was developed based on the principle of rotation

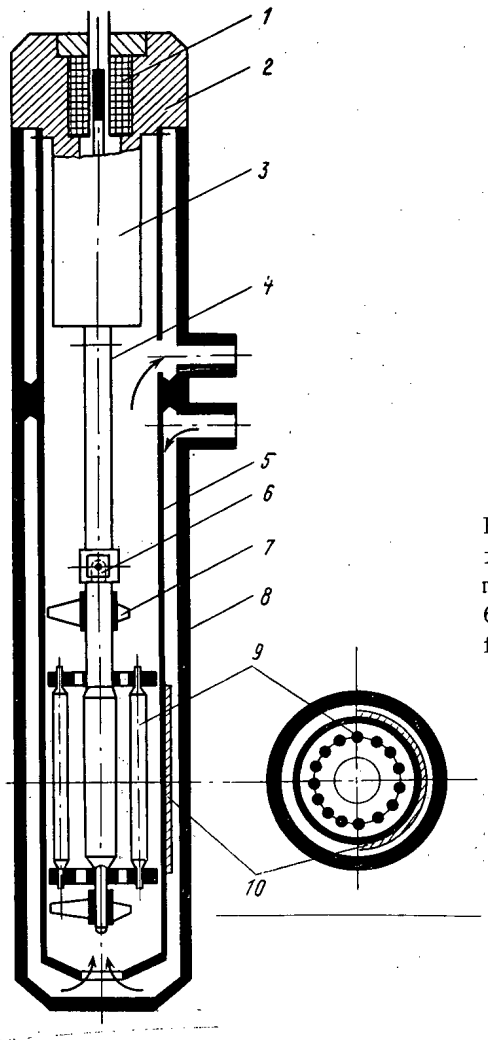

Fig. 5. TTs-2M irradiation facility: 1) position indicator of the assembly; 2) head; 3) rotation mechanism; 4) suspension bracket; 5) flow separator; 6) hinge; 7) spacing sprocket wheel; 8) casing; 9) fuel element; 10) shield.

of the fuel-element assembly in a heterogeneous neutron field, formed by means of a fixed absorbing shield installed in the irradiation facility. The periodic change of orientation of the loop fuel-element assembly by its rotation relative to the shield leads to a redistribution of the power release between the fuel elements. The total thermal power of the fuel-element assembly remains constant, which is the distinctive feature of the method, leading to the minimum effect of the variable regime of testing of the fuel elements in the loop channel during operation of the reactor. The TTs-2M facility, in which this method of power variation is effected, is shown in Fig. 5. The assembly is moved by means of a rotation mechanism installed in the head of the facility. The absorbing shield is fixed immovably to the coolant flow separator. In the TTs-2M facility, up to 15 VVÉR simulated fuel elements can be loaded simultaneously. The amplitude and nature of the change of power of the fuel elements depend on the angle of rotation of the assembly, the maximum value of which in the TTs-2M facility amounts to 90° (Fig. 6).

From the data presented, it follows that the spectrum of the simultaneously achieved regimes with respect to the power level of the fuel elements and its range of variation is quite extensive. This allows, in a single experiment, the dependence of the individual fuel-element characteristics on the parameters of the power cycle to be obtained. In order to reduce the number of variable regimes with simultaneous increase of the number of fuel elements irradiated in specified conditions in the TTs-2M facility, profiling of the fuel charge over the cross section of the fuel element assembly can be used (Fig. 7).

The rate of change of power of the fuel elements is provided by stepwise rotation of the fuel-element assembly with a choice of the necessary number of stages and the time of stay of the assembly at each of them. In the design of the fuel-element assembly, provision is made for the possibility of remote control recharging of the fuel elements in the conditions of a shielded chamber. This allows in the TTs-2M facility, without shutting down the experiment

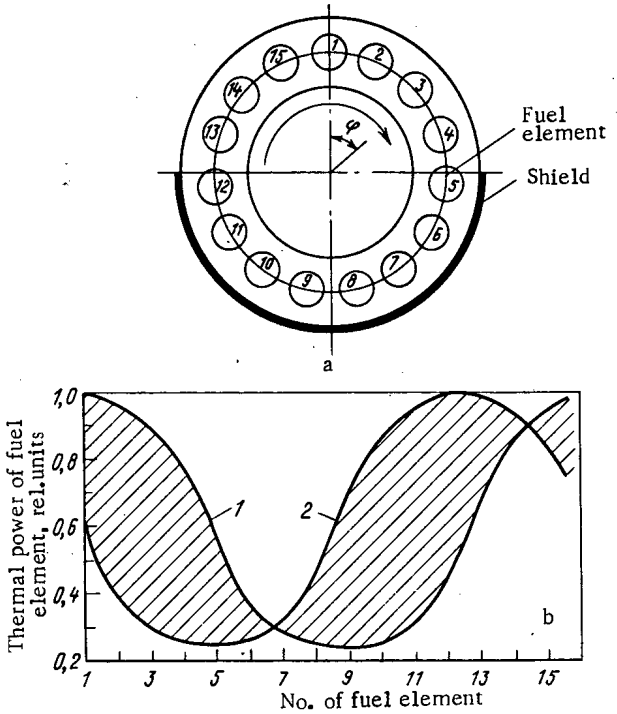

Fig. 6. Orientation of fuel elements relative to the shield (a) and the range of variation of their power by rotation of the assembly with a nonprofiled fuel charge (b) for the initial ($\varphi = 0$) position of the assembly (1) and after rotation by an angle of $\varphi = 90°$ (2).

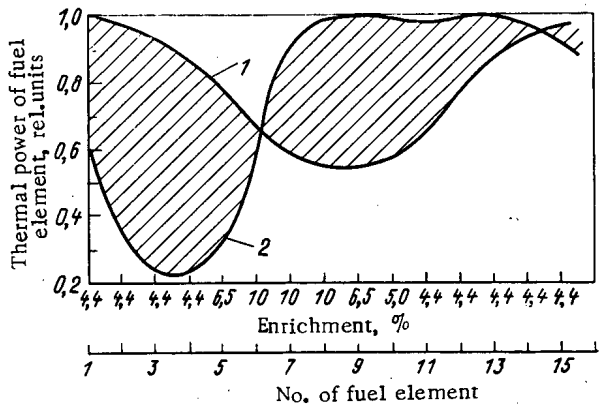

Fig. 7. Range of variation of power of fuel elements during rotation of the assembly, with a profiled fuel charge, in the TTs-2M facility with an initial ($\varphi = 0$) position of the assembly (1) and after rotation by an angle $\varphi = 90°$ (2).

as a whole, the testing of fuel elements up to a different number of power cycles. In addition, such recharging makes it possible to use fuel elements in the experiment which have been irradiated previously up to different fuel burnups in other simpler facilities. The special feature of the TTs-2M design lies in that directly in the course of irradiation, by a change of reactivity in the loop circuit during rotation of the fuel-element assembly, the location of a fuel element losing hermeticity can be determined.

CONCLUSIONS

The procedures and irradiation facilities developed for testing fuel elements at a variable power have received experimental verification in the SM-2 and MIR reactors, and have

shown satisfactory operating efficiency of all units. During the experiments, no appreciable effect of the facilities was noted on the operation of the reactors into which they were loaded, and on the testing conditions in other channels. These procedures at the present time are being used in investigations conducted in the SM-2 and MIR reactors, for verification of the operating efficiency of the fuel elements of power reactors in different variable operating cycles.

LITERATURE CITED

1. G. Thomas, "The Studsvik INTER RAMP PROJECT: An international power ramp experimental program," J. Nucl. Mater., 87, No. 2, 215-226 (1979).
2. I. Firing and E. Kolstad, "Evaluation of in-reactor measurements of fuel rod deformations," in: Proceedings of an International Conference on Nuclear Power and the Fuel Cycle, IAEA-CN-36/495, Vienna, Vol. 2 (1977), pp. 629-633.
3. V. I. Andreev, P. M. Ergorenkov, V. N. Kolyadin, et al., "Application of a gaseous absorber for fuel element tests in nonstationary conditions," At. Energ., 51, No. 5, 302-304 (1981).
4. V. A. Tsykanov and B. V. Samsonov, Techniques of Irradiation of Materials in High Neutron Flux Reactors [in Russian], Atomizdat, Moscow (1973).
5. P. G. Aver'yanov, B. A. Zaletnykh, E. P. Klochkov, et al., Development and Modernization of Research Material-Study Reactors of the Institute, and Intrareactor Methods of Investigation [in Russian], Preprint NIIAR-2 (455), Dimitrovgrad (1981).

MATHEMATICAL MODEL OF THE BEHAVIOR OF OXIDE MICROFUEL-ELEMENTS IN A HIGH-TEMPERATURE GAS-COOLED REACTOR

S. A. Balankin and E. A. Rybakova

UDC 621.039.524.2.034.3:001.57

One of the main reasons for the destruction of microfuel-elements in high-temperature gas-cooled reactors is the amebic effect [1]. This effect consists of the migration of the fuel kernel against the temperature gradient and is caused by the transport of carbon driven by the temperature gradient from the "hot" side of the inner pyrocarbon coating to the "cold" side.

The amebic effect is characteristic for microfuel-elements with uranium, thorium, and also mixed uranium–thorium oxide and carbide kernels [1-7]. The phenomenon of amebic destruction of carbide microparticles has been studied in detail [2, 7], but there are no models which adequately describe the amebic process in oxide microfuel-elements. The purpose of this paper is to develop a mathematical model of the amebic behavior of microfuel-elements with uranium dioxide kernels in a reactor at temperatures in the range 1273-1523°K and a burnup of 0.5-5% of the initial number of metallic atoms.

According to published reports [1-7], one of the important factors characterizing the work of microfuel-elements and leading to their destruction, together with high temperature, is the temperature gradient along the particle.

A temperature gradient can appear in a particle for a number of reasons: asymmetry of the particle and the concomitant asymmetry of heat release within it, the presence of a temperature gradient in the active zone, and any extremal conditions of reactor operation. The temperature gradient caused by the asymmetry of heat release in the particle can be evaluated with the help of the method proposed in [8]. We shall study a homogeneous spherical particle with radius a, heat release per unit volume $q(r) = \text{const} = q_0$, and an axisymmetrical distribution of heat release over the surface $H(\theta) = H_0 + h(\theta)$, where H_0 is the average value of the coefficient of heat release ($H_0 = 0.3 \cdot 10^4$ W·m^{-2}·K [8]), $h = (\delta_0/2k_g)\cos\theta$. This formulation of the problem corresponds to the case when the kernel of the particle is not a perfect sphere or to the case when for one reason or another, for example, in the process of fabrication of the microfuel-element, the kernel separated from the coatings. Then δ_0 is the maximum gap and k_g is the coefficient of thermal conductivity of the gas filling the interlayer. The remain-

Translated from Atomnaya Énergiya, Vol. 58, No. 2, pp. 101-104, February, 1985. Original article submitted January 10, 1983.

0038-531X/85/5802-0111$09.50

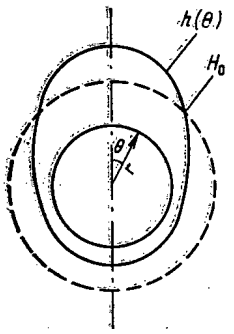

Fig. 1. Diagram of the distribution of heat release in an asymmetrical microfuel-element.

ing variables are elucidated in Fig. 1. The equation of heat conduction for the stationary state of heat transport in the sphere has the form

$$k\Delta T(r, \theta) + q_0 = 0, \tag{1}$$

and under the assumption that heat exchange with the external medium occurs according to Newton's law the boundary condition is written as follows:

$$k \frac{\partial T(r, \theta)}{\partial r}\Big|_{a, \theta} + [H_0 + h(\theta)]\, T(a, \theta) = 0, \tag{2}$$

where T is the temperature with respect to the external medium and k is the coefficient of thermal conductivity of the particle.

We seek the solution of the system of equations (1) and (2) in the form

$$T(r, \theta) = Q_0 \sum_{i=0}^{N} H_i(\cos\theta)\, Q_i(r), \tag{3}$$

where Q_0 = const t; $H_i(\cos\theta)$ are the Legendre polynomials; and $Q_i(r)$ are twice continuously differentiable functions of r. If we retain the first three terms in the series (3), then the system under study can be solved analytically. The temperature gradient is determined by the difference $T(a, o) - T(a, \pi)$. Using the data from [3, 9-11], we find that it is equal to $0.1 \cdot 10^5 - 0.2 \cdot 10^5$ K·m^{-1}.

Estimates of the values of the temperature gradient in the particle, arising due to the nonuniformity of heat release in the reactor, based on the dependences of the temperature distribution on the distance away from the center of the active zone [3] show that the temperature gradient in the particle caused by the temperature gradient in the active zone coincides with the estimate based on the assumption that the microfuel-element is asymmetrical.

Knowing the temperature gradient imposed on the microfuel-element in the reactor and taking into account the other working parameters of the microparticle (pressure of gaseous fission products reaching 10^6-10^7 Pa, a temperature of 1173-1573°K, and fluences of fast neutrons of the order of 10^{25}-10^{27} m^{-2}), a conclusion can be drawn concerning the destructive processes that can occur in the particle.

The main process is mechanical failure, which is not a subject of this paper. In addition, under these conditions the coating materials can interact chemically with the fuel and the fission products. Finally, the presence of a temperature gradient can give rise both to the chemical and physical transport of matter.

Following [11-13], we shall assume that the qualitative composition of the gas phase filling the pores of the buffer layer of the microfuel-element is determined by the gaseous fission products (Xe and Kr) as well as by the products of the interaction of the oxygen liberated in the fission process with the inner pyrocarbon coating (CO and CO_2).

Let the pressure of these gases depend on the temperature according to the perfect-gas law. Then, for xenon and krypton, we obtain

$$p_p = \frac{d_0 V_0 N_A h_0 b \gamma_p f_p}{M_0 V_p 100} kT, \tag{4}$$

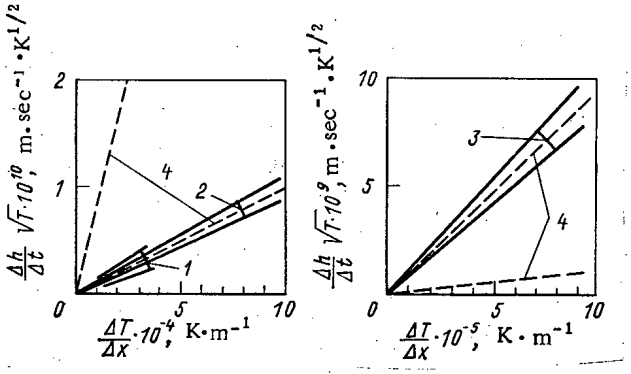

Fig. 2. Dependence of the amebic process on the temperature gradient: 1, 2, 3) regions obtained by analyzing the AERE, ORNL, and KFA data, respectively, by the method of least squares [5]; 4) boundaries of the theoretically obtained region.

where p in the index is Xe and Kr; N_A is Avogadro's number; M_o is the molecular mass of the kernel material; h_o is the number of metal atoms in the fuel molecule; γ_r is the radiation yield of the fission product; f_p is the relative fraction of gas liberated from the kernel into the coating; b is the burnup, expressed as a percent of the initial number of metal atoms; k is Boltzmann's constant; V_o is the volume of the kernel; V_p is the volume of the pores which can be occupied with gas; and d_o is the density of the kernel.

The pressure of CO and CO_2 as a function of the temperature is determined by the relation

$$p_i = \frac{\left(2+y_0-\sum S_k Y_k - y_1\right) d_0 V_0 N_A \alpha_i b}{M_0 V_p} kT, \tag{5}$$

where i = CO, CO_2; y_o is the initial deviation from stoichiometry, Y_k is the number of atoms of the k-th fission product; S_k is the value of O/M for the k-th fission product; the sum $\Sigma S_k Y_k$ includes only the fission products whose oxide forms are more stable than CO; α_i is a coefficient determining the relative fraction of oxygen atoms used up in the formation of the i-th gas ($\alpha_{CO} + 2\alpha_{CO_2} = 1$); and y_1 is a term that takes into account the relative fraction of the oxygen used up in measuring the stoichiometry of the fuel. In [11] an iterative process, in which the usual temperature dependences of thermodynamic equilibrium are used, is proposed for determining p_i. As indicated in [13], irradiation markedly changes the conditions of equilibrium in the CO — CO_2 system. There are no data in the literature on the effect of neutron irradiation on this system, but the effect of fast electrons and gamma rays on it was studied in [13]. Extrapolating the results obtained to the conditions of reactor operation and using the data in [11, 12] for burnup of 0.5-5% of the initial number of metal atoms and temperatures of 1273-1523°K, we find (in Pa):

$$p_{CO} = 0{,}07 \cdot 10^3 \; b \cdot T; \tag{6}$$

$$p_{CO_2} = 3{,}2 \cdot 10^3 \; b \cdot T; \tag{7}$$

$$p_{Xe} = 1{,}3 \cdot 10^3 b \cdot T; \tag{8}$$

$$p_{Kr} = 0{,}26 \cdot 10^3 \; b \cdot T. \tag{9}$$

To construct the mathematical model of the amebic processes in an oxide microfuel-element, it is necessary to elucidate the mechanism that controls the attainment of the equilibrium values of the CO and CO_2 pressures in the gas phase of the buffer layer of the microparticle.

The following processes are identified in [14] as possible processes:

on the surface

$$\langle C\rangle \rightarrow [C]_{UC_2}; \tag{10}$$

diffusion from the surface through the interface

$$[C]_{UC_2}; \tag{11}$$

reaction at the interface

$$2\,[C]_{UC_2} + UO_2 \rightarrow UC_2 + 2\,[O]_{UC_2}; \tag{12}$$

diffusion to the surface of the kernel

$$[O]_{UC_2}; \tag{13}$$

and the surface reaction

$$[O]_{UC_2} + \langle C\rangle \rightarrow (CO). \tag{14}$$

Here the square brackets indicate a solid solution of the element enclosed in the material denoted by the subscript; the angular brackets enclose the solid materials and the parentheses enclose gaseous materials.

The most probable mechanism [14], however, is diffusion of oxygen through the boundary layer between UO_2 and UC_2, and the coefficient of diffusion is determined by the relation $k_d = 21.0 \cdot \exp(-90{,}000/RT)$, cm^2/sec (the activation energy is expressed in cal/mole). According to [15], the time over which the equilibrium state is reached, assuming that it is controlled by diffusion, is equal to

$$\theta = a^2/\pi^2 D, \tag{15}$$

where a is the diffusion length and D is the coefficient of diffusion. Therefore, making the assumption that the boundary layer between UO_2 and UC_2 is equal to several micrometers, we find that for a given burnup the equilibrium pressure in the temperature range studied is established within several hours, i.e., much more rapidly than the burnup increases and the temperature in the microfuel-element changes.

Thus, the values of the CO and CO_2 pressure, determined by formulas (6) and (7), are equivalent with given burnup and temperature.

The difference between the conditions of equilibrium on the hot and cold sides of the inner pyrocarbon coating will unavoidably lead to the transport of carbon. Here an analysis showed that only the concentration-driven gas-phase diffusion of carbon oxides contributes to the indicated process in the burnup and temperature ranges studied. According to Fick's law, the flux of the i-th component in the gas mixture is equal to

$$\mathbf{j}_i = \frac{D_i}{RT} \operatorname{grad} p_i, \tag{16}$$

where T is the absolute temperature, R is the universal gas constant, and p_i is the partial pressure of the component.

In a porous medium the coefficient of diffusion D_i is determined by the formula [16]

$$D_i^{-1} = D_{ik}^{-1} + D_{iM}^{-1}, \tag{17}$$

where D_{ik} is the coefficient of Knudsen diffusion and D_{iM} is the coefficient of molecular diffusion. In the case studied $D_i \approx D_{iM}$.

Using the formula [17] for calculating binary diffusion coefficients and Wilk's formula for determining the diffusion coefficients in a gaseous mixture based on the binary coefficients [18], with the help of relations (6)-(9) it is possible to find the coefficients of diffusion of CO and CO_2:

$$D_{CO} = 0{,}58 \cdot 10^{-7} \sqrt{T} b^{-1} \, m^2 \cdot sec^{-1} \tag{18}$$

$$D_{CO_2} = 0{,}19 \cdot 10^{-7} \sqrt{T} b^{-1} \, m^2 \cdot sec^{-1} \tag{19}$$

Next, with the help of Eqs. (16), (18), and (19), we calculate the CO and CO_2 fluxes, transporting carbon from the hot side of the inner pyrocarbon coating to the cold side:

$$j_{CO} = \frac{0{,}49 \cdot 10^6}{\sqrt{T}} \frac{dT}{dx} \, mole \cdot m^{-2} \, sec^{-1} \tag{20}$$

$$j_{CO_2} = \frac{0{,}73 \cdot 10^{-5}}{\sqrt{T}} \frac{dT}{dx} \, mole \cdot m^{-2} \, sec^{-1} \tag{21}$$

The amebic effect in the microfuel-element is associated not only with the transport of carbon from the hot to the cold side under the action of the temperature gradient but also with the motion of the fuel kernel against the temperature gradient and the change in its shape. However, the motion of the atoms in the kernel was not studied in any of the papers on the amebic effect, and the motion of thorium and oxygen against the temperature gradient is postulated only in [6] in the study of the amebic effect on microfuel-elements with thorium dioxide kernels, initially irradiated and then subjected to annealing in the presence of a

temperature gradient. But this assumption [6] does not agree with the interreactor experiments, because if diffusion of the fissioning atoms in the coating does occur inside the microfuel-element, then it occurs along the temperature gradient. In this case, the coefficient of diffusion of uranium or thorium from the oxide or carbide kernels into the pyrocarbon coating, according to [19, 20], depends on the properties of the pyrocarbon, in particular, on the density, and this leads to the predominant lengthening of the kernel toward the lower density part of the buffer coating, i.e., in the direction of the hotter pole.

The diffusion of atoms of the fissioning material into the bulk of the inner coating and gas-phase transport of carbon from the hot to the cold side of the microfuel-element are two parallel processes, leading to the destruction of the inner pyrocarbon coating. Therefore, in order to calculate the rate of destruction of the inner coating it is necessary to know which of these processes proceeds most rapidly. Estimates based on the results of [19] showed that gas-phase transport in an oxide microfuel-element occurs more rapidly than diffusion of atoms in the kernel into the bulk of the coating. This suggests that the last process does not affect the rate of amebic destruction, but affects the change in the shape of the kernel, which, strictly speaking, is responsible for the name of the phenomenon under study.

Comparing, in accordance with the formula (15), the process of oxygen flow up to the buffer coating and the gas-diffusion transport of carbon in the form of CO and CO_2, we find that the controlling link in the formation of carbon oxides and gas-phase transport is precisely the diffusion of CO, described by Eq. (20), from the hot pole of the microfuel-element to the cold pole. In accordance with this the rate of amebic migration $\Delta h/\Delta t$ in the temperature intervals studied and the rate of burnup can be described by the relation

$$\frac{\Delta h}{\Delta t} = \beta \frac{1}{\sqrt{T}} \frac{\Delta T}{\Delta x}, \qquad (22)$$

where β is a coefficient determined by the geometric and physical properties, $\beta = (10^{-4}-10^{-5})$ $m^2 \cdot K^{1/2} \cdot sec^{-1}$. The calculations performed using formula (22) are reflected in the graphs in Fig. 2. Thus the present model takes into account the constant change in the conditions of equilibrium accompanying a change in the burnup, manifested in the constant flow of oxygen up to the buffer coating and the accumulation of carbon oxide and dioxide in the volume of the pores in the buffer layer, and assumed a unidirectional transport of oxygen from the cold pole to the hot one. This enables the rejection of the improbable hypothesis of cyclical displacement, in particular, the necessity of modeling the outflow of oxygen from the cold pole to the hot one, which gave rise to considerable difficulties in the previously existing models. For example, in [5] two more probable mechanisms of oxygen transport from the cold pole of the microfuel-element to the hot one are indicated: gaseous diffusion of CO and solid-phase diffusion of oxygen. In this case, the first leads to a quadratic dependence of the amebic process on time and gives unsatisfactory results when a gap is present between the kernel and the inner coating [5], and the second leads to dependence of the rate of amebic migration analogous to the law of thermodiffusion, but it is impossible to interpret theoretically the constants in this dependence [5]. In addition, it is pointed out in [13] that under irradiation the number of oxygen molecules, atoms, and ions in the system $CO - CO_2 - C$ is negligibly small compared to the number of CO and CO_2 molecules. In this connection it seems to us that the dependence presented in [5] has more of an a priori character rather than that of a strictly theoretically proven result.

Thus, in the analysis we introduced the change in the shape of the fuel kernel of the microfuel-element as a result of diffusion of fissioning atoms into the bulk of the buffer coating. A primary mathematical model of amebic behavior of an oxide microfuel-element in a reactor in the temperature range 1273-1523°K and burnup of 0.5-5% of the initial number of metal atoms was developed.

LITERATURE CITED

1. R. Bullock, "Fuel-fluence tests of experimental thermosetting fuel rods for the high-temperature gas-cooled reactor," Nucl. Technol., 52, No. 2, 246 (1981).
2. O. Stansfield, C. Scott, and J. Chin, "Kernel migration in coated fuel particles," Nucl. Technol., 25, 517 (1974).
3. L. Wolf, G. Ballensiefen, and W. Frokling, "Fuel elements for high temperature pebble-bed reactor," Nucl. Eng. Design, 34, 93 (1975).
4. T. Gulden, J. Scott, and C. Moreau, "Present thorium-cycle concepts and performance limitations," in: ANS Conference Gas-Cooled Reactors, Gutlinburg (1974), p. 176.

5. M. Wagner-Loffler, "Amoeba behavior of UO_2 coated particle fuel," Nucl. Technol., 35, 392 (1977).
6. C. Smith, "Migration of ThO_2 kernels under the influence of a temperature gradient," Nucl. Technol., 35, 402 (1977).
7. T. Gulden, "Carbon thermal diffusion in the UC_2—C system," J. Am. Ceram. Soc., 55, 14 (1972).
8. Z. Holy, "A synthesis technique for the variable surface heat transfer," Nucl. Eng. Design, 8, 289 (1968).
9. V. V. Goncharov et al., Effect of Irradiation on Graphite in Nuclear Reactors [in Russian], Atomizdat, Moscow (1978).
10. R. B. Kotel'nikov, High-Temperature Nuclear Fuel [in Russian], Atomizdat, Moscow (1978).
11. M. Dalle Donne and G. Chumacher, "Consideration on PyC and SiC coated particles for gas cooled fuel reactor application," J. Nucl. Mater., 40, 27 (1971).
12. H. Walther, "On mathematical models for calculating the mechanical behavior in coated fuel particles," Nucl. Eng. Design, 18, 11 (1072).
13. G. P. Zhitneva and S. Ya. Pshezhetskii, "Mechanism of heterogeneous reaction of CO_2 with carbon under bombardment by fast electrons," Zh. Fiz. Khim., 41, 1707 (1967).
14. T. Lindemer et al., "Kinetics of the graphite–uranium dioxide reaction from 1400 to 1756°C," J. Am. Ceram. Soc., 52, 233 (1969).
15. J. Shaw and W. Oates, "Thermomigration of carbon in metals," Metall. Trans., 2, 2127 (1971).
16. R. Evans and G. Watson, "Gaseous diffusion in porous media at uniform pressure," J. Chem. Phys., 35, No. 6, 2076 (1961).
17. J. Hirschfelder et al., Nuclear Theory of Gases and Liquids, New York (1954).
18. R. Reed and T. Sherwood, Properties of Gases and Liquids [Russian translation], Khimiya, Leningrad (1971).
19. P. Coss, E. Balthesen, and H. Nickel, "Diffusion of uranium and thorium in pyrocarbon," in: USAEC Conference 730601, p. 53.
20. G. B. Fedorov and E. A. Smirnov, Diffusion in Reactor Materials [in Russian], Atomizdat, Moscow (1978).

RADIATION EROSION OF WELDED JOINTS IN STEELS PROMISING FOR FUSION SYSTEMS

B. A. Kalin, V. I. Pol'skii,
D. M. Skorov, E. E. Goncharov,
I. L. Artemenkov, and A. P. Morozov

UDC 621.039.531

Welding is one of the major operations in making the discharge chambers for various types of fusion system [1, 2]. The first wall in a discharge chamber is exposed to intense neutron bombardment and heat loads, as well as variable mechanical stresses and high fluxes of neutral and charged particles [2, 3]. Therefore, the welded joints in the first wall have to have not only high mechanical strength and good vacuum quality but also considerable radiation resistance under bombardment by neutrons and charged particles, as well as thermal stability in the presence of plasma and compatibility with the coolant.

Here we present results on two forms of effect from a fusion plasma on the first wall: bombardment by helium ions of energy 20 and 40 keV and irradiation by plasma bunches. We examined stainless steels of the austenite and ferrite classes made not only by powder-metallurgy methods but also by traditional methods. These steels are taken as being promising materials for fusion-reactor chambers, while they have been thoroughly tested and have a well-developed and cheap welding technology.

Methods. The bombardment by 20-keV helium ions was performed with a double-focusing mass monochromator, while the 40-keV bombardment was performed with an ILU-3 accelerator. The ion dose in both cases was $1 \cdot 10^{22}$ m^{-2}, while the target temperature during irradiation did not exceed 350°K. Deuterium-plasma bunches were used with an MK-200 pulsed plasma accelerator

Translated from Atomnaya Énergiya, Vol. 58, No. 2, pp. 104-110, February, 1985. Original article submitted March 1, 1984.

 0038-531X/85/5802-0116$09.50

TABLE 1. Experimental and Calculated Parameters* of Welded Joints in Austenitic Steels

Temperature °K	12Kh18N10T				ÉI-847			
	$y_e \cdot 10^{-3}$, m	$y_t \cdot 10^{-3}$, m	t_h, sec	$1/2h \cdot 10^{-3}$, m	$y_e \cdot 10^{-3}$, m	$y_t \cdot 10^{-3}$, m	t_h, sec	$1/2h \cdot 10^{-3}$, m
773-1173	—	3,29	5,9	1,76	—	3,36	2,7	1,40
1173-1323	2,71	2,52	2,0	1,76	2,61	2,67	4,0	1,40
Over 1323	2,17	2,21	6,9	1,76	2,10	2,25	1,5	1,40

*Here and in Table 2, y_e and y_t are the experimental and theoretical values of the distance from the weld center to the edge of the given temperature region, while t_h is the time for which the middle of the given region was in the given temperature range, and 1/2 h is the weld half-width.

(1-3 pulses of mean energy density 400 kJ/m^2 and duration up to 50 μsec) [4]. The maximum energy of the deuterium ions in a bunch was 10 keV.

The specimens for irradiation were cut from welds in steel sheets of thickness $(0.8\text{-}1.5)\cdot10^{-3}$ m. Welding was performed with a tungsten electrode with direct polarity in argon at a rate of $(4\text{-}6)\cdot10^{-3}$ m/sec. The specimens irradiated in the mass monochromator were of size $10 \times 10 \times 10^{-3}$ m. The irradiated area was a spot of diameter not more than $5\cdot10^{-3}$ m and covered half of the weld and a small part of the surrounding zone. The specimens of size $8 \times 5 \times 10^{-3}$ m irradiated on the ILU-3 were placed in a cassette and irradiated by a beam scanning over the area, which provided identical irradiation conditions for the surface of the weld and the surrounding material as well as identical irradiation for the different steels.

Track autoradiography was used to examine the distribution of the implanted helium and the redistribution during intermediate annealing. The method is based on the reaction $^3He(n, p)^3H$ and has a sensitivity in determining ^3He of 10^{18} atoms/m^2 when one uses CN-85 cellulose nitrate track detectors [5]. The replica method was used with an ÉMV-100L transmission electron microscope to obtain a resolution in the helium distribution of approximately 0.1 μm. The microstructure and microhardness were examined correspondingly with Neofot-21 and PMT-3 instruments, while the surface topography was examined with an RÉM-200 scanning electron microscope with a step of $(0.2\text{-}0.5)\cdot10^{-3}$ m. The erosion coefficients, the blister density, and the mean and maximum blister sizes were calculated by a standard method [6].

The sizes of the temperature regions y near the welded joints were calculated from the following equation [7]:

$$T(y) = \frac{0{,}484q}{2v\rho C_p \delta y}\left(1 - \frac{ay^2}{\lambda\delta}\right), \quad (1)$$

where T(y) is the function for the temperature propagation perpendicular to the weld line, $q = 0.24\ \eta vI$ is the effective arc thermal power ($\eta = 0.7\text{-}0.85$), v is welding speed, ρ is density, C_p is specific heat, δ is plate thickness, α is the heat-transfer coefficient, and λ is the thermal conductivity. One specifies a critical temperature for the given material in order to calculate the distances from the center of the weld for typical temperature regions. The following formula [7] defines the time for which any region near the weld is heated above a temperature T(y):

$$t_h = f\frac{(q/v\delta)^2}{\lambda C_p \rho\,[T_{max} - T(y)]}, \quad (2)$$

where f is a coefficient given by nomograms. The temperature conditions were deduced from the properties of the materials. For example, three heating ranges were selected for ferrite steels [8, 9]: above 1073°K, where there is accentuated gain growth; 1073-773°K, the region of high-temperature tempering and residual tensile-stress fields; and below 773°K, the region of low-temperature tempering and thermal hardening. Four regions have been selected for austenite steels [9, 10]: above 1323°K, the region of accentuated grain growth and of partial $\gamma \rightarrow \alpha$ transformation; 1323-1173°K, the region of initial accelerated austenite grain growth; 1173-773°K, the region of residual tensile stresses and high-temperature tempering; and below 773°K, the region of low-temperature tempering and thermal hardening.

TABLE 2. Experimental and Theoretical Parameters of Welded Joints in Ferritic Steels

Temperature °K	Kh13M2S2				Kh13M2Yu2				Kh13M2S1Yu + 1.5% TiO_2			
	$y_e \cdot 10^{-3}$, m	$y_t \cdot 10^{-3}$, m	t_h, sec	$1/2h \cdot 10^{-3}$, m	$y_e \cdot 10^{-3}$, m	$y_t \cdot 10^{-3}$, m	t_h, sec	$1/2h \cdot 10^{-3}$, m	$y_e \cdot 10^{-3}$ m	$y_t \cdot 10^{-3}$, m	t_h sec	$1/2h \cdot 10^{-3}$, m
773-1073	—	3,85	3,6	1,75	—	3,73	3,6	1,63	—	3,55	4,2	1,90
Over 1073	2,81	2,81	0,9	1,75	2,65	2,69	0,9	1,63	2,71	2,98	1,7	1,90

Results. Figure 1 gives typical microstructure photographs, while Fig. 2 gives microhardness data for different parts of the weld. Tables 1 and 2 give the sizes of the thermally and mechanically affected regions together with the heating times, which have been derived from the surface isotherms for the single passage of a line heat source over an infinitely thin plate with heat transfer to a water-cooled copper substrate and on the basis of complete temperature equalization over the thickness. Table 3 gives the blistering parameters for the welds on bombardment by helium ions of energy 20 and 40 keV. Figure 3 gives the calculated erosion coefficients. Figure 4 shows electron micrographs of the most characteristic forms of these steels after exposure to the plasma bunches. Figure 5 gives autoradiographs of the helium patterns in the steel.

The microstructure is characterized by zones differing in grain shape and size: the zone of the welding bath having long crystals elongated perpendicular to the weld line, the zone around the weld having enlarged grains, and the zone of initial microstructure.

The microstructure in the weld-bath zone is determined by the type of steel: dendritic with steels Kh13M2S2 and Kh13M2Yu2 (Fig. 1a), cellular for 12Kh18N10T and ÉI-847 (Fig. 1b), and mixed for steel Kh13M2S1Yu1 + 1.5% TiO_2 (Fig. 1c). Figure 1 shows that the microstructure of the welding bath is inhomogeneous. New crystals grow from the edge towards the center on the basis of melted grains in the zone around the weld, while the orientation and transverse dimensions are maintained. New crystals on the other hand are initiated at the center of the weld. As a result, the two crystal-growth fronts coincide, and this gives a region of crushed grains. The first form of growth is caused by thermal supercooling, and the second by concentration supercooling [8].

The zone around the weld was of the same type in all materials, but the extents and grain sizes varied. The most marked tendency to grain growth occurred in the ferritic steels Kh13M2S2 and Kh13M2Yu2. The zones around the welds were also wider in these steels. The austenitic and ferritic dispersion-hardened steels showed less extended transitions from the welded-joint structure to the initial one.

The third transitional zone following the zone around the weld does not differ in grain size and shape from the initial material, but it is characterized [8-10] by active low-temperature adsorption, residual welding stresses, and high densities for the initial finely divided carbides.

The microstructure changes correspond to changes in microhardness, which are dependent on the type and composition of the steel. The microhardness is reduced in the welding-bath zone somewhat below the initial value in the austenitic steels, whereas it is substantially increased in the region around the weld. The microhardness falls gradually to the initial level away from the edge of the weld (Fig. 2a). Ferritic steels show two microhardness peaks: in the region of the welding bath and in the region of low-temperature tempering (below 773°K). There was less variation in the microhardness, although the dependence on y was the same, in the ferritic steel containing dispersed TiO_2 particles (Fig. 2b).

The damage due to the radiation erosion alters considerably away from the center of the weld, and there are marked differences between the ferritic and austenitic steels. In the region of crystal collision and crushing, at $(0.8\text{-}1.3)\cdot10^{-3}$ m from the center of the weld, there are minima in the erosion for the austenitic steels but maxima for the ferritic steels, the exact effect being dependent on the material and sheet thickness. The erosion increases markedly for the austenitic steels but decreases for the ferritic steels at the edges of the welding bath and in the region of accelerated grain growth. The erosion coefficients and the blistering parameters for the two types of steel are dependent on the irradiation energy. For example, on bombardment with 20-keV helium ions, the ferritic steels show a pronounced advantage over the austenitic steels in the region of the welded joint. The erosion of the Kh13M2S2 steel at the peak does not exceed 0.05 atom/ion, whereas the erosion coefficient for

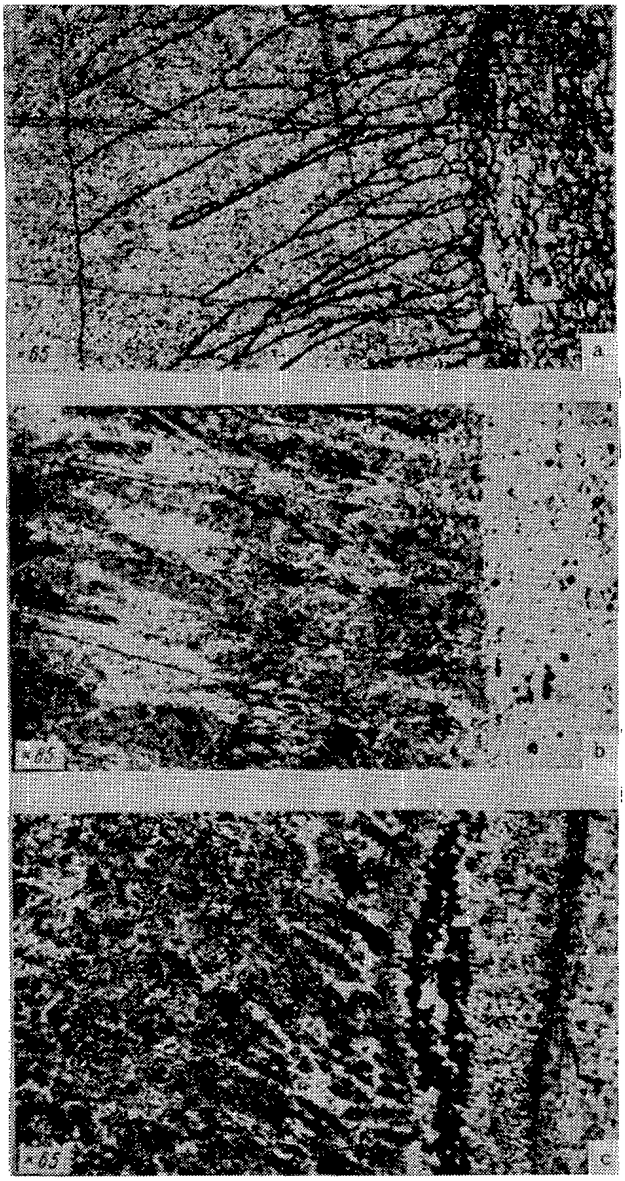

Fig. 1. Microstructures in welded joints: a) Kh13-M2S2, dendritic, ×65; b) ÉI-847, cellular, ×85; c) Kh13M2S1Yu1 + 1.5% TiO_2, mixed, ×65.

12Kh18N10T steel at the edge of the welding bath is almost 10 times larger. The mean diameter of the blisters on the ferritic steels was almost half that on the austenitic steels at the same density. An exception was represented by Kh13M2S1Yu1 + 1.5% TiO_2, on which the blisters did not burst.

The same S(y) relation applied for the 40-keV ions, but the peak amplitude for the ferritic steels increased by almost a factor 30, while the erosion coefficient for Kh13M2S2 steel attained 1.38 atoms/ion at $1.25 \cdot 10^{-3}$ m from the weld center. In all zones, the damage occurred by the flaking mechanism (Fig. 4a and b). However, the erosion of the ferritic steel containing TiO_2 was determined mainly by the blistering and the bursting of the blisters, as in the austenitic steels, and the erosion of the blisters themselves remained at the level of the steels bombarded by 20-keV ions. The average blister size (Table 3) increased in all zones, whereas the density was reduced by the increased energy. At $(4-5) \cdot 10^{-3}$ m from the weld center, the erosion coefficients for the austenitic steels fell to the initial values. In the ferritic steels, the erosion coefficient had a second maximum at $(5-6) \cdot 10^{-3}$ m, after which there was a gradual fall to the value characteristic of the steel in the initial state. An exception was represented by Kh13M2S1Yu1 + 1.5% TiO_2, for which the erosion coefficient fell to the initial level within the weld-bath zone. With a weld width of $(3-4) \cdot 10^{-3}$ m, the width of the zone of anomalous damage on the surface was about $12 \cdot 10^{-3}$ m, being dependent on

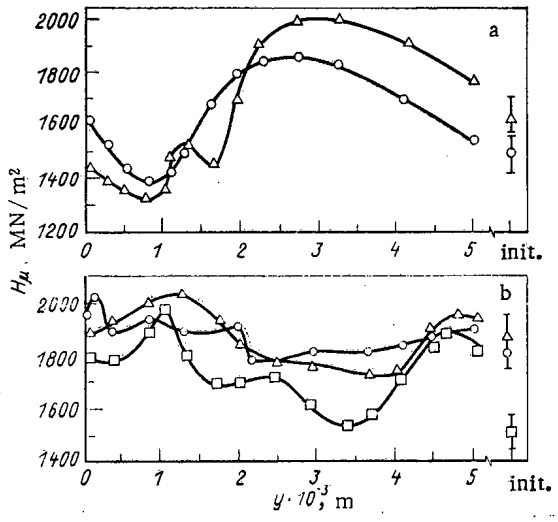

Fig. 2. Dependence of microhardness on distance from weld center for austenitic steels (a) and ferritic ones (b). a: ○) ÉI-847; Δ) 12Kh18N10T; b: ○) Kh13M2S1-Yu1 + 1.5% TiO_2; Δ) Kh13M2S2; □) Kh13M2Yu2.

TABLE 3. Welded Joint Blistering Parameters*

E, keV	$y \cdot 10^{-3}$, m	12Kh18N10T			ÉI-847			Kh13M2S2			Kh13M2Yu2			Kh13M2S1Yu1 + 1.5% TiO_2		
		d_{max}, μm	d_{av}, μm	$\rho \cdot 10^{-11}$, m^{-2}	d_{max}, μm	d_{av}, μm	$\rho \cdot 10^{-11}$, m^{-2}	d_{max}, μm	d_{av}, μm	$\rho \cdot 10^{-11}$, m^{-2}	d_{max}, μm	d_{av}, μm	$\rho \cdot 10^{-11}$, m^{-2}	d_{max}, μm	d_{av}, μm	$\rho \cdot 10^{-11}$, m^{-2}
20	0	1,97	1,23	15,4	2,01	0,79	14,3	1,30	0,81	2,2	1,02	0,82	4,3	0,83	0,45	15,4
	0,5	2,05	1,31	12,6	2,07	0,82	12,6	1,52	0,79	3,1	1,42	0,73	6,3	0,92	0,53	19,7
	1,0	2,21	1,54	10,6	2,15	0,99	8,3	1,01	0,63	8,2	1,51	0,57	13,5	1,12	0,62	12,5
	1,5	2,12	1,67	5,3	2,14	1,02	11,3	1,97	0,83	4,3	1,42	0,59	7,2	0,72	0,40	27,5
	2,0	2,72	1,60	11,5	1,96	0,89	15,3	2,01	0,88	5,7	1,75	0,82	9,4	0,32	0,12	35,2
40	0	1,85	1,14	2,0	1,93	1,33	1,7	—	—	—	—	—	—	2,12	1,29	1,7
	0,5	1,99	1,28	1,9	2,23	1,64	1,9	—	—	—	—	—	—	2,42	1,51	1,6
	1,0	2,55	1,56	1,8	2,38	1,93	1,6	—	—	—	—	—	—	2,58	1,51	2,4
	1,5	2,41	1,70	2,0	2,02	1,49	2,6	—	—	—	—	—	—	2,42	1,51	1,7
	2,0	2,34	1,56	3,2	1,64	1,19	2,7	—	—	—	—	—	—	2,27	1,36	1,5
	2,5	1,75	1,02	3,5	2,23	1,27	2,0	—	—	—	—	—	—	2,04	1,21	0,5
	3,0	2,05	1,43	2,1	2,33	1,34	1,7	—	—	—	1,99	1,44	4,6	1,57	1,06	0,7
	3,5	2,70	1,70	1,7	2,14	1,79	1,4	—	—	—	1,45	1,32	6,5	1,59	0,77	0,3
	4,0	2,73	1,82	1,5	2,45	1,83	1,4	2,20	1,77	4,3	1,52	1,21	10,7	1,62	0,91	0,3
	init.	2,14	1,51	1,6	2,16	1,29	1,3	3,92	1,96	2,7	2,57	1,76	2,7	2,39	1,47	0,5

*d_{max} and d_{av} are the maximal and averaged dimensions of a blister, while ρ is the blistering density.

the thermophysical parameters of the material, the plate thicknesses and the welding mode. The deuterium-plasma bunches produced the most damage to 12Kh18N10T steel, and the least to ferritic steel Kh13M2S1Yu1 + 1.5% TiO_2.

Discussion. These results show that the radiation erosion in welded joints varies substantially perpendicular to the weld line because of the various phase transitions and structural alterations occurring from the inhomogeneous heating during welding, the exact effect being dependent on the type and composition of the material.

In essence, welding can be considered as inhomogeneous heat treatment involving melting in the central part, heating to various temperatures, and rapid cooling around the weld, particularly in the presence of temperature and stress gradients [8]. The changes in microstructure and mechanical parameters are largely determined by the speed and energy deposition in the welding. The estimates of the heating and the sizes of the thermally affected zones correlate with the observed zones of altered microstructure (Table 1) and microhardness (Fig. 2). Changes in the erosion coefficients for the two types of steel reproduce the form of the microhardness curves (Figs. 2 and 3). The microhardness gives an integral evaluation of the

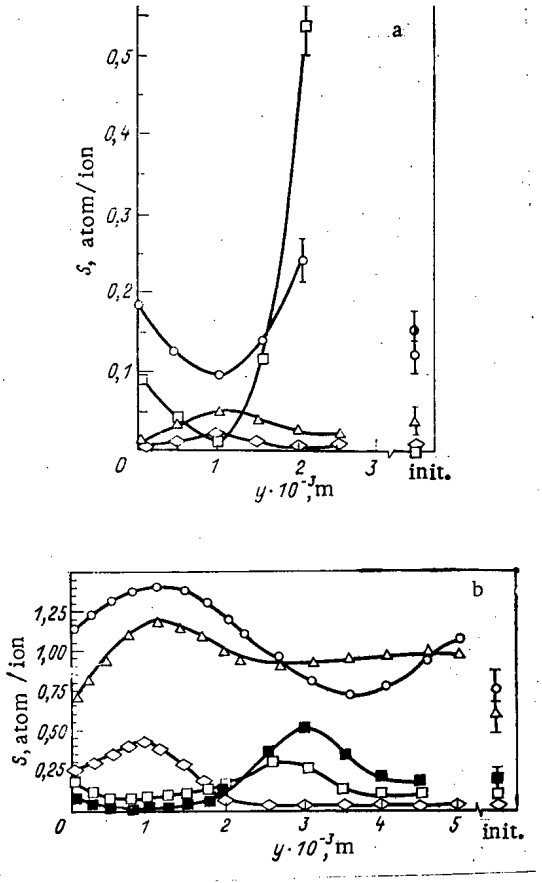

Fig. 3. Dependence of the erosion coefficient on the distance from the center of the weld at 20 keV, ion dose $1 \cdot 10^{22}$ m^{-2} (a) and at 40 keV, $1 \cdot 10^{22}$ m^{-2} (b). a: ○) powder ÉI-847; □) cast 12Kh18N10T; △) powder Kh13M-2S2; ◇) powder Kh13M2Yu2; ◑) cast ÉI-847; b: ○) powder Kh13M2S2; △) powder Kh13M2Yu2; ◇) powder Kh13M2S1Yu1 + 1.5% TiO_2; □) powder ÉI-947; ■) cast 12Kh18N10T.

microstructure as affected by the alloying-element redistribution during welding, the changes in the internal stresses, and so on. However, while there are persistent trends in microstructure over the zones, the structure of each zone is determined by the nature of the material. Therefore, the damage to the ferritic steels, which are of bcc structure, differs from that for the austenitic steels, which have fcc lattices.

In steels of the austenitic class, the S(y) and $H_\mu(y)$ curves are complicated but of similar character. The microhardness is related to the ultimate strength (yield) in a linear fashion, so one can say that the erosion in the austenitic steels increases with the strength. The relationships are complicated because the welding of an austenitic steel causes the zones in the joint to differ considerably in state of stress (residual stresses of the second kind), plastic strain produced by these stresses, carbide-phase and dislocation densities, supersaturation of the austenite with alloying elements, and grain size [10]. Considerable tensile stresses arise in the weld and around it, which exceed the yield point of the material in the region of the welding bath, but which go over gradually to compressive stresses in the zone around the weld [11], which explains why S(y) and $H_\mu(y)$ behave in the same way. These stresses may produce partial $\gamma \rightarrow \alpha$ decomposition [11], which accentuates the inhomogeneity in the internal stresses. In the welding bath, these stresses may exceed the yield point, so they will relax by plastic strain, but relaxation is more difficult in the zone around the weld. Tensile stresses exceeding σ_y reduce the erosion considerably [12], whereas at $0.4\text{-}0.5\sigma_y$ they increase the erosion by comparison with the unstressed material. This appears to be the reason for the minimum in the welding-bath zone and also for the maximum erosion around the weld. This minimum is somewhat displaced from the axis of the weld because of the structural inhomogeneity. The minimum-erosion range at 40 keV (Table 3) corresponds to the largest blisters, which may be related to the helium redistributing in the stress fields into the target [12].

Fig. 4. Electron micrographs of welded joints bombarded by deuterium plasma for steels 12Kh18N10T (a) and Kh13M2S1Yu1 + 1.5% TiO_2 (b).

The maximum erosion occurs in the zone of the welding bath in steels of the ferritic class and also in TsM-6 molybdenum-base alloy, which also has a bcc lattice [13], with some displacement towards the surrounding zone. In Kh13M2S2 and Kh13M2Yu2 steels, this maximum coincides with the zone of elongated dendritic grains, i.e., with the zone of rapid grain growth, and thus with the region of maximal residual stresses. The published data [8, 9] show that the stress pattern in a welded ferritic steel is compressive in the region of the welding bath, but tensile at the periphery and in the surrounding zone. Hardening of the solid solution by impurities and alloying elements and reduction in the plastic-strain resistance together with the internal stresses would appear to be the factors responsible for the brittle failure (flaking) and considerable surface swelling over the entire grain area in the welding-bath zone. Silicon in α-Fe favors surface damage. In that respect, the erosion in ferritic steels is extremely sensitive to the composition and decreases in the sequence Kh13M2S2—Kh13M2Yu2—Kh13M2S1Yu1 + 1.5% TiO_2. Also, Fig. 3b shows that the dependence of the erosion on the composition is more marked than that on the structure change in the weld zone. The addition of 1.5% TiO_2 to the ferritic steel substantially alters the erosion and suppresses the swelling. The steel containing TiO_2 also shows a microstructure stable under welding, which prevents the grain growth in all the weld zones.

A difference between the erosion in the ferritic steels relative to TsM-6 alloy [13] is that there is a second erosion maximum in the region of low-temperature tempering. The peak in the microhardness indicates hardening in this zone on welding (Fig. 2b). It is possible that the reason for the elevated erosion in this steel after heating to the embrittlement temperature is the accelerated aging due to the internal tensile stresses.

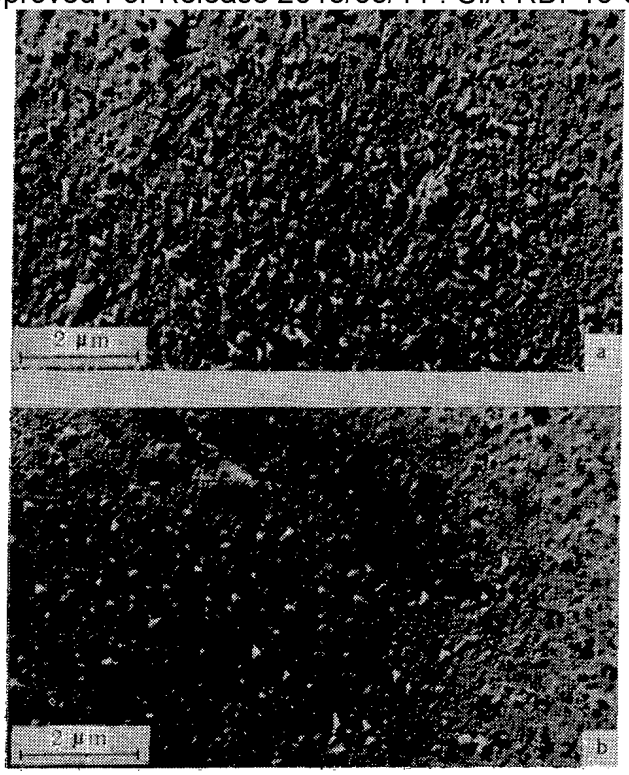

Fig. 5. Track electron-microscope autoradiography of the welding bath zone in Kh13M2S2 steel after irradiation (a); after irradiation and annealing at 1073°K for 0.5 h in argon (b).

In [13], a reason was given for the increased erosion around the center of the weld in a bcc material: the grain-boundary volume is reduced, which reduces the effect of the helium sinks, so the helium accumulates in the grain bodies. The distribution of ^3He and the redistribution on annealing show that there are no substantial changes in the trek disposition before and after annealing. There is a reduction in the trek density after annealing (Fig. 5), which is due to helium escaping from the irradiated material. The main reason for the changes in erosion coefficient in the various welded regions is that there are differences in mechanical properties and state of strain.

The erosion results for the bcc and fcc materials are such that the least occurs in Kh13M2S1Yu1 + 1.5% TiO_2, i.e., a bcc material. Similar results were obtained on irradiating welds in steels with plasma bunches. The erosion in 12Kh18N10T steel was greater than that in Kh13M2S1Yu1 + 1.5% TiO_2 because firstly there is a radiation-induced reaction of deuterium with carbon, of which there is four times as much in 12Kh18N10T steel. This gives rise to CD_4 molecules, which is confirmed by the presence of the mass M = 20 in the thermal desorption spectrum, as well as by the occurrence of large blisters (up to 10 μm). Secondly, the properties of an austenitic steel are inferior to those of a ferrite steel (thermophysical properties, heat resistance, and thermal stability), as is evident from the considerable cracking in the first and the absence of cracks at the surface of the second.

Welding in steels and alloys causes accentuated erosion near the welded joints because of changes in microstructure and redistribution of the alloying elements and internal stresses. On the whole, there is more damage to large irregular grains in zones of rapid growth.

LITERATURE CITED

1. International Tokamak Reactor, Phase One, IAEA, Vienna (1982).
2. B. P. Maksimenko, "A scheme for protecting the first wall of a fusion reactor with inertial containment," At. Tekh. Rub., No. 5, 27-31 (1980).
3. G. Kulcinski and G. Emmert, J. Nucl. Mater., 53, No. 1, 31-38 (1974).
4. N. V. Goryachev, A. M. Zhitlukhin, I. V. Ilyushin, et al., in: Proceedings of the Fifth All-Union Conference on Plasma Accelerators and Ion Injectors [in Russian], Nauka, Moscow (1982), pp. 14-15.

5. E. E. Goncharov, T. G. Kyabova, and D. A. Sorochan, "Local analysis for He by trek autoradiography from the reaction $^3He(n, p)^3H$," At. Energ., 54, No. 3, 204-205 (1983).
6. B. A. Kalin, N. M. Kirilin, A. A. Pisarev, et al., "A study of the damage to blisters at the surfaces of metals," At. Energ., 40, No. 3, 252-253 (1976).
7. L. A. Kozdoba, Methods of Solving Nonlinear Thermal-Conduction Problems [in Russian], Nauka, Moscow (1975).
8. N. N. Prokhorov, Processes in Metals on Welding [in Russian], Vol. 2, Metallurgiya, Moscow (1976).
9. Welding in Engineering [in Russian], Vol. 2, Mashinostroenie, Moscow (1978).
10. Yu. F. Yurchenko and G. I. Agapov, The Corrosion of Welded Joints in Oxidizing Media [in Russian], Mashinostroenie (1976).
11. E. A. Rumyantsev, V. F. Savel'ev, and V. M. Sagalevich, Metalloved. Term. Obrab. Met., No. 2, 39-41 (1983).
12. B. A. Kalin, S. N. Korshunov, D. M. Skorov, and V. L. Yakushin, Aspects of Nuclear Science and Engineering, Series: Physics of Radiation Damage and Radiation Metallography [in Russian], Issue 2(25) (1983), pp. 61-67.
13. B. A. Kalin, M. I. Guseva, V. L. Yakushin, D. M. Skorov, and S. N. Korshunov, "The effects of microstructure in a welded joint on erosion during ion bombardment," At. Energ., 51, No. 6, 385-387 (1981).

LEAKAGE OF TRITIUM IN A THERMONUCLEAR REACTOR

Yu. V. Martynenko and Yu. N. Yavlinskii

UDC 621.039.633

The leakage of hydrogen through metallic membranes recently has become the subject of an intensive study in connection with the transportation and storage of this rapidly diffusing gas for the users of hydrogen power generation. In a thermonuclear reactor, this problem has additional difficulties, which are associated with the leakage of tritium from the body of the reactor through the first wall, and which is undesirable because of its high cost, radioactivity, and complexity of separation from the coolant cooling the wall. Therefore, when designing a reactor, it is necessary to calculate the flow of gas through the metal (mostly stainless steel), and also the amount of tritium contained in the wall.

The calculation of the leakage of tritium is a diffusion problem, the complexity of which consists in the difficulty of determining the boundary conditions and the necessity of taking account of the temperature gradient in the wall.

The special feature of the conditions at the surface of the wall as applied to the plasma is that the tritium enters the wall in the form of accelerated ions with energy 100-1000 eV. As the depth of penetration of these ions is much less than the thickness of the wall d, then the homogeneous equations of diffusion can be solved, and the inflow of gas can be calculated in the boundary condition with $x = 0$. In some papers [1-3] the behavior of hydrogen in the surface layer was considered on the basis of models in which the union of the hydrogen atoms into stationary complexes one with another and with the lattice defects was taken into account. It would appear that this approach can be useful for understanding the processes taking place; however, the use of these models leads to complex systems of differential equations with nonlinear boundary conditions. The results of numerical solutions of these equations contain several indeterminate constants, which makes their interpretation impossible. Moreover, in the near-surface layer, equal to the depth of penetration of the ions, the concentration of tritium can attain 10^{22}-10^{23} cm^{-3}. The properties of the material in this layer (energy of dissolution of hydrogen, energy of diffusion activation, etc.) can be significantly different from the parameters of the pure material (for a discussion of these problems, see [4]).

If the flow of tritium from the plasma j is much greater than the diffusion flow from the surface $x = 0$ deep into the wall, i.e., if $j \gg D\partial C(0, t)/\partial x$ (D is the coefficient of diffusion; $C(x, t)$ is the gas concentration in the wall), then in order to solve the diffusion problem it is sufficient to specify $C(0, t)$. Experiments on the penetration of hydrogen from a gas discharge into stainless steel [1, 5, 6] have shown that a stream of gas q through the wall is a factor of several less than the incident stream j. In addition, the amount of

Translated from Atomnaya Énergiya, Vol. 58, No. 2, pp. 111-113, February, 1985. Original article submitted May 30, 1983.

 0038-531X/85/5802-0124$09.50

hydrogen implanted in the sample with a dose exceeding 10^{-4} - 10^{-3} cm^{-3} is unchanged [2]. Hence, it follows also that almost all the hydrogen implanted in the wall is released back into the volume containing the plasma, and the flow of hydrogen deep into the sample from the irradiated surface is small $q \ll j$.

It follows from the experiments of [2] that the time for the hydrogen concentration to reach saturation amounts to ~10 sec. In future thermonuclear reactors, the period of a cycle of pulses — interval — may be equal to 10^2-10^3 sec. The time of establishment of a stationary distribution of tritium in the first wall (with its thickness of 1 cm) even at a temperature of 900°K (when the coefficient of diffusion is greater than in realistic conditions) amounts to $d^2/D \sim 10^5$ sec. Therefore, variations of $C(0, t)$ with time will be expressed only at a depth much less than the thickness of the wall. Assuming that $C(0, t)$ depends only very slightly on the time, we can introduce $C_0 = C(0, t) = \text{const}$, equal to the concentration $C(0, t)$ averaged with respect to time. The boundary conditions at the wall surface when $x = d$ can be simplified considerably by assuming that $C(d) = 0$ if $C(d) \ll C_0$.

The gradient of the concentration at the rear boundary $\partial C(d)/\partial x \leqslant (C_0 - C(d))/d$, and the equation is satisfied only for $t \to \infty$ and with a constant coefficient of diffusion. When $C(d) = 0$, the error in the determination of the diffusion flow for $x = d$ is small, which means that the solution of $C(x, t)$ will be insignificantly different from the true solution.

Thus, the mathematical formulation of the problem concerning the penetration of tritium through the wall has the form

$$\frac{\partial C(x, t)}{\partial t} = \frac{\partial}{\partial x} D(x) \frac{\partial C(x, t)}{\partial x}; \tag{1}$$

$$C(x, 0) = 0; \tag{2}$$

$$C(0, t) = C_0 = \text{const}; \tag{3}$$

$$C(d, t) = 0. \tag{4}$$

The dependence of the coefficient of diffusion $D(x)$ of tritium on the coordinate is related with the presence in the wall of a temperature gradient $\nabla T \simeq (T_0 - T_1)/d$, where T_0 is the temperature at the front surface of the wall turned towards the plasma; T_1 is the temperature of the wall surface in contact with the coolant. The coefficient of diffusion in these conditions can be represented in the form

$$D(x) = D(0) \exp(-E_D/T_0 - x\nabla T), \tag{5}$$

where E_D is the energy of diffusion activation and the temperature here and in the future is measured in units of energy.

As the purpose of the present paper consists in obtaining at least an approximate but simple analytical solution of $C(x, t)$, applicable for engineering calculations, in the future in place of Eq. (5), the approximate formula

$$D(x) = D_0 e^{-\alpha x} \tag{6}$$

will be used, which for small temperature differentials $T_0 - T_1$ approximates to the function (5). If the constants D_0 and α are chosen from the condition of coincidence of Eqs. (5) and (6) at $x = 0$ and $x = d$, then

$$D_0 = D(0) \exp(-E_D/T_0), \quad \alpha = E_D \nabla T/T_0 T_1 = E_D (T_0 - T_1)/T_0 T_1 d. \tag{7}$$

In the majority of engineering calculations, the working temperature of the wall usually is assumed to be 600°K, and the temperature differential 100°K. With these values and also with $E_D = 0.6$ eV (typical value for steel) the error of the approximation by Eq. (6) is ≈10% in all. However, if the temperature differential amounts to 200°K, then the error amounts to 50%, which all the same is of considerably better accuracy than that with which the coefficients of diffusion are determined. In addition, if the temperature depends on the depth, then the limit of solubility also depends on the depth. However, the effect of this factor on the diffusion can be taken into account by a change of α, but this is unnecessary here in view of the smallness of the correction.

Equation (1) with the coefficient of diffusion determined by Eq. (6) has the exact autonomous solution

$$C(x, t) = \text{const} \exp(-e^{\alpha x}/\alpha^2 D_0 t). \tag{8}$$

This solution describes the propagation of a wave of tritium concentration in an unbounded medium from $x = -\infty$ to $x = +\infty$. We note that when $\alpha x > 1$, the wave front is steep and at a distance $x > 1/\alpha$ from the source, the concentration depends very slightly on the initial distribution, and is described by the autonomous solution (8). However, with $x < 1/\alpha$ the function $C(x, t)$ cannot reach an autonomous solution, but at this distance the coefficient of diffusion can be assumed independent of x. The solution (8) enables the time of diffusion through the wall of thickness d to be estimated

$$t_d = (e^{\alpha d} - 1)/\alpha^2 D_0. \tag{9}$$

With a large time $t >> t_d$, a stationary distribution of the concentration $C(x, \infty)$ is established, so that

$$D(x)\frac{\partial C(x, \infty)}{\partial x} = \text{const} \tag{10}$$

and $C(x, \infty)$, satisfying the boundary conditions (3) and (4), is equal to

$$C(x, \infty) = C_0[1 - (e^{\alpha x} - 1/e^{\alpha d} - 1)]. \tag{11}$$

The flow of the gas q through the wall is interesting and not the distribution with respect to depth of the tritium C(x). In the steady-state case

$$q(\infty) = D(d)|\partial C(x, \infty)/\partial x|_d = \alpha D_0 C_0/(e^{\alpha d} - 1). \tag{12}$$

The flow q for $t < t_d$ is small, and for $t > t_d$ it reaches a steady value $q(\infty)$. In order to find the exact function for q(t) it is necessary to solve Eq. (1) with the boundary conditions (3) and (4) and the initial condition (2). This solution has the form of a series of cylindrical functions, in which summing is carried out over the number of roots of a certain equation containing a combination of Bessel functions of the first and second species. The use of this solution is difficult, as summing of the series is more complex than the numerical solution of this problem.

For practical purposes, an approximate solution [4] was found, which enabled the function q(t) to be obtained and also the amount of tritium buried in the wall of the reactor. With an error not exceeding 15%, the gas flow through the wall is found by the formula

$$q(t) = \frac{\alpha D_0 C_0}{e^{\alpha d} - 1}\exp\left(\frac{-4e^{-\alpha d}}{e^{4D_0\alpha^2 t e^{-\alpha d}} - 1}\right). \tag{13}$$

It can be seen from Eq. (13) that the flow q is exponentially small with $t < e^{\alpha d}/4D_0\alpha^2$, and with the inverse inequality it rapidly (exponent into exponent) attains the steady-state value (12).

The amount of hydrogen found in the wall in unit surface $N(t) = \int_0^d C(x, t)\,dx$ also steeply attains its maximum value for $t = e^{\alpha d}/4D_0\alpha^2$. For $e^{\alpha d} >> 1$ $N(t)$

$$N(\infty) \approx (C_0/\alpha)(\alpha d - 1). \tag{14}$$

Expressions (12) and (14) for determining the flow of tritium atoms through the wall of a thermonuclear reactor and the amount of tritium buried in the wall during operation of the reactor are simple and give an accuracy sufficient for engineering calculations.

The value of C_0 must be determined in each specific case, as the concentration of mobile hydrogen x = 0 can depend on the material and temperature of the wall, energy and flux density of the incident ions. From experiments [1, 5, 6] devoted to an investigation of the leakage of hydrogen from a gas discharge through a plate of stainless steel, it follows that C_0 is proportional to the incident ion flux j, and it is independent of the temperature for $T < 650°K$, and for $T > 650°K$, $C_0 \sim \exp(-U/kT)$, where $U \approx 0.6$ eV and k is Boltzmann's constant. C_0 is independent of the energy of the incident ions in the range 100-2000 eV.

For the parameters assumed for INTOR ($T_0 = 300°C$, $T_1 = 200°C$, $j = 3.3 \cdot 10^{16}$ cm^{-2}·sec^{-1} and d = 1.3 cm), C_0 is found to be approximately equal to $2 \cdot 10^{18}$ cm^{-3}. We note that the total concentration of hydrogen close to the surface x = 0 (including the hydrogen found in the stationary complexes) can exceed C_0 by 4-5 orders. The values of the steady flux passing through the INTOR wall, the amount of tritium located in the wall in steady-state conditions, and the time of emergence of the diffusion flow into the steady-state regime are $q(\infty) = 10^{11}$ cm^{-2}·sec^{-1}, $N(\infty) \approx 2 \cdot 10^{18}$ cm^{-2}, $t_{t_d} \approx 7.5 \cdot 10^6$ sec. In view of the large spread of the experimental data, these quantities are determined with an error up to a coefficient of ~ 3.

In conclusion, the authors thank G. E. Shatalov for valuable discussions.

LITERATURE CITED

1. V. M. Sharapov, A. I. Pavlov, and A. P. Zakharov, Zh. Fiz. Khim., 56, No. 1, 5 (1982).
2. G. Standenmeier, J. Roth, R. Behrisch, et al., "Trapping of deuterium implanted in carbon and silicon; a calibration for particle energy measurements in the plasma boundary of tokamaks," J. Nucl. Mater., 84, 149-156 (1979).
3. B. Doyle, Hydrogen Trapping, Detrapping and Reemission from the Fusion First Wall, Institute of Plasma Physics, Nagoija University, IPPJ-AM-21, pp. 37-72.
4. Yu. V. Martynenko and Yu. N. Yavlinskii, Penetration of Hydrogen through the Wall of a Thermonuclear Reactor [in Russian], Preprint IAÉ-3767/8, Moscow (1983).
5. S. A. Grashin, Yu. A. Sokolov, A. E. Gorodetskii, et al., Interaction of Hydrogen with the Material of the Discharge Chamber of the Tokamak TM-4 [in Russian], Preprint IAÉ-3622/7, Moscow (1982).
6. A. I. Livshits, M. E. Notkin, Yu. M. Pustovoit, and S. V. Yakoslev, "Transmission and Absorption of Atoms and Ions of Hydrogen by 1Kh18N9T Stainless Steel," Problems of Nuclear Science and Technology, Series Thermonuclear Fusion [in Russian], Issue 2(10) (1982), p. 73.

PROVIDING RADIATION SAFETY IN HANDLING RADIOACTIVE WASTES FROM NUCLEAR POWER STATIONS

E. I. Vorob'ev, L. A. Il'in,
A. S. Belitskii, O. A. Pavlovskii,
and V. D. Stepanova

UDC 621.039.56:621.039.7

Throughout human history, the increase in energy consumption has exceeded the increase in the number of energy users [1]. As a result, the necessary level of energy production in the industrially developed countries cannot be provided by a single source, and consequently, it is necessary to develop all possible energy sources and to use various energy resources. In the next stage in power engineering (up to the year 2000), the main producers will be coal and nuclear power based on thermal-neutron reactors. The proportion of nuclear power stations in the electrical power production in the USSR will increase.

Ensuring radiation safety in handling radioactive wastes will largely determine the prospects for the development of nuclear power as a whole. This problem is being given serious attention in many countries. At present, substantial researches are being conducted in the Soviet Union on the design and implementation of technology that produces little or no waste, but at present it is hardly feasible to implement the latter at nuclear power plants. The design of these plants envisages discharges of certain amounts of radionuclides to air and water, as well as the formation of liquid and solid radioactive wastes, which have to be isolated from the biosphere. The main line of provision for radiation safety in handling and storing radioactive wastes from nuclear power stations in the USSR is to concentrate them, with a subsequent selection of storage methods that provide reliable radionuclide containment [2].

Nuclear power stations produce three forms of radioactive waste: gaseous, liquid, and solid. Before the gaseous wastes are discharged to the atmosphere, they pass through a complicated system designed to remove aerosols and iodine, and they are also stored temporarily in gas holders of radio chromatographic systems, which greatly reduce the activities from the radioactive inert gases (RIG), which are released through the stack. Table 1 gives the normalized values for gaseous discharges from nuclear power stations containing water-cooled–water-moderated (VVÉR) and high-boiling channel (RBMK) reactors derived from the actual data on air discharges at Soviet stations [1-3]. Although the actual gas-aerosol discharges from the nuclear power stations in the USSR are substantially below the set limits [4], it is important to store the gases temporarily before discharge to the atmosphere for RBMK reactors.

The contaminated water formed on operating the reactor and carrying out maintenance is purified and reused. The liquid radioactive waste consists mainly of distillation residues

Translated from Atomnaya Énergiya, Vol. 58, No. 2, pp. 113-116, February, 1985. Original article submitted May 10, 1983; revision submitted October 11, 1984.

0038-531X/85/5802-0127$09.50

TABLE 1. Activities of Gaseous Wastes from Nuclear Power Stations, Bq/GW(el)•yr

Radionuclide	VVÉR	RBMK
RIG	$1{,}6\cdot10^{14}$	$4{,}7\cdot10^{15}$
^{3}H	$7{,}4\cdot10^{12}$	$1{,}9\cdot10^{12}$
^{14}C	$3{,}0\cdot10^{11}$	$1{,}4\cdot10^{12}$
$^{89,90}Sr$	$6{,}2\cdot10^{7}$	$7{,}7\cdot10^{7}$
^{131}I	$1{,}3\cdot10^{10}$	$3{,}6\cdot10^{10}$
Mixture of long-lived nuclides*	$7{,}2\cdot10^{9}$	$1{,}7\cdot10^{10}$

*With half-lives $T_{1/2}$ > 24 h, apart from ^{3}H, ^{14}C, $^{89,90}Sr$, ^{131}I.

from evaporation equipment and slimes from filter materials. We have examined the concentrated liquid wastes from existing nuclear power stations held in stores, which has enabled us to define closely the volumes of liquid wastes, the chemical and radionuclide compositions, and the physicochemical states of the nuclides in the liquid. Table 2 gives quantitative characteristics of the liquid wastes from reactors of various types.

Nuclear power station liquid wastes are highly concentrated solutions with salt contents of 150-200 g/liter. The liquid part always has a strongly alkaline reaction (pH > 11), no matter what the type of reactor, and high oxygen demand (up to 7 mg of O_2/liter). At all nuclear stations, the chemical compositions of the medium-activity liquid wastes are dominated by various sodium salts. The content of nitrates is 30 g/liter for the VVÉR but up to 90 g/liter for the RBMK. The wastes also contain sodium oxalates and the sodium salt of EDTA, while the wastes from stations having VVÉR reactors contain sodium borates.

At Soviet and other nuclear power stations, liquid wastes are usually stored in special reinforced-concrete vessels faced with steel sheet. The specific activity in the liquid fraction is $3\cdot10^{6}$-$1.2\cdot10^{8}$ Bq/liter and is due mainly to ^{137}Cs (50-90%), ^{134}Cs, and ^{51}Cr (10-35%). The contribution from other nuclides is less than 5%. The tritium concentrations in wastes at stations with VVÉR are higher by an order of magnitude than those at ones with RBMK, and they constitute 10^{4}-10^{5} Bq/liter (a few percent). The ^{90}Sr contents do not exceed 0.1%. Also, the vessels contain dense sediments, whose activity in the main is determined by the contents of ^{106}Ru, ^{95}Zr, ^{95}Nb and activated corrosion products. When concentrates from the VVÉR reactor have been stored for long times, dense sediments are formed, which are composed of borates.

Soviet power stations recirculate the technical water, which contains or potentially may contain radionuclides. During power station operation, there may also be a certain amount of excess (unbalanced) water: from traps, from decontamination, and from laundries, which will have passed through a purification cycle, which is discharged to cooling ponds after appropriate radiation checks [5]. If the reactor operates without faults, the normalized radionuclide discharges to water are small: the tritium is about 5 and 1 TBq/GW(el)•yr for the VVÉR and RBMK, respectively, while the levels for other radionuclides are lower by 5-7 orders of magnitude [3, 5]. Such low levels of liquid radionuclide discharge to cooling ponds represent virtually no radiation hazard to the population.

The most promising way of handling liquid wastes is to convert them to the solid state, which involves binding the radionuclides to prevent leaching and the entry of them into the environment. One of most reliable methods of binding radionuclides in liquid wastes is bitumening, which is being introduced at Soviet stations.

Improvements in the existing system for handling liquid wastes must be designed to reduce the volume of primary wastes, as well as to develop and implement methods of storing waste temporarily that eliminate the formation of sparingly soluble compounds in the vessels; in addition, one should improve the design of building and installation operations to ensure that the vessels are free from leaks. The vessels should also be equipped with reliable monitoring systems, and effective ventilation should be fitted in the storage areas together with radiation shielding for working areas.

The solid radioactive wastes formed at nuclear power stations are represented by discarded equipment, used filters from ventilation systems, contaminated building rubble, cleaning

TABLE 2. Volumes of Liquid Radioactive Wastes from Nuclear Power Stations, 10^3 m^3/GW(el)•yr

Liquid waste	VVÉR	RBMK	BN
Distillation residue: with actual salt content	1,0–4,6	0,7	0,6
with design salt content (400 g/liter)	0,4–1,7	0,35	0,06
Spent ion-exchange resin	0,01–0,04	0,04	—
Spent activated charcoal	0,002–0,0025	0,003	—
Perlite	—	0,15–0,20	—

material, special clothing, etc. The volume of these wastes is dependent on the equipment design and installation, as well as on the power station operation. Table 3 gives the normalized values for the volumes of solid wastes of various specific activities as calculated from our figures obtained with the VVÉR-440, RBMK-1000, and BN-350 reactors. The data show that low-activity wastes predominate (70–80% of the total volume), with 40–60% of these constituted by organic wastes.

A serious problem in dealing with solid wastes is the low filling coefficient for the stores, which is only 0.6–0.7. This could be increased by using methods of cutting and pressing cumbersome waste items, melting plastics, and burning combustible wastes. As power station wastes represent a radiation hazard, the methods and locations for storing them must prevent the population being affected by the radiation for the time necessary for the wastes to reach a harmless state. The time required is dependent on the radiochemical composition and initial specific activity, as well as on the specific activity adopted as the threshold above which the wastes are considered as radioactive [6]. The storage times required to reach the safe state are 300–500 years for wastes with specific β activity in bitumen products containing ^{90}Sr and ^{137}Cs of $4 \cdot 10^7$–$4 \cdot 10^9$ Bq/kg (for solidified liquid wastes and spent ion-exchange resins) and for a minimal activity in solid wastes of $7.4 \cdot 10^4$ Bq/kg [4].

The localization of stored wastes is provided primarily by natural conditions (geological and hydrogeological ones). Engineering designs capable of isolating radioactive wastes are to be considered only as additional artificial barriers preventing the migration of radioactive substances. The natural conditions and the engineering measures are related one to the other: the worse the natural conditions, the more complicated and expensive it is to take the additional measures. When the conditions are less favorable, the solidified wastes must have more stable mechanical and physicochemical parameters.

At present, it is most realistic to provide reliable isolation of solidified or solid wastes in the lithosphere. Other methods of storing these wastes (for example, in the glaciers in Greenland or the Antarctic, or in space, etc.) are not at present applicable for technical, economic, and other reasons. We also do not consider the disposal of radioactive wastes in the oceans, which is practiced by certain capitalist countries but to which considerable objection is made by the world scientific community.

Migration in the lithosphere is very low [7]. Pools of oil and gas have persisted in the earth for many millions of years. One of the most mobile substances in the lithosphere is groundwater, whose complete exchange on average requires 5000 years, although the value for the active exchange zone is 330 years, while the values may be thousands or millions of years for zones of retarded exchange or stagnation [8]. Many rocks can adsorb radionuclides present in power station wastes, and consequently their rates of propagation in polluted groundwater are in many cases lower by 1–3 orders of magnitude than the speed of the water itself.

The following basic specifications must be met in order to ensure radiation safety in these methods of storing wastes:

1) It should be possible to set up a health-protection zone within which restrictions are placed on the use of the area and the subsoil on the basis of natural and health conditions, as well as the current and possible future economic activities in the region, while

TABLE 3. Volumes of Solid Radioactive Wastes from Nuclear Power Stations, $m^3/GW(el) \cdot yr$

Waste group	γ-ray dose rate at 0.1 m from the surface of wastes, mSv/h	Specific β activity, Bq/kg	VVÉR	RBMK	BN
High specific activity	>10	$3{,}7 \cdot 10^9$	20	10	20
Medium specific activity	0,3—10	$3{,}7 \cdot 10^6$—$3{,}7 \cdot 10^9$	170	150	150
Low specific activity	$3 \cdot 10^{-4}$—0,3	$7{,}4 \cdot 10^4$—$3{,}7 \cdot 10^6$	660	500	600
Total	—	—	850	660	770

no one must be permitted to live there. The width of this zone is defined in relation to the volume of the waste, the storage method, and the local conditions. It is desirable that it should not be less than 0.5-1.0 km wide from the outer boundaries of the store.

2) The radioactive contamination should not extend outside the outer boundary of the health-protection zone during any stable or emergency state in the stores and repositories throughout the period for which it is necessary to store the wastes.

3) In shallow repositories, there must be no contact between the wastes and groundwater. Also, surface waters must not be allowed to enter these repositories, while the infiltration of precipitation should be minimized.

4) The waste stores are best placed in regions of low seismic activity, where the tremor intensity is not more than six points (on a 12 point scale), in regions with stable plains but possibly with rolling relief remote from rivers and other surface bodies of water (not nearer than 500 m). Unfavorable regions for stores are mountainous ones, highly dissected areas, as well as marshy lowland areas, river floodplains, gorges, etc.

In the building of stores for solid or solidified wastes near the surface, preference should be given to regions formed by sediments of thickness not less than 20 m. The groundwater level should be at a depth of 10 m or more from the bottom of the repositories. Calculations show that the high sorption capacities of dry sediments (clays, loams, and sands) with a thickness of 10 m enable one to guarantee for many plains in the USSR that ^{90}Sr and ^{137}Cs would not enter groundwater horizons within the necessary storage periods.

The geological and hydrogeological conditions vary greatly in the USSR. Many regions are possible for ways of storing solid and solidified power station wastes. For example, in the Caspian area, in the Ural foothills, and in certain places in western and central regions of the European part of the USSR there are thick rocksalt formations suitable for underground stores. In many regions, there are also areas with thick aeration zones (over 20 m), where shallow repositories may be built.

In the design of storage locations, it is also necessary to provide safety in transporting the wastes from their sources. Experience with existing stores shows that this problem can be handled reliably and economically if the repositories are equipped with special containers and transportation, while the wastes are shipped on request from the power stations.

It is commonly assumed that improving systems for handing radioactive wastes will be expensive. However, calculations by foreign experts indicate that the costs for processing and storing power station wastes up to the year 2000 will not exceed 0.3% of the total costs of building and operating the stations [9]. We consider that as the costs are comparatively low, the optimum solution to the safe storage of power station wastes will have hardly any effect on the overall cost of building and operating these stations, although it will improve their competitiveness by comparison with other energy sources.

This evidence shows that one can provide radiation safety in handling power station wastes in two stages: the first includes extensive purification for gaseous and liquid wastes together with the collection, sorting, processing, transportation, and storage of solidified or solid wastes; the second provides reliable localization of the stored wastes for the time required for their activity to fall to a level safe for the environment and man.

Radiation safety in storing radioactive wastes is provided in the main by choosing favorable hydrogeological conditions for repositories or underground stores. The natural conditions in the USSR make it possible to solve this problem.

LITERATURE CITED

1. N. S. Babaev et al., Nuclear Power, Man, and the Environment [in Russian], Énergoizdat, Moscow (1981).
2. L. A. Buldakov et al., Radiation Safety in Nuclear Power Engineering [in Russian], Atomizdat, Moscow (1981).
3. E. I. Vorob'ev et al., At. Energ., 54, No. 4, 277 (1983).
4. Health Rules for Designing and Operating Nuclear Power Stations, SPAÉS-79 [in Russian], Énergoizdat, Moscow (1982).
5. O. A. Pavlovskii et al., in: Papers from the Conference of Comecon Member Countries on Providing Radiation Safety in Operating Nuclear Power Stations, Issue 5 [in Russian], Énergoizdat, Moscow (1984), pp. 41-47.
6. Radiation Safety Standards NRB-76 and Basic Health Rules for Operating with Radioactive Substances and Other Sources of Ionizing Radiation OSP-72/80 [in Russian], Énergoizdat, Moscow (1981).
7. A. S. Belitskii, Protecting Natural Resources in Disposing of Industrial Liquid Wastes Underground [in Russian], Nedra, Moscow (1976).
8. M. I. L'vovich and L. L. Rossolimo, in: Man, Society, and the Environment [in Russian], Mysl', Moscow (1973).
9. Nucl. Power Eng., 86, No. 2, 16 (1982).

MEASUREMENT OF THE CROSS SECTIONS OF THE REACTION $^{237}Np(n, 2n)^{236}Np$ (22.5 h) FOR NEUTRON ENERGIES IN THE RANGE 7-10 MeV*

N. V. Kornilov, V. Ya. Baryba, A. V. Balitskii,
A. P. Rudenko, B. D. Kuz'minov, O. A. Sal'nikov,
E. A. Gromova, S. S. Kovalenko, L. D. Preobrazhenskaya,
A. V. Stepanov, Yu. A. Nemilov, Yu. A. Selitskii,
B. I. Tarler, V. B. Funshtein, V. A. Yakovlev,
Sh. Darotsi, P. Raich, and I. Chikai

UDC 539.172.4

The structure of nuclear power with fast reactors incorporates a closed fuel cycle with expanded production of nuclear fuel.

The fuel cycle includes the storage, transportation, and reprocessing of spent fuel assemblies and the fabrication of new assemblies. The economic efficiency of implementation of these processes is in many ways determined by the nuclide composition of the spent fuel assemblies.

One of the inconvenient, in this sense, nuclei is ^{232}U. It cannot be separated chemically from ^{238}U and accompanies it at all stages of motion along the closed fuel cycle. The half-life of ^{232}U is about 80 years, and its decay is accompanied by a series (about 10) of decays of daughter nuclei with short half-lives and emission of "hard" γ rays ($E_\gamma \approx 2.6$ MeV) [1].

*This work was supported by the State Committee on Technical Development of the Hungarian People's Republic.

L. Koshut Institute of Experimental Physics, Debretsen, Hungarian People's Republic.
USSR. Translated from Atomnaya Énergiya, Vol. 58, No. 2, pp. 117-120, February, 1985. Original article submitted April 19, 1984.

0038-531X/85/5802-0131$09.50

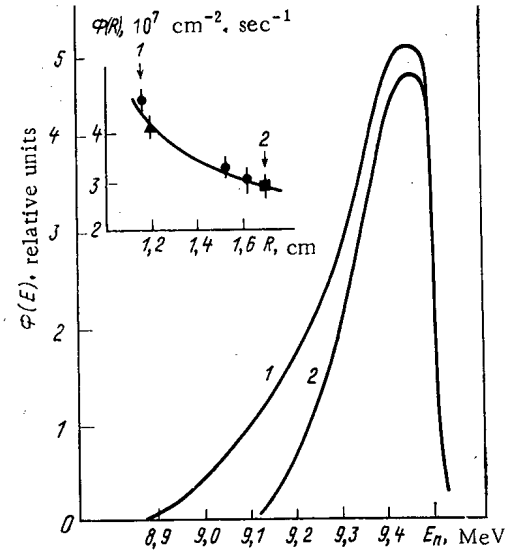

Fig. 1. Dependence of the neutron flux on the energy for two points in the assembly of the samples, denoted in the inset by the numbers 1 and 2 ($\overline{E_n}$ = 9.37 MeV): ●) $^{27}Al(n, \alpha)$; ▲) $^{238}U(n, 2n)$; ■) $^{238}U(n, f)$. The inset shows the experimental values of the neutron flux density, measured with the help of different reference reactions. The solid line shows the curve (normalized to the experiment) which was used to determine the density of the neutron flux passing through the Np sample.

Thus, with its comparatively long (compared with the duration of the fuel cycle) lifetime ^{232}U is an intense emitter of "hard" γ rays. In addition, the daughter nuclei contain gaseous radioactive products.

One of the main paths for the formation of ^{232}U nuclei in fast reactors is via the reaction (n, 2n) according to the following scheme:

$$^{238}U\,(n,\ 2n)^{237}U \xrightarrow{\beta^-} {}^{237}Np$$

$$^{237}Np\,(n,\ 2n)^{236}Np \begin{cases} \xrightarrow{e.c.} {}^{236}U \\ \xrightarrow{\beta^-} {}^{236}Pu \end{cases}$$

$$^{236}Pu \xrightarrow{\alpha} {}^{232}U.$$

The energy dependence of the cross section of the first reaction was studied in detail previously [2], and the estimated cross sections for this reaction are given in [3].

The cross section of the reaction $^{237}Np(n, 2n)$ was measured only in the neutron energy range 14-15 MeV [4-7], with the exception of the single measurement by Nishi et al. [8] at E_n = 9.6 MeV.

The reaction $^{237}Np(n, 2n)$ leads to the formation of the nuclides ^{237}Np in the short-lived s ($T_{1/2}$ = 22.5 ± 0.4 h) and long-lived l ($T_{1/2} = 1.15 \cdot 10^5$ years) states with spins 1^- and 6^-, respectively [9]. A direct experiment which would determine which of these two states is the ground state and the energy of excitation of the metastable state has not yet been performed. The latest approximate value of the excitation energy is ~50 keV [8, 9]. Each of the isomeric states accompanying β^- decay transforms into ^{236}Pu or, by capturing an electron, into ^{236}U. Forty-eight percent of the s states and 8.9% of the l-states transform into ^{236}Pu [9]. From the viewpoint of applied problems, it is most important to know the cross section of the reaction $^{237}Np(n, 2n)^{236}Np$ (s) → ^{236}Pu. This paper is concerned with the study of this process.

We measured the cross section of the reaction by a relative method using as the reference reactions $^{27}Al(n, \alpha)$, $^{238}U(n, f)$, and $^{238}U(n, 2n)$. We placed neptunium in the form of an oxide

TABLE 1. Cross Sections of the Reaction $^{237}Np(n, 2n)^{236}Np$ (s)

$E_n \pm E$, MeV	$\sigma_{2n} \pm \Delta\sigma$, mb	E_{min}, MeV	E_{max}, MeV
7,99±0,10	49±3	6,85	7,31
7,47±0,10	86±4	7,18	7,68
7,90±0,09	123±7	7,60	8,07
8,32±0,11	191±9	7,97	8,52
8,90±0,11	256±13	8,54	9,10
9,37±0,12	338±13	9,0	9,56
9,90±0,10	335±13	9,54	10,08

into thin-walled containers with a diameter of 10 mm and 2-3 mm high. The mass of the samples was 140-400 mg. We obtained neutrons with energies of 7-10 MeV on the ÉRP-10M accelerator with the help of a gaseous deuterium target in the reaction D(d, n). The input window was made of molybdenum foil (8.2 ± 0.1 mg/cm^2) and the bottom consisted of platinum 0.3 mm thick. The target was 50 mm long and the deuterium pressure was equal to ~150 kPa. Metallic foils consisting of ^{27}Al (h = 0.2 mm) and ^{238}U (h = 0.36 mm) were placed on the front and rear walls of the container with the neptunium. The entire assembly was fastened to the ionization chamber with the ^{238}U target. The distance between the end-face of the neutron source and the assembly with the samples was 10 mm. Each neptunium sample was irradiated for 80-100 h with a current of 2-3 μA. The correction to the fluctuation of the neutron flux in the course of irradiation did not exceed 10%.

We calculated the average energy of the neutrons taking into account the kinematics of the reaction D(d, n), the dependence of the cross section on the exit angle of the neutrons, the geometry of the experiment, and the losses of energy of the deuterons in the gas in the target and in the molybdenum window of the target. Typical energy distributions of the neutron flux are shown in Fig. 1 for E_n = 9.37 MeV. The values of dE/dx used in the calculation are taken from [10]. The accuracy of the calculation of the average energy of the neutrons was checked in the experiments by measuring the neutron-transmission function of the graphite block for neutron energies in the range 5-6.5 MeV. It is shown in [11], to within ±3 keV, that the total cross section for scattering of neutrons by carbon has sharp resonances at neutron energies of 5.369 and 6.293 MeV. The computed values of E_n, corresponding to the minima in the transmission function turned out to be higher than the values presented by ~24 keV. This correction was taken into account in the calculation of the average energies of the neutrons. The estimated error in the calculation of the average neutron energies is ~8 keV at $E_n \approx 6$ MeV and ~17 keV at $E_n = \sim 10$ MeV.

The average energy of the neutrons varies by ~7 and ~30 keV/mm when the sample is displaced parallel and perpendicular to the axis of the neutron beam. The corresponding uncertainties in the position of the samples are equal to ±0.2 and ±0.5 mm. Thus, the total error in the determination of the average neutron energy does not exceed +20 and −30 keV. The average values and the rms spreads in the energies are presented in Table 1. The table also shows the values of the minimum and maximum neutron energies.

We measured the activity of ^{237}U and ^{24}Na with a Ge (Li) detector, whose absolute efficiency was determined in the energy range 200-1500 keV to within 2-3%. In addition, we measured the activity of ^{24}Na with a β–γ coincidence detector. The results of the measurements of the activity with different detectors agree to within 2%. The cross sections of the reactions $^{27}Al(n, \alpha)$ and $^{238}U(n, f)$ are taken from [12], and for the reaction $^{238}U(n, 2n)$ we used the data from [3] (the method of γ measurements is described in greater detail in [2, 13]). The dependence of the neutron flux on the distance is shown in Fig. 1.

The reactions (d, n) and (d, np) on the construction materials of the deuterium target created the background neutron flux. It was measured by neutron detectors while evacuating deuterium from the gaseous target. We calculated the neutron flux from the reaction D(d, np) based on the data in [14]. With respect to the neutron flux from the main working reaction D(d, n), the background flux in the reaction $^{238}U(n, f)$ varied in the range E_d = 4-7 MeV from 1 to 14%. The detectors for the neutron flux based on the reactions $^{238}U(n, 2n)$, $^{27}A(n, \alpha)$ and $^{237}Np(n, 2n)$, however, because of the high thresholds, were virtually insensitive to the background neutrons.

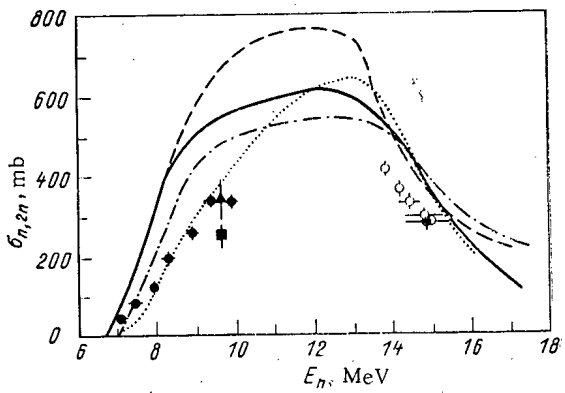

Fig. 2. Experimental cross sections of the reaction ^{237}Np(n, 2n)^{236}Np (s) (● — this work and [7] for E_n = 14.8 Mev, ▲ — [18], ■ — [8], ○ — [5]) and the computed dependences of the cross section of the reaction ^{237}Np(n, 2n)^{236}Np (s + l) on the neutron energy [——) [19], ---) [20], -·-) [21], ...) [8]].

To determine the number of ^{236}Np(s) nuclei formed under irradiation, we used the α emission of ^{236}Pu as a marker and a carrier in the chemical separation of ^{236}Pu from the irradiated target — ^{239}Pu. Prior to injecting into the neptunium a definite amount of ^{239}Pu, it was necessary to remove the poorly controlled background impurity of plutonium isotopes from the preparation. The ^{239}Pu, ^{238}Pu, and ^{236}Pu impurity in the starting neptunium preparation were equal to 10^{-2}, 10^{-4}, and 10^{-9}% of the neptunium mass, respectively. Prior to irradiation we removed plutonium from the starting preparation using the method described in [15]. As a result of the purification, the plutonium content was decreased by a factor of 10^5. The ^{236}Pu impurity in the purified neptunium did not exceed 0.1% of the amount of this nuclide formed under irradiation. The plutonium was removed from the irradiated preparation in an ion-exchange chromatographic column with AG^R 1-X2(BiO — Rad) brand resin.

The α-spectrometrical sources, prepared from the plutonium fraction by the method of evaporation in a vacuum, contained on the average 35% of all of the ^{236}Pu accumulated under irradiation. The form of the α spectra was analogous to the one we presented previously in [7]. The counting rate of alpha particles from ^{236}Pu varied from 1.26 to 3.76 sec^{-1}. We measured the mass of ^{237}Np in the irradiated preparation based on the alpha activity of ^{237}Np [$T_{1/2}$ = (2.14 ± 0.01)·10^6 years] in the aliquots extracted from this preparation [16].

We calculated the cross section of the reaction ^{237}Np(n, 2n)^{236}Np (s) from the formula

$$\sigma^s_{n,2n}(^{237}\mathrm{Np}) = A\frac{N_\alpha(^{236}\mathrm{Pu})}{N_\alpha(^{239}\mathrm{Pu})}\frac{1}{N\Phi_n\lambda W},$$

where A is the activity of ^{239}Pu introduced into the neptunium preparation as a marker; N_α (^{236}Pu)/N_α (^{239}Pu) is the ratio of the alpha emission intensities of ^{236}Pu and ^{239}Pu in the α spectrum obtained; N is the number of ^{237}Np nuclei in the target; Φ_n is the integral flux of neutrons through a unit area of the neptunium target; λ is the decay constant of ^{236}Pu [16]; W is the probability of β^- decay of ^{236}Np, equal to 0.48 ± 0.01 [17].

The results of the measurements of the cross sections of the reaction ^{237}Np(n, 2n)^{236}Np (s) and the errors of these measurements are presented in Table 1. The error in the cross section of the reaction (n, 2n) includes the error in determining the density of the neutron flux (rms error based on the data from different reference reactions, constituting 4%), the number of ^{237}Np nuclei (0.8%), the activity of ^{239}Pu introduced as a marker (~1%), the ratio N_α (^{236}Pu)/N_α (^{239}Pu) (equal to ~3%), and the probability of β^- decay (2%). Figure 2 shows, in addition to the data from this work, the experimental cross sections from other studies and the computed total cross sections of the (n, 2n) reaction. At E = 9.6 MeV the cross section measured by Nishi et al. is presented as two values taken from the figures in [8, 18]. In the range E_n = 14-15 MeV the most detailed results of measurements from [5] and the cross section measured in [7] by two methods, based on the α activity of ^{236}Pu and the γ activity of ^{238}U, are presented. The four curves in Fig. 2 are different variants of the calculation of the cross sections of the (n, 2n) reaction. All variants were constructed taking into account the experimentally obtained cross section in the region E_n = 14-15 MeV, where from

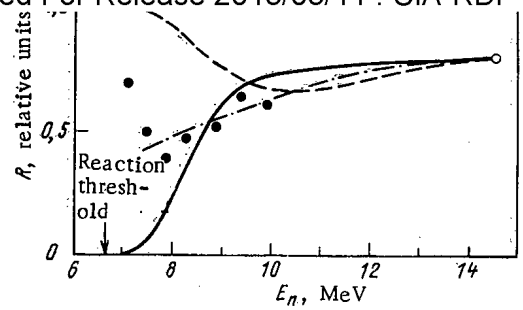

Fig. 3. Energy dependence of the ratio $R = \sigma^s_{n,2n}/\sigma_{n,2n}$: ●) the values of $\sigma^s_{n,2n}$ from this work are scaled to $\sigma_{n,2n}$ from [19]; ○) the experimental value from [22]; ——, ---) the energy dependences of R, proposed in [8], for the cases when the short-lived state is an excited or a ground state; -.-) the energy dependence of R proposed from the results of this work and based on the values of $\sigma_{n,2n}$ from [19].

an experiment on neutrons from a thermonuclear explosion it is known that the ratio of the cross sections of the reactions ^{237}Np(n, 2n)^{236}Np (l) and ^{237}Np(n, 2n)^{236}Np (s) is equal to 0.35 ± 0.05 [2]. The difference between the computed curves increases as E_n decreases. It is evident from Fig. 2 that the calculation in [8] does not agree with the measurements performed in this work, since the total cross section for the formation of the short- and long-lived isomers is even smaller than the experimental cross section for the formation of ^{236}Np (s).

The graph of the dependence of the ratio $R = \sigma^s_{n,2n}/(\sigma^s_{n,2n} + \sigma^l_{n,2n})$ on the neutron energy (Fig. 3) studied in [8] is of interest for discussing the characteristics of the ground and metastable states of ^{236}Np. Depending on whether the ^{236}Np (s) state is the ground or metastable state, the curve $R = f(E_n)$ at the threshold rises to 1 or drops to 0. The curves in [8] with the much too protracted descent and ascent near the threshold only reflect the qualitative behavior. The increase in R at E_n = 7.5 MeV, according to our work and the total cross section calculated in [19], indicates that ^{236}Np (s) is the ground state. But the accuracy of the computed cross section $\sigma_{n,2n}$ is apparently inadequate to make such an assertion in this region.

The experimental results of this work are the culmination of the first careful study of the energy dependence of the cross section for the formation of ^{236}Pu in the reaction ^{237}Np(n, 2n). Together with the results in [4, 7], for neutron energies near 14 MeV they present the possibility for describing this cross section in the entire energy interval of importance for fast reactors. The urgency of a theoretical study of the reaction examined here, taking into account the quantum characteristics of the low-lying levels, remains.

LITERATURE CITED

1. T. S. Zaritskaya, S. M. Zaritskii, A. K. Kruglov, et al., "Dependence of the formation of ^{232}U in nuclear fuel on the neutron spectrum," At. Energ., 48, No. 2, 67-70 (1980).
2. N. V. Kornilov, B. V. Zhuravlev, O. A. Sal'nikov, et al., "Measurement of the cross section of the reaction ^{238}U(n, 2n)^{237}U for neutron energies in the range 6.5-10.5 MeV," At. Energ., 49, No. 5, 283-286 (1980).
3. N. V. Kornilov, V. N. Vinogradov, E. V. Gai, et al., Problems in Atomic Science and Engineering, Series on Nuclear Constants [in Russian], No. 1 (45) (1982), p. 33.
4. J. Perkin and R. Coleman, Nucl. Energy, 14, Part A/B, 69 (1961).
5. I. Landrum, I. Nagle, and M. Lindner, Phys. Rev. C, 8, 1938 (1970).
6. K. Lindeke et al., Phys. Rev. C, 12, 1507 (1975).
7. E. A. Gromova, S. S. Kovalenko, Yu. A. Nemilov, et al., "Measurement on the cross section of the reaction ^{237}Np(n, 2n) with 14.8-MeV neutrons," At. Energ., 54, No. 2, 108-111 (1983).
8. E. Fort, H. Derrien, and J. Doat, Nucl. Data for Sci. and Technol., Antwerp (1982), p. 673.
9. M. Schmorak, Nucl. Data Sheets, 36, No. 3, 367 (1982).
10. J. Janni, Atomic Data and Nuclear Data Tables, Vol. 27, No. 2/3 (1982).
11. W. Galati, J. Brandenberger, and J. Weil, Phys. Rev., C, 5, 1508 (1972).

12. B. Magurno, ENDF-B Dosimetry File for Ver. 5, IAEA-208, Vol. 1 (1980), p. 375.
13. Sh. Darotsi, in: Neutron Physics, Proceedings of the 6th International Conference, Moscow (1984), Vol. 3, p. 191.
14. M. Drosg, in: Proceedings of the IAEA Consultant's Meeting on Neutron Source Prop., Vienna (1980), p. 201, INDC(NDS)-114/CT.
15. V. N. Ushatskii, L. S. Preobrazhenskaya, and E. S. Gugel', Radiokhimiya, 15, No. 3, 450 (1973).
16. Yu. V. Khol'nov et al., Characteristics of the Emissions from Radionuclides Used in the Economy [in Russian], Atomizdat, Moscow (1980).
17. IDDC (NDS)-108/N, Vienna, IAEA (1979).
18. M. F. Andreev and V. I. Serov, in: Neutron Physics, Proceedings of the 5th All-Union Conference, TsNIIatominform, Moscow (1980), Part 3, p. 301.
19. M. Segev and M. Caner, Ann. Nucl. Energy, 5, 239 (1978).
20. ENDF-76, UKRL-50014, Vol. 15, Part D, Rev. 1 (1978).
21. V. M. Bychkov, V. I. Plyaskin, and É. F. Toshinskaya, Problems in Atomic Science and Engineering, Series on Nuclear Constants [in Russian], No. 3(42) (1981), p. 26.
22. W. Meyers, M. Lindner, and R. Newbury, J. Inorg. Nucl. Chem., 37, 637 (1975).

CALCULATION OF THE NEUTRON YIELD FROM THICK TARGETS BOMBARDED BY ELECTRONS WITH ENERGIES UP TO 500 MeV

N. L. Emets, B. A. Shilyaev, and V. A. Yamnitskii

UDC 539.124:539.125.517.5:681.3.001.24

High-energy electron and γ-ray beams are being increasingly used in applied problems [1]. However, the presence of high-energy products of nuclear reactions (primarily neutrons) requires special attention to the shielding of the target complexes. Experimental data on the parameters of photoneutrons in the energy range of the order of hundreds of megaelectron volts are inadequate, especially data on the spectrum of photoneutrons for energies exceeding 70 MeV, where the penetrability of neutrons is maximum.

Formulation of the Problem. In connection with the obvious inadequacy of experimental data on the photocreation of neutrons, the presently most accessible method for obtaining these data is mathematical modeling using different nuclear models. Such a "mathematical experiment" will greatly decrease the amount of time required for the studies.

In this work we studied three groups of materials: light materials — oxygen and aluminum (Z = 8 and 13); materials with intermediate atomic numbers — iron and nickel (Z = 26 and 28); and heavy materials — tungsten and lead (Z = 74 and 82). Iron, nickel, and aluminum are constituents of the samples studied in applied experiments, tungsten is used as a converter for obtaining γ-ray bremmstrahlung on electron beams, and oxygen and lead were studied in connection with their possible application in neutron-radiation shielding systems. In addition, the largest amount of experimental data on photocreation of neutrons is available precisely for lead, which makes it possible to check the mathematical models used.

The energy range 34-300 MeV was chosen because of the use of the LUÉ-360 electron accelerator for purposes of simulation, while the range of target thicknesses studied — up to tens of radiation lengths — was determined during the course of the experiment as the thickness at which the onset of "saturation" of the secondary neutron emission in the electron energy range chosen occurs. In one case, for purposes of making a quantitative check of the mathematical model, we studied an electron beam with an energy of 1200 MeV.

In a real experiment, three different neutron sources can be used: a convertor, a target, and the burial ground for electrons and γ quanta. It is correspondingly necessary to take into account the layered structure of the target in the calculations.

Nuclear Models Used. The cascade-evaporation model of the nucleus, which is part of the IMITATOR program complex, oriented for the solution of simulation problems, is used for

Translated from Atomnaya Énergiya, Vol. 58, No. 2, pp. 120-123, February, 1985. Original article submitted February 9, 1984; revision submitted June 7, 1984.

 0038-531X/85/5802-0136$09.50

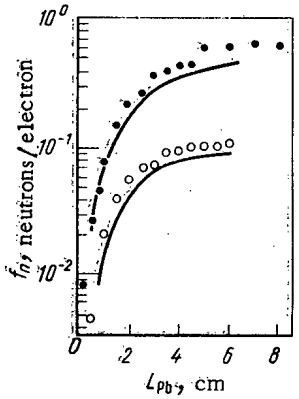

Fig. 1. Comparison of the experimental [7] (●, ○) and computed (——) data on the yield of photoneutrons from a lead target with a thickness L_{Pb} for electron energies of 230 (○) and 1200 (●) MeV.

calculations of photoneutron yields [2]. In the energy range studied, the cross sections of the electronuclear processes (for example, (e, n), (e, 2n), and similar reactions) are two orders of magnitude smaller than the cross sections of photonuclear processes, as a result of which both primary and secondary electrons arising as a result of the development of an electromagnetic cascade in the target material are taken into account only in calculating the primary defect formation, while the cross sections for the yield of the products from nuclear reactions are calculated only using photonuclear models which include γ rays from the electromagnetic cascade as primary particles.

The model of the development of the electromagnetic cascade is constructed based on the transport model, which takes into account electron bremmstrahlung and creation of electron–positron pairs by γ rays, which processes are balanced at each point of space.

The probability for the emission of a neutron from a nucleus when the nucleus absorbs one quantum of fixed energy is calculated from the cascade-evaporation model, obtained by combining the cascade [3] and the evaporation-fission models [4]. At the cascade stage of the nuclear model it is assumed that the γ ray was constrained to interact with one of the nucleons in the nucleus, transferring a definite momentum to it. Then, a cascade process, similar to the atom–atom cascade in a solid, but differing by the inclusion of some quantum limitations, develops in the nucleus.

It is assumed that the energy remaining in the nucleus after the completion of the cascade stage is expended on the excitation of the nucleus, and then the evaporation-fission model, which regards the nucleus as a drop of Fermi liquid, from which separate nucleons are evaporated, is used. The process of evaporation itself is also modeled by the Monte Carlo method as a competition between alternate emission of different particles (up to α particles inclusively) and the fission process.

The cross section for the interaction of a γ ray with a single nucleon and a quasideuteron as well as the cross section for the interaction of nucleons with one another are determined from experimental data stored in the computer memory in the form of a table together with subsequent interpolation just as the cross sections for the absorption of γ rays by the target material $\sigma_{\gamma tot}$ in regions of the quasideuteron and the 3,3 resonance; the cross sections $\sigma_{\gamma tot}$ in the region of the giant resonance are obtained by an appropriate approximation of the experimental data presented in [5].

The neutron yield from a thick target is calculated from the formula

$$f_n = \int_0^{x_{max}} dx N_0 \int_{E_n}^{E_{\gamma\,max}} P_n(E_\gamma)\,\sigma_{\gamma\,tot}(E_\gamma)\,\frac{dN_\gamma}{dE_\gamma}\,dE_\gamma,$$

where x_{max} is the thickness of the sample; N_0 is its atomic density; E_n is the emission threshold for photoneutrons; E_γ^{max} is the maximum energy of the bremmstrahlung spectrum of γ rays;

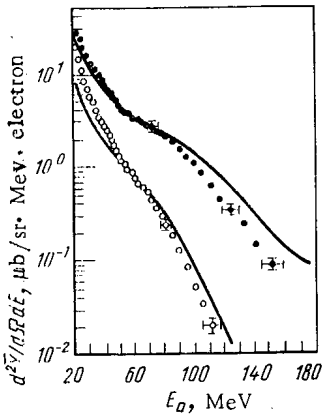

Fig. 2

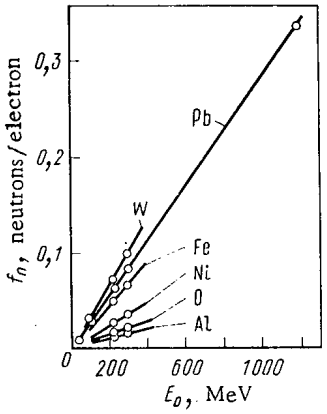

Fig. 3

Fig. 2. Comparison of experimental [8] (●, ○) and computed (——) energy distributions of photoneutrons from a lead target with a thickness of 4.3 radiation lengths irradiated at an angle of 90° by electrons with energies of 150 (○) and 266 (●) MeV ($\bar{Y}$ is the neutron output cross section averaged over the energy of the γ rays and the thickness of the sample).

Fig. 3. Dependence of the yield of photoneutrons on the energy of primary electrons E_0 with a target thickness of 10 radiation lengths.

P_n (E_γ) is the probability for emission of a neutron accompanying the capture of a γ ray with energy E_γ by the nucleus; $\sigma_{\gamma tot}$ ($E\gamma$) is the total cross section for capture of a γ ray with this energy by the nucleus; and dN_γ/dE_γ is the energy distribution of γ-rays bremmstrahlung. The angular and energy distributions are convoluted in an analogous manner, but P_n ($E\gamma$) is replaced by the value of the corresponding distribution.

Quantitative Check of the Models. Most of the experimental data on the photoneutron yield has been obtained for lead. We used these data to make a quantitative check of the models used. The earliest results [6] were obtained with electron energies of 34 MeV for targets with a thickness of $3.94X_0$ (f_n = 0.0077 neutrons per electron) and $5.93X_0$ (f_n = 0.0089 neutrons per electron), where X_0 = 0.57 cm is the radiation length in lead and f_n is the neutron yield calculated using formula (1). The computed values for this thickness are equal to 0.0077 and 0.0078 neutrons per electron, respectively. Much more detailed data are given in [7], where the dependences of the total neutron yield on the thickness of the lead target are presented for electron energies of 236 and 1200 MeV. In Fig. 1 these experimental data are compared with the corresponding calculations. The fact that the experimental values are somewhat higher than the theoretical ones can be explained by the experimental procedure: since the number of neutrons was recorded by an activation method, in order to obtain the value of the total yield it was necessary to know the energy spectrum of the neutrons, which within the framework of [7] was approximated by a single exponential, which does not entirely correspond to the data in [8]. The use of these spectra for analyzing the results obtained improves the agreement between the experimental and theoretical data.

It should be noted that the neutron energy spectra, measured by the time-of-flight method [8], also do not completely agree with the computed spectra (Fig. 2). This difference can be explained by the scattering of fast neutrons inside the target, which decreases the number of fast neutrons and correspondingly increases the number of low-energy neutrons due to (n, xn) reactions. We also compared the computational results obtained in this work with the computational data obtained abroad, for example in [9]. It was found that they agree to within 10-15%.

Thus, the data obtained on the yield and distributions of photoneutrons adequately represent the real situation. The average error, in our opinion, does not exceed 20%.

Computational Results. Figure 3 shows the energy dependences of the total yield of neutrons from the mentioned targets as a function of the energy of the primary electron beam. Here we took into account all neutrons arising in photonuclear reactions independent of their

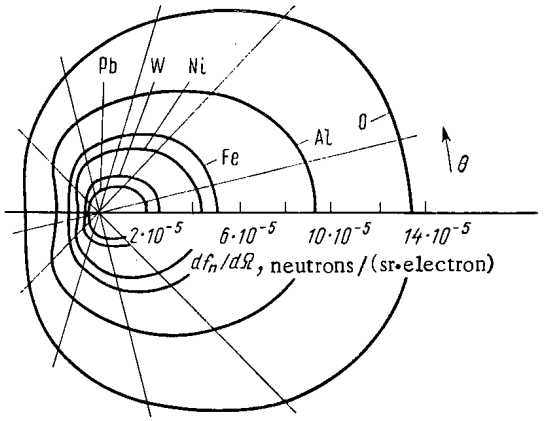

Fig. 4. Angular distribution of fast neutrons with energies exceeding 70 MeV with electron energies of 300 MeV and a target thickness of $10X_0$.

energy. It follows from Fig. 3 that these dependences are linear, as noted in [7, 9]. However, if we study the dependence of the yield of photoneutrons on the mass number with fixed electron energy, then it is easy to see that the monotonicity breaks down. Thus, the yield of neutrons from oxygen is higher than from aluminum, it is higher from iron than from nickel, and it is higher from tungsten than from lead. Svanson [9] proposed a power-law dependence for the neutron yield on the mass of the target nucleus, but this dependence is satisfied, as follows from the graphs presented by Svanson himself, only on the average with deviations of up to 50%.

In analyzing the additional data it was noted that the total neutron yield is lower for aluminum, nickel, and lead, i.e., for those elements in which the helium yield in photonuclear reactions is large. This can be explained to some extent by the presence of materials with the natural composition of the magic (^{58}Ni) and doubly magic (^{208}Pb) nuclei in the nuclides of the materials. This explanation, however, is not valid for monoisotopic aluminum and, in addition, the doubly magic nuclei constitute only part of the isotopic composition of nickel and lead. The increased yield of helium is apparently realized not only for magic but also for close to magic nuclei, rivaling at the evaporation stage the intranuclear process with neutron production. The angular distribution of the total neutron flux is practically isotropic in the absence of separate energy groups.

The group of neutrons with energies exceeding 70 MeV, which are most dangerous from the viewpoint of their biological effect and which are most difficult to shield, are of special interest. Figure 4 shows the angular distributions of neutrons in this group for the above-enumerated elements. All distributions are similar: if the intensity of the forward neutron flux along the trajectory of the electron beam is taken to be 1, then at an angle of 90° it is equal to 0.5, while the intensity of the backward neutron flux at an angle of 180° is equal to 0.25. The drop in the intensity of the high-energy component of the photoneutron flux with an increase in the mass of the target nucleus with other conditions remaining the same is very interesting (see Fig. 4).

Figure 5 shows the energy distributions of photoneutrons computed under the conditions analogous to those indicated in Fig. 4. In the 3-7-MeV range the energy distributions change places: at the lower energy the order (increasing) of the neutron energy distributions corresponds to the increase in the total neutron yield, while at higher energies it corresponds to the growth in the high-energy (cascade) group. This can be explained as follows. High-energy neutrons are prevented from leaving nuclei with a high atomic mass by the fact that any neutron which has obtained significant energy from the γ ray can interact within such a nucleus with other nucleons, thereby decreasing the maximum energy of neutrons and simultaneously increasing the number of nucleons entrained into the cascade process. At the same time, the probability of formation of highly excited nuclear fragments as a result of these processes increases. Taking into account the lower binding energy of nucleons in heavy nuclei, it is possible to explain the higher yield of all neutrons from nuclei with high atomic mass. A detailed study of the group of neutrons with energies exceeding 70 MeV shows that their yield is a nonlinear function of the energy of the primary beam (Fig. 6).

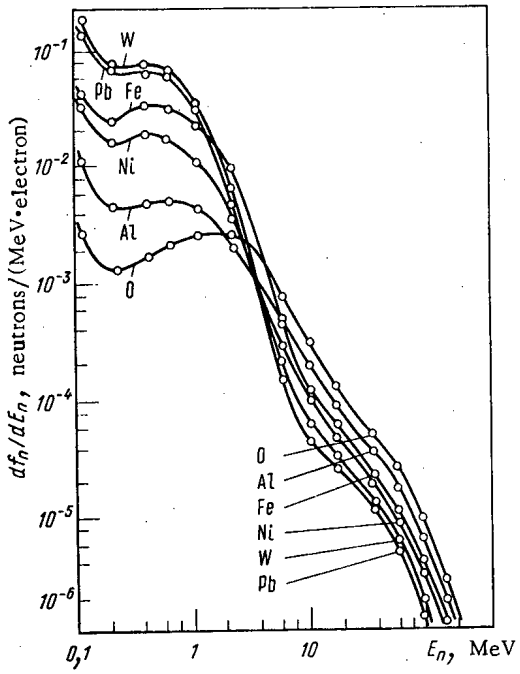

Fig. 5. Energy distributions of photoneutrons in different targets for 300 MeV electrons and a target thickness of $10X_0$.

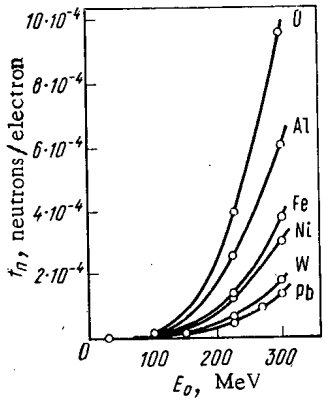

Fig. 6. Dependence of the yield of fast photoneutrons (E_n > 70 MeV) on the electron energy with a target thickness of $10X_0$.

Conclusions. A procedure was proposed for mathematical modeling of the yield of photoneutrons from thick targets, prepared from different materials, for a wide range of energies of the primary electrons. The method was tested on experimental data.

Dependences of the total yield of neutrons on the energy of the electron beam and the target material were obtained. Anomalies were noted in the yield of photoneutrons near the magic and doubly magic nuclei.

The values of the yield of fast neutrons from thick targets, their spatial distribution, and the dependence on the energy of the primary electrons and target thickness were determined. It was noted that the total yield of fast neutrons drops significantly as the atomic mass of the target material increases.

In conclusion the authors thank Yu. N. Ranyuk, who initiated and participated in the development of the model of cascade-evaporation process in a nucleus.

LITERATURE CITED

1. V. F. Zelenskii, V. A. Stratienko, V. N. Mushnikov, and N. L. Emets, "Rapid simulation of reactor damage to materials with the help of gamma ray beams," in: Proceedings of the Conference on Reactor Materials Engineering, Vol. 1, TsNIIatominform, Moscow (1978), pp. 154-193.
2. V. V. Gann, V. A. Yamnitskii, and A. M. Vaisfel'd, "IMITATOR — complex of programs for mathematical simulation of radiation damage processes," Problems in Atomic Science and Engineering. Series on the Techniques of Physical Experiments [in Russian], No. 1(5), (1980), pp. 39-43.
3. N. L. Emets, G. Ya. Lyubarskii, Yu. N. Ranyuk, and P. V. Sorokin, "The KASKAD program for simulating the interaction of high-energy photons with atomic nuclei," Preprint No. 72-37, Kharkov Physicotechnical Institute, Kharkov (1972).
4. N. L. Emets and Yu. N. Ranyuk, "Modeling of the evaporation-fissioning cascade in nuclei," Problems in Atomic Science and Engineering. Series on the Physics of Radiation Damage and Radiation Materials Engineering [in Russian], (1979), No. 1(9), pp. 31-37.
5. B. Bülow and B. Forkmen, Reprint from Technical Reports Series No. 156, Handbook on Nuclear Activation Cross Section (Photonuclear Cross Section), Vienna (1974).
6. W. Barber and W. Georg, "Neutron yields from targets bombarded by electrons," Phys. Rev., 116, 1551 (1959).
7. V. I. Noga, Yu. N. Ranyuk, Yu. N. Telegin, and P. V. Sorokin, "Neutron yield from a thick lead target bombarded by high-energy electrons," Preprint No. 78-34, Kharkov Physicotechnical Institute (1978).
8. H. Von Eyss and G. Lührs, "Photoproduction of high-energy neutrons in thick targets by electrons with energy from 150 to 270 MeV," Z. Phys., 262, No. 393, 419 (1973).
9. W. Svanson, "Calculation of neutron yields released by electrons incided on selected materials," SLAC-PUB-2042, November (1977) (A).

EVALUATION OF THE CHARACTERISTICS OF THE EMISSION OF SECONDARY ELECTRONS FROM A METAL BOMBARDED BY PHOTONS WITH ENERGIES IN THE RANGE 0.05-1.0 MeV

M. L. Gol'din and V. D. Tkachenko

UDC 539.12.04

In a number of problems of applied nuclear physics it is necessary to calculate the energy and number of secondary electrons knocked out by photon radiation from metallic single- and multilayered targets in the energy range E_0 = 0.05-1.0 MeV. Let us assume that a beam of photons with an initial energy of E_0 is incident on a homogeneous metallic plate with a thickness d at an angle θ_0 to the normal. For the range E_0 studied, Compton scattering and photoelectric absorption must be taken into account. In the first case we shall study in detail the forward scattering of photons with the formation of comparatively slow electrons and back-scattering with the formation of fast electrons. In the second case we shall study the forward and backscattering of photoelectrons. For each of the four groups of electrons, taking into account the available data on their transmission and reflection, we shall find the quantum yield in the forward and backward directions, as well as the average energy. Then, in a similar manner, we shall taken into account the contribution of the secondary scattered Compton photons.

1. Compton Forward-Scattering of Photons. We shall determine the linear coefficients of the Compton interaction μ_1 and scattering μ_1^s from the formulas [1]

$$\mu_1 = NZ\int_0^{\pi/2}\frac{d\sigma}{d\Omega}\,d\Omega = \pi r_0^2 NZ\{[(4+10k+8k^2+k^3)/2k^2(1+k)^2]+(k^2-2k-2)\,k^{-3}\ln(1+k)\}; \quad (1)$$

$$\mu_1^s = NZ\int_0^{\pi/2}\frac{d\sigma^s}{d\Omega}\,d\Omega = \pi r_0^2 NZ\,[k^{-3}\ln(1+k)-(6+15k+3k^2-12k^3-8k^4)/6k^2(1+k)^3], \quad (2)$$

Translated from Atomnaya Énergiya, Vol. 58, No. 2, pp. 124-127, February, 1985. Original article submitted January 9, 1983.

0038-531X/85/5802-0141$09.50

where N is the density of atoms, r_0 is the classical electron radius, $k = E_0/0.511$, and σ and σ^s are the cross sections for Compton interaction and scattering, respectively.

The average energy of the scattered photons is

$$E_1 = (\mu_1^s/\mu_1) E_0, \tag{3}$$

and the energy of the knocked-out electron is

$$T_1 = E_0 - E_1. \tag{4}$$

We find the average values of the cosines of the exit angles of the photon θ_1 and electron φ_1 from the relations

$$E_1 = E_0/[1 + k(1 - \cos\theta_1)]; \tag{5}$$

$$\operatorname{ctg}\varphi_1 = (1 + k)(1 - \cos\theta_1)/\sin\theta_1. \tag{6}$$

The average cosine of the angle between the direction of the electron velocity and the normal to the plate is

$$u_1 = \cos\theta_0 \cos\varphi_1. \tag{7}$$

We determine the quantum yield of electrons n_N^+ and also the yield with respect to energy n_E^+ from the formula [2]

$$n_{N,E}^+ = (\mu_1/\cos\theta_0) \int_0^d \exp[-\mu_{0t}(d-x)/\cos\theta_0]\ T_{N,E}(x)\, dx, \tag{8}$$

where μ_{0t} is the total coefficient of attenuation, and $T_{N,E}(x)$ is the transmission coefficient for electrons with respect to the number of particles and energy, respectively. Empirical relations for T_N and T_E were obtained in [3]:

$$T_{N,E}(x) = \exp[-\delta (x/r)^{\alpha}], \tag{9}$$

where r is the extrapolated range of the electrons, cm:

$$r_N = \frac{1+u}{2\rho}\left[\frac{107{,}2-Z}{5{,}442Z-1312{,}0} + \frac{292{,}7-Z}{4{,}163Z+561{,}3}\,T + \frac{Z-2{,}797}{63{,}86Z+587{,}5}\,T^2\right]; \tag{10}$$

$$r_E = \frac{1+u}{2\rho}\left[\frac{Z-137{,}0}{2344{,}0-7{,}625Z} + \frac{1400-Z}{37{,}32Z+3303{,}0}\,T + \frac{Z+14{,}14}{80{,}0Z+2207{,}0}\,T^2\right]; \tag{11}$$

u is the cosine of the angle between the direction of motion of the electron and the normal to the plate; ρ is the density; Z is the atomic number of the material; α and δ are empirical constants:

$$\alpha_N = 1 + \frac{5{,}5-0{,}1(3{,}4-T)^2}{Z^{0{,}398-0{,}032T}}(u-0{,}1564); \tag{12}$$

$$\alpha_E = 0{,}708 + (Z+24)(u-0{,}1564)/(0{,}93Z+13{,}7); \tag{13}$$

$$\delta_N = 2{,}59 - 0{,}0076(Z-6), \quad \text{for} \quad Z \geqslant 6; \tag{14}$$

$$\delta_E = (Z+32{,}6)/(0{,}524Z+10{,}8). \tag{15}$$

The formulas (9)-(15) are valid for energies in the range 0.4-6.0 MeV. The error of the approximation does not exceed 10% for u > 0.7 and values of x for which $T_{N,E}(x) > 0.1$. In the other cases, it is equal to 20-30%.

To use formula (9) with T < 0.4 MeV, we proceed as follows. Since α_N is virtually indepent of energy, and α_E, δ_N and δ_E do not depend on the energy, we determine the parameters α and δ from the formulas (12)-(15).

For normal incidence and T > 300 eV we find the extrapolated range from Tabat's formula [4]:

$$r_T = a_1\{[\ln(1+a_2\tau)/a_2] - a_3\tau/(1+a_4\tau^{a_5})\}/\rho, \tag{16}$$

where

$$\tau = T/0{,}511;\quad a_1 = 0{,}2335AZ^{-1{,}209};\quad a_2 = 1{,}78\cdot10^{-4}Z;$$
$$a_3 = 0{,}9891 - 3{,}01\cdot10^{-4}Z;\quad a_4 = 1{,}468 - 1{,}18\cdot10^{-2}Z;$$
$$a_5 = 1{,}232Z^{-0{,}109};$$

A is the atomic mass.

TABLE 1. Electron Yield from Targets with an Equilibrium Thickness, 10^{-3} Electrons per Photon

Z	E_0, MeV							
	0,0415		0,1		0,279		0,662	
	n^+	n^-	n^+	n^-	n^+	n^-	n^+	n^-
13	0,29	0,11	0,14	0,24	0,58	0,037	2,49	0,15
29	2,59	1,45	1,20	0,46	0,81	0,16	2,02	0,37
73	4,76	3,45	2,37	1,69	3,51	1,54	3,08	0,99

A comparison of the values of the ranges calculated from formulas (10), (11), and (16) in the energy range 0.4-0.6 MeV shows that for u = 1, $r_N = 1.15r_T$ and $r_E = 0.92r_T$. Therefore, for T < 0.4 MeV we assumed that

$$r_N = 1{,}15\,(1+u)\,r_T/2;\ r_E = 0{,}92\,(1+u)\,r_T/2. \tag{17}$$

To check the adopted assumptions, we calculate $T_N(x)$ for electron energies of 0.25 and 0.159 MeV. A comparison with Seliger's experimental data [5] shows that the error for this energy is equal to 10-20%. Taking into account the fact that the electron range is much shorter than the mean free path length of the photon, we obtain

$$n_1^+ = (\mu_1/\cos\theta_0)\exp(-\mu_{0t}d/\cos\theta_0)\,r_{ef}(T_1,\ u_1), \tag{18}$$

where

$$r_{ef} = \int_0^d \exp[-\delta\,(x/r)^\alpha]\,dx. \tag{19}$$

For d < r the integral is calculated numerically. For d > r the upper limit may be assumed to be equal to infinity. Then

$$r_{ef} = r\Gamma(1+1/\alpha)\,\delta^{-1/\alpha}, \tag{20}$$

where $\Gamma(x)$ is the γ function.

Calculating with the help of the formulas (18) and (20) the electron yield with respect to the number of particles n_{1N}^+ and with respect to energy n_{1E}^+, we find the average electron energy

$$T_1^+ = (n_{1E}^+/n_{1N}^+)\,T_1. \tag{21}$$

Electrons forming at a depth x from the front wall of the target can be knocked out backwards under two conditions: when they are reflected backwards and when they leave the target at an angle of 39° to the normal [6]. We shall examine these two cases.

Backward Reflection. The coefficient of reflection is equal to [7]

$$\eta_1 = 0{,}891\,(\eta_0/0{,}891)^{u_1}, \tag{22}$$

where

$$\begin{gathered}\eta_0 = b_1\,(1+b_2\tau^{b_3})^{-1};\\ b_1 = 0.9384\exp(-9.3088Z^{-0.6041});\\ b_2 = 0.0135+13.99Z^{-1.5415};\\ b_3 = 1.6359-5.312/Z;\\ \tau = T_1/0.511.\end{gathered} \tag{23}$$

The energy of the reflected electron [8] is

$$T_1' = T_1\,(1-c_1\tau^{c_2}-c_3\tau^{-c_4}). \tag{24}$$

Here $c_1 = 1.33Z^{-0.385}$, $c_2 = 0.066Z^{0.33}$, $c_3 = 0.048Z^{-0.35}$, $c_4 = 0.47Z^{0.122}$.

The quantum yield of the electron is

$$n_1^- = (\mu_1/\cos\theta_0)\,\eta\,(T_1,\ u_1)\,r_{ef}(T_1',\ 39°). \tag{25}$$

Their energy is

$$T_1^{-1} = (n_{1E}^{-1}/n_{1N}^{-1})\, T_1'. \tag{26}$$

2. Compton Backscattering of Photons. The linear coefficients of Compton interaction μ_2 and scattering μ_2^s are equal to

$$\mu_2 = NZ \int_{\pi/2}^{\pi} \frac{d\sigma}{d\Omega}\, d\Omega = 2\pi r_0^2 NZ \{[(1+k)/k^2][2(1+k):(1+2k) - \ln(1+2k)/k] + [\ln(1+2k)/2k] - (1+3k)/(1+2k)^2\} - \mu_1; \tag{27}$$

$$\mu_2^s = NZ \int_{\pi/2}^{\pi} \frac{d\sigma^s}{d\Omega}\, d\Omega = \pi r_0^2 NZ \{[\ln(1+2k)/k^3] + [2(1+k)(2k^2-2k-1)/k^2(1+2k)] + 8k^2/3(1+2k)\} - \mu_1^s. \tag{28}$$

The energy of the scattered photons is

$$E_2 = (\mu_2^s/\mu_2) E_0. \tag{29}$$

The energy of the electron knocked-out in the forward direction is

$$T_2 = E_0 - E_2. \tag{30}$$

We determine the forward and backward yields of the electrons as well as their energy using the new values of μ, T, u, and T' analogously by formulas (18)-(26).

3. Forward Scattering of Photoelectrons. We find the numerical value of the linear coefficient of the photoeffect from the formula

$$\mu_{0\tau} = \rho \sum_{i=0}^{3} \tau_i E_0^{-i}, \tag{31}$$

where the coefficients τ_i for different elements are presented in [9]. We assume that the energy of the electrons formed T_3 is equal to the difference of E_0 and the energy of the K shell. The angular dependence of the scattered electrons is described by Sauter's formula [10]:

$$J(\varphi) = [\sin^3\varphi/(1-\beta\cos\varphi)^4] + C[\sin^3\varphi/(1-\beta\cos\varphi)^3], \tag{32}$$

where $C = (3 - 3\sqrt{1-\beta^2} - 2\beta^2)/2\,(1-\beta^2)^{3/2}$, $\beta = v/c$.

The linear coefficient of interaction, corresponding to forward scattering, is

$$\mu_3 = \mu_{0\tau} \int_0^{\pi/2} J(\varphi)\, d\varphi \Big/ \int_0^{\pi} J(\varphi)\, d\varphi = \mu_{0\tau} (d_1^+ + Cd_2^+)/(d_1 + Cd_2). \tag{33}$$

The average cosine of the scattering angle of electrons is

$$\cos\varphi_3 = \int_0^{\pi/2} J(\varphi)\cos\varphi\, d\varphi \Big/ \int_0^{\pi/2} J(\varphi)\, d\varphi = (d_3^+ + Cd_4^+)/(d_1^+ + Cd_2^+). \tag{34}$$

Here

$$d_1 = 4/3(1-\beta^2)^2;\quad d_1^+ = (2-\beta)/3(1-\beta)^2;$$
$$d_2 = \{[2\beta/(1-\beta^2)] - \ln[(1+\beta)/(1-\beta)]\}/\beta^3;$$
$$d_2^+ = \{[(\beta^3-\beta^2+2\beta)/2(1-\beta)] + \ln(1-\beta)\}/\beta^3;$$
$$d_3 = \left\{\left[\left(\frac{10}{3}\beta^3 - 2\beta\right)/(1-\beta^2)^2\right] + \ln[(1+\beta)/(1-\beta)]\right\}/\beta^4;$$
$$d_3^+ = \{[(\beta^4 - 2\beta^3 + 9\beta^2 - 6\beta)/6(1-\beta)^2] - \ln(1-\beta)\}/\beta^4;$$
$$d_4 = \{[(6\beta - 10\beta^3 + 4\beta^5)/(1-\beta^2)^2] - 3\ln[(1+\beta)/(1-\beta)]\}/\beta^4;$$
$$d_4^+ = \{[(6\beta - 3\beta^2 - \beta^3)/2(1-\beta)] + 3\ln(1-\beta)\}/\beta^4.$$

The cosine of the angle between the direction of motion of the electron and the normal to the plate is

$$u_3 = \cos\theta_0 \cos\varphi_3. \tag{35}$$

The forward yield is

$$n_3^+ = (\mu_3/\cos\theta_0) \exp(-\mu_{0t} d/\cos\theta_0)\, r_{ef}(T_3, u_3). \tag{36}$$

TABLE 2. Yield of Electrons from a Lead Plate with Different Thicknesses, 10^{-3} Electrons per Photon

Direction of emergence	d, cm			
	0,01	0,1	0,5	0,8
n^+	3,65	3,41	2,44	1,81
n^-	1,24	1,30	1,31	1,31

The backward yield is

$$n_3^- = (\mu_3/\cos\theta_0)\,\eta\,(T_3,\ u_3)\,r_{ef}(T_3',\ 39°). \tag{37}$$

We determined the energy of the knocked-out electrons by formulas (21) and (26).

4. Photoelectrons Knocked-Out in the Backward Direction. In this case $T_4 = T_3$;

$$\mu_4 = \mu_{0\tau}\int_{\pi/2}^{\pi} J(\varphi)\,d\varphi \Big/ \int_0^{\pi} J(\varphi)\,d\varphi = \mu_{0\tau}(d_1^- + Cd_2^-)/(d_1 + Cd_2); \tag{38}$$

$$\cos\varphi_4 = \int_{\pi/2}^{\pi} J(\varphi)\cos\varphi\,d\varphi \Big/ \int_{\pi/2}^{\pi} J(\varphi)\,d\varphi = (d_3^- + Cd_4^-)/(d_1^- + Cd_2^-). \tag{39}$$

Here $d_i^- = d_i - d_i^+$ (i = 1, 2, 3, 4).

The backward yield of electrons is

$$n_4^- = (\mu_4/\cos\theta_0)\,r_{ef}(T_4,\ u_4); \tag{40}$$

and the forward yield is

$$n_4^+ = (\mu_4/\cos\theta_0)\exp(-\mu_{0t}d/\cos\theta_0)\,\eta\,(T_4,\ u_4)\ \ r_{ef}(T_4',\ 39°). \tag{41}$$

Thus, in the cases examined we took into account the contribution of electrons formed by singly scattered photons. The contribution of photons with the parameters $(E_1,\ \theta_1)$ — n_5–n_8 and $(E_2,\ \theta_2)$ — n_9–n_{12} is taken into account analogously.

For example, the primary photon at a depth x can undergo Compton backward scattering. A secondary photon at some depth y can also interact by one of the four mechanisms. If this is once again the mentioned type of scattering, then we denote the electron yields n_5^+ and n_5^- by

$$n_5^- = [\mu_1\mu_5\eta\,(T_5,\ u_5)/\cos^2\theta_0\cos\theta_1]\int_0^d dx\int_x^d T(y)\,dy. \tag{42}$$

The double integral in expression (42) cannot be solved analytically. It can be shown by numerical integration that even in the limit $d \to \infty$ it does not exceed r^2 (T'_5, 39°). Thus, the contribution of n_5^- (as well as of n_6^-, n_7^-, n_8^-, n_9^+, n_{10}^+, n_{11}^+, n_{12}^+) is negligibly small.

For i = 5, 6, and 7

$$n_i^+ = [\mu_1\mu_i/(\mu_{1t}\cos\theta_0 - \mu_{0t}\cos\theta_0\cos\theta_1)]\,[\exp(-\mu_{0t}d/\cos\theta_0) - \exp(-\mu_{1t}\,d/\cos\theta_0\cos\theta_1)]\,r_{ef}(T_i,\ u_i); \tag{43}$$

$$n_8^+ = [\mu_1\mu_8\eta\,(T_8,\ u_8)/(\mu_{1t}\cos\theta_0 - \mu_{0t}\cos\theta_0\cos\theta_1)]\,[\exp(-\mu_{0t}\,d/\cos\theta_0) - \exp(-\mu_{1t}\,d/\cos\theta_0\cos\theta_1)]\,r_{ef}(T_8',\ 39°). \tag{44}$$

For i = 9, 10, and 11

$$n_i^- = [\mu_2\mu_i/(\mu_{2t}\cos\theta_0 - \mu_{0t}\cos\theta_0\cos\theta_2)]\,\{1 - \exp[(\mu_{2t}\,d/\cos\theta_0\cos\theta_2) - \mu_{0t}\,d/\cos\theta_0]\}\,r_{ef}(T_i,\ u_i); \tag{45}$$

$$n_{12}^- = [\mu_2\mu_{12}\eta\,(T_{12},\ u_{12})/(\mu_{2t}\cos\theta_0 - \mu_{0t}\cos\theta_0\cos\theta_2)]\,\{1 - \exp[(\mu_{2t}\,d/\cos\theta_0\cos\theta_2) - \mu_{0t}\,d/\cos\theta_0]\}\,r_{ef}(T_{12}',\ 39°). \tag{46}$$

TABLE 3. Dependence of the Electron Yield on the Thickness of a Lead-Coated Copper Plate, 10^{-3} Electrons per Photon

Direction of emergence	d, cm					
	0,1	0,2	0,3	0,4	0,5	1,0
n^+	3,60	3,55	3,50	3,45	3,38	3,08
n^-	1,32	1,39	1,45	1,49	1,53	1,65

In formulas (42)-(46) μ_5, μ_6, μ_7, and μ_8 are calculated just as μ_1, μ_2, μ_3, and μ_4, but for the energy E_1; μ_{9-12} are calculated for the energy E_2; $u_i = \cos\theta_0 \cos\theta_1 |\cos\varphi_i|$ (i = 5-8);

$$u_i = \cos\theta_0 |\cos\theta_2 \cos\varphi_i| \ (i = 9 \div 12);$$

$$\mu_{0t} = \sum_{i=1}^{4} \mu_i;\ \mu_{1t} = \sum_{i=5}^{8} \mu_i;\ \mu_{2t} = \sum_{i=9}^{12} \mu_i.$$

For $d \gg 1/\mu_{0t}$ the significant contribution to the electron yield from multiply-scattered photons begins to grow. For $d \leq 1/\mu_{0t}$ this contribution is taken into account approximately by replacing μ_{1t} by $\sum_{i=6}^{8} \mu_i$, and μ_{2t} by $\sum_{i=10}^{12} \mu_i$.

The computed values of the quantum yields of electrons for targets with an equilibrium thickness with Z = 13, 29, 73 and E_0 = 662, 279, 100, 41.5 keV are presented in Table 1. A comparison with the experimental data in [11] shows that the forward yields are approximately 20% too low and the backward yields are approximately 30% too low. This disagreement can be explained as follows. In [11] all electrons with energies >50 eV are registered. In the computational scheme proposed here, electrons with energies exceeding 22 keV and 800 eV for E_0 = 0.662 and 0.0415 MeV, respectively, are included. The error of ~50% for Z = 73 and E_0 = 100 keV is explained by the closeness of E_0 to the K absorption edge. A separate inclusion of the contributions from the K and L shells decreases this error.

Table 2 shows the dependence of the quantum yield on d for Z = 82 and E_0 = 0.662 MeV. As d is increased, the electron forward yield decreases, but the backward yield increases.

The method described here can be applied to multilayer targets. As an example, Table 3 shows the results of a calculation of the electron yield from a copper plate with a thickness d, coated on both sides by a layer of lead, whose thickness is comparable to the range of electrons with maximum energy. We substituted the values of μ_i for lead and μ_{0t}, μ_{1t} and μ_{2t} for copper into the formulas for the quantum yield presented above.

We used the method presented to select the optimum parameters of the GR-10 level alarm [12].

LITERATURE CITED

1. S. V. Starodubtsev, Complete Collection of Scientific Works in Six Volumes [in Russian], Vol. 3, FAN, Tashkent (1971).
2. P. Ebert and A. Lauson, IEEE Trans. Nucl. Sci., NS-13, No. 1, 735 (1966).
3. A. F. Akkerman et al., Monte Carlo Solution of Problems of Electron Transport in Matter [in Russian], Nauka, Alma-Ata (1972).
4. T. Tabata et al., Nucl. Instrum. Method., 103, No. 1, 85 (1972).
5. H. Seliger, Phys. Rev., 100, No. 4, 1029 (1955).
6. V. F. Baranov, Dosimetry of Electron Radiation [in Russian], Atomizdat, Moscow (1974).
7. J. Kalef-Ezra et al., Nucl. Instrum. Method., 195, No. 3, 587 (1982).
8. T. Tabata et al., Jpn. J. Appl. Phys., 11, No. 8, 1220 (1972).
9. O. S. Marenkov, At. Energ., 27, No. 5, 462 (1969).
10. F. Sauter, Ann. Phys., 9, 217 (1931).
11. M. Ya. Grudskii, "Experimental study of the characteristics of secondary electrons knocked-out of matter by γ rays," Author's Abstract of Candidate's Dissertation, Physico-mathematical Sciences, V. G. Khlopin Radium Institute, Leningrad (1981).
12. M. L. Gol'din and V. K. Shestialtynov, At. Energ., 54, No. 6, 438 (1983).

CROSS SECTION OF THE ^{58}Ni(n, p) REACTION FOR NEUTRON ENERGIES OF 7-10 MeV

N. V. Kornilov, V. Ya. Baryba,
A. V. Balitskii, A. N. Rudenko,
S. Daroci, P. Raics, and Z. Papp

UDC 539.172.4

The ^{58}Ni(n, p) reaction is widely used in reactor dosimetry, a fact which explains the severe requirements imposed on the accuracy with which its cross section in the range from the threshold energy to 20 MeV must be known. In the World Request List for Nuclear Data (WRENDA) 81/82 [1], it is noted that the error must not exceed 2-5% for the entire range of neutron energies. For the energy interval from 7 to 10 MeV, in which the cross section of the ^{58}Ni(n, p) reaction reaches its maximum value, the available experimental data cannot meet these requirements. The most detailed and accurate determinations (with an error of about 5%) of the reaction cross section were made in [2] for $E \leq 10$ MeV. The data of [3, 4], obtained with lower accuracy, are about 10% higher than the results of [2]. An analogous situation is observed for different versions of the estimates. Thus, the estimates of ENDF/B IV [5] and BOSPOR [6] are about 10% higher than those of ENDF/B V [7]. These facts have prompted the present study.

The cross sections of the reaction ^{58}Ni(n, p)^{58}Co were measured by the activation method in experiments described in [8, 9]. We used the ^{27}Al(n, α), ^{238}U(n, f), and ^{238}U(n, 2n) reactions to determine the neutron flux. Foils of metallic nickel with natural isotopic composition, 10 mm in diameter and 0.1 mm thick, were irradiated together with neptunium specimens and foils used for determining the neutron flux [9]. Neutrons with energies of 7-10 MeV were obtained on the ÉGP-10M tandem generator using a gaseous deuterium target in the D(d, n) reaction. The activity of ^{58}Co ($T_{1/2}$ = 70.8 days) was determined from the yield of γ quanta with an energy of 810.8 keV when I_γ = 99.5%. The spectra of γ quanta were measured for 50-300 h after irradiation, thereby ensuring that we measured the total cross section of the ^{58}Ni(n, p)$^{58m+g}$Co reaction. The statistical error of the values of the initial neutron energy was no more than 1%. The contributions made by the background neutrons from the (d, n) reaction on the target materials and from the decomposition reaction D(d, np) to the activity of the nickel specimens did not exceed 1.7% and 2.8%, respectively. The experimental error was determined mainly from the accuracy in the measurement of the neutron flux (error $\leq$4%) and the efficiency of the Ge(Li) detector (error of 2-3%). The experimental technique is described in more detail in [8, 9].

In Fig. 1a we show the experimental data on the cross section of the ^{58}Ni(n, p) reaction obtained by various authors. The cross-section values we determined earlier [8] are in good agreement with the results of the present study. The average cross sections for the initial neutron energies 8.91, 9.37, and 9.90 MeV, as well as for other energy values, are shown in Table 1. Table 1 also shows the average neutron energy, the mean-square standard deviations of the energy and the errors in the cross section of the ^{58}Ni(n, p) reaction. The data of [3, 4], within the limits of experimental error (about 10%), agree both with the results of the present study and with those of [2]. In [3] the cross section of the ^{58}Ni(n, p) reaction was measured in relation to the ^{235}U(n, f) reaction. In Fig. 1a the results of [3] have been renormalized, taking account of the latest data (ENDF/B V) on the cross section of the ^{235}U(n, f) reaction. The results of [10] are close to the data of [2]. All of the aforementioned measurements were made by the activation method. The only exception is [4], in which the cross section was obtained by starting from an analysis of the proton spectrum.

Our data convincingly support the estimates of ENDF/B IV and BOSPOR. Thus, the average ratio of the σ values obtained in the present study to those in the BOSPOR library is 1.014 $\pm$ 0.021. The reason for the substantial difference (more than two standard deviations) between our data and the results of [2] is not clear. It should be noted that [2] yielded lower values for the cross sections of other reactions as well. In [11] we observed that the cross section

USSR. Hungarian People's Republic. Translated from Atomnaya Énergiya, Vol. 58, No. 2, pp. 128-129, February, 1985. Original article submitted February 21, 1984.

0038-531X/85/5802-0147$09.50

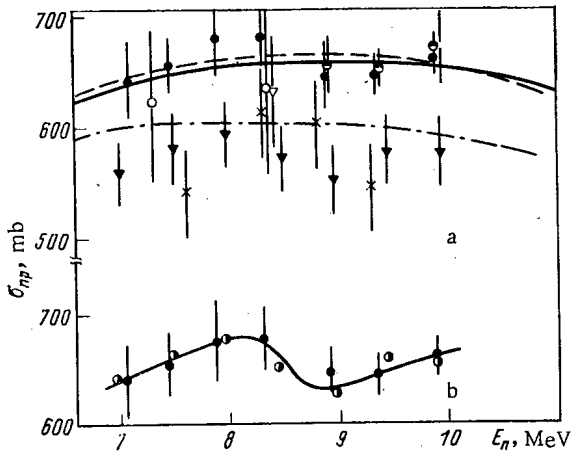

Fig. 1. Experimental data on the cross section of the ^{58}Ni(n, p) reaction (a) and comparison of the results of the present study with the renormalized results of [2] (b): ●) present study; ◓) data of [8]; ○) [3]; ▽) [4]; ×) [10]; ▼) [2]; ——) BOSPOR [6]; ---) ENDF/B IV [5]; -·-) ENDF/B V [7]; ◑) renormalized results of [2]. The solid curve in Fig. 1b was drawn by hand.

TABLE 1. Cross Sections of the ^{58}Ni(n, p) Reaction

$E_n \pm \Delta E_n$, MeV	$\sigma \pm \Delta\sigma$, mb	$E_n \pm \Delta E_n$, MeV	$\sigma \pm \Delta\sigma$, mb
7,07±0,10	641±33	8,91±0,11	649±27
7,45±0,10	655±25	9,37±0,12	646±20
7,88±0,09	677±35	9,90±0,10	664±18
8,31±0,11	679±27		

of the ^{56}Fe(n, p) reaction taken from [2] is about 10% lower, on the average, than our results and other published data.

Some cross-section values in the present study and in [2] were measured at practically the same neutron energy. The average normalization coefficient, as determined from these points, is 1.146 ± 0.021. Figure 1b shows our data together with the renormalized results of [2].

The relative behavior of the cross section reveals a structure that is common to the various experiments. It is difficult to suppose that the observed correlation is mere coincidence. Evidently there exist fluctuations in the reaction cross section. The energy resolution of the two experiments is about 100 keV (in [2] the values of the total energy dispersion are given), and therefore it is possible to obtain similar energy-dependence curves when the cross section is averaged.

On the basis of the foregoing, we can conclude that despite the appearance of new experimental data, in the 7-10 MeV neutron-energy range we have not yet attained the required accuracy in measuring the cross section of the ^{58}Ni(n, p) reaction. Solving this problem will require new experiments carried out with an error of less than 5% and high energy resolution.

LITERATURE CITED

1. WRENDA 81/82, INDC(SEC)-78/URSF. World Request List for Nuclear Data (1981).
2. D. Smith and J. Meadows, Nucl. Sci. Eng., 58, No. 3, 314 (1975); ANL/NDN-10 (1975).
3. J. Barry, Reactor Sci. Technol., 2, 467 (1962).
4. K. Debertin et al., Nucl. Phys., 70, 89 (1965).
5. B. Magurno, ENDF/B IV, Dosimetry File. BNL-NCS-50446 (1975).
6. V. M. Bychkov et al., Cross Sections of Threshold Reactions Produced by Neutrons [in Russian], Moscow (1982).

7. M. Divadeeman, BNL-NCS-51346, ENDF-294 (1979).
8. S. Daroci et al., "Measurement of the cross sections of the ^{58}Ni(n, p), ^{93}Nb(n, 2n), and ^{197}Au(n, 2n) reactions at neutron energies of 9, 9.5, and 10 MeV," Report at the Sixth All-Union Conference on Neutron Physics, Kiev (1983).
9. N. V. Kornilov et al., At. Energ., this issue, 117.
10. Yu. A. Nemirov and Yu. N. Trofimov, Nuclear-Physics Research in the USSR [in Russian], Vol. 25 (1977), p. 47.
11. P. Raics et al., in: Neutron Physics. Materials of the Fifth All-Union Conference on Neutron Physics, Vol. 1 [in Russian], TsNIIatominform, Moscow (1980), p. 236.

GASEOUS SATURATION OF THE PRIMARY CIRCUIT COOLANT IN NUCLEAR STEAM SUPPLY SYSTEMS OF WATER-MODERATED WATER-COOLED POWER REACTORS

Yu. A. Kalaida, A. P. Lastochkin, V. I. Esin, V. S. Sysoev, Yu. D. Katkov, M. G. Khor'kov, G. E. Perfil'ev, and V. A. Dobrogorskii

UDC 621.039.5.629.1

An analysis of the data published ([1, 2] and others) on nitrogen solubility in water has confirmed the ambiguity of the temperature dependence of the gas concentration. With regard to the functioning of the main components of the primary circuit system (circulating pumps, cleanup system filters, fuel assembly), the question arises on what is the maximum nitrogen concentration in the primary circuit coolant in the nuclear steam supply systems (NSSS). Although a high nitrogen concentration in the aqueous coolant (C = 2000-3000 normal cm^3 N_2 in 1 kg H_2O) can disrupt the proper functioning of the main components, until now the importance of the maximum nitrogen concentration in the heated primary circuit coolant during the operation of systems where gaseous-type compensating devices are used has not been established.

One of the reasons for this appears to be the particular complication and difficulty of performing a reliable and representative monitoring of the gas concentration in the heated coolant in the NSSS when operating. It is thought that the maximum nitrogen concentration in the primary circuit cannot be higher than the nitrogen concentration in the water of the compensators [3, 4] and that, when the NSSS are operating, an equalization of gas concentration in the water of the primary circuit and that of the volume compensators is taking place [4]. The deductions referred to are based on the results of monitoring the gas concentration in the "cooled" sections of the primary circuit, in particular downstream of the cleanup filter cooler.

The inconsistency in the determination of the gas concentrations in the cooled and heated sections of the primary circuit is obvious. In this connection the authors posed the problem of carrying out an experimental gaseous transfer and gaseous saturation study in a closed system possessing coolant parameters characteristic of an NSSS primary circuit system with a gaseous-type compensating system.

The study was carried out in a special facility equipped with a gaseous-type compensating system and also with gas concentration monitoring systems in the cooled (compensating system) and heated (primary circuit system) sections of the facility (Fig. 1).

As seen in Fig. 1, heated vessel 25, equipped with coiled heat exchanger 21, is located in electric oven 22. Vessel 25, simulating the primary circuit system, is connected to chambers 14 and 10 by a connecting pipe fitted with shutoff valves 24, 16, and 11. Vessel 25 is fitted with thermocouple 23 and chamber 14 with thermocouple 15. The volume compensator water chamber 14 is connected to expansion vessel 6 through a pipe fitted with shutoff valve 7. Expansion vessel 6 is fitted with standard manometer 3 and valves 4 and 5.

The experimental facility was equipped with standard manometers 3, 13, and 17 for pressure measurements (maximum error ±0.0025 MPa), vacuum gauges (not shown in figure, maximum

Translated from Atomnaya Énergiya, Vol. 58, No. 2, pp. 129-130, February, 1985. Original article submitted February 21, 1984; revision submitted June 1, 1984.

0038-531X/85/5802-0149$09.50

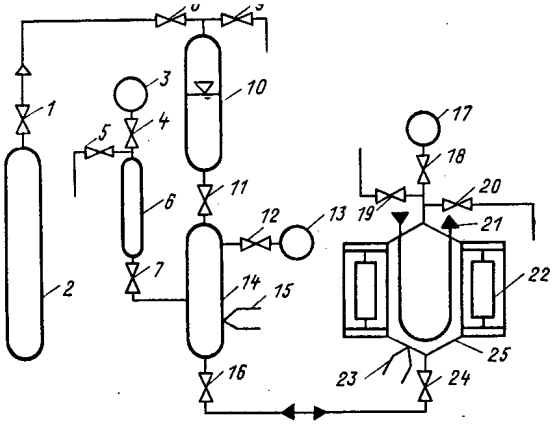

Fig. 1. Scheme of the experimental facility: 1, 4, 5, 7, 8, 9, 11, 12, 16, 18, 19, 20, 24) shutoff valves; 2) gas cylinder; 3, 13, 17) standard manometers; 6) expansion vessel; 10, 14) compensator gas and water chambers; 15, 23) thermocouples; 21) coiled heat exchanger; 22) electric oven; 25) heated vessel.

error ±0.001 MPa), differentially transforming induction transducers with secondary indicating and recording instruments (maximum error ±0.06 MPa, also not shown in Fig. 1), and thermocouples 15 and 23 for temperature measurements (maximum error ±1°C) with the same secondary instruments.

The monitoring of the gas concentration in heated vessel 25 was done by the two methods described in [1]. The percentage error in determining the gas concentration in heated vessel 25 was at most ±2-3%.

The monitoring of the gas concentrations in volume compensator water chamber 14 was carried out with the use of expansion vessel 6. In order to determine the gas concentrations in the volume compensator water, valves 11 and 16 were shut and then valve 7 was opened to connect expansion vessel 6 to volume compensator water chamber 14, following which the pressure rise in expansion vessel 6 was read from manometer 3 with the aid of valve 4.

Having read the pressure p_e, the gas concentration in the compensator water is given by the formula:

$$C_{co} = \frac{p_e}{p_0}\left(\frac{E_e}{\gamma^w_{t_{co}} E^w_{co}} \frac{T_0}{T_{co}} + C_{res}\right),$$

where E_e is the expansion vessel volume in cm^3; E^w_{co} is the volume of compensator water chamber 14 in cm^3; T_{co} and T_0 are the temperatures of the gas in the compensator and under normal conditions in °K; p_e and p_0 are the gas pressures in the expansion vessel and under normal conditions in MPa; $\gamma^w_{t_{co}}$ is the density of the water in the compensator water chamber in kg/cm^3; C_{co} is the gas concentration in the water of compensator 14 in normal cm^3 N_2 in 1 kg H_2O; and C_{res} is the residual gas concentration in the compensator water in normal cm^3 N_2 in 1 kg H_2O.

The experimental sequence for determining the maximum gaseous saturation of the heated vessel consisted of the following. Heated vessel 25 and compensator water chamber 14 were filled with water. The volume compensator gas chamber 10 was filled with nitrogen and the initial pressure, e.g., 10 MPa, adjusted. Expansion vessel 6 was evacuated and isolated from the system by the use of valve 7. Cyclic temperature changes were induced in vessel 25 by periodic connections and disconnections of the power supply to electric oven 22 followed by cooling water admissions to the coiled heat exchanger 21. The mass transfer in one heating–cooling cycle ΔG (kg/cycle) was obtained from the density difference between cooled and heated coolant in vessel 25. The temperature ranges and mass transfers in heated vessel 25 were: Δt_1 = 300-80°C, Δt_2 = 310-210°C, and Δt_3 = 270-145°C; ΔG_1 = 0.260 kg/cycle, ΔG_2 = 0.165 kg/cycle, and ΔG_3 = 0.128 kg/cycle. The temperature in vessel 6 and chamber 10 was about 20-30°C.

After every 20 heating–cooling cycles check measurements were made on the gas concentration in the water present in heated vessel 25. At the end of the experiment the gas concentration in the water chamber of volume compensator 14 was checked.

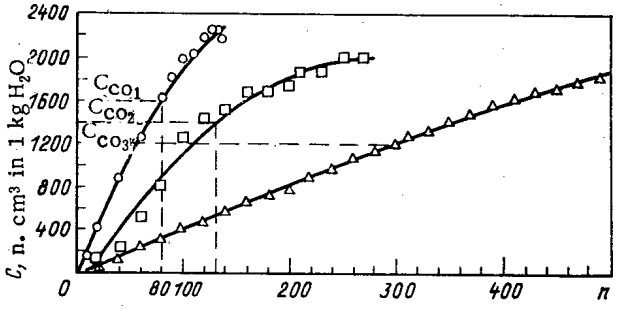

Fig. 2. Graphs showing the gas concentrations measured in heated vessel 25 versus numbers of heating–cooling cycles. ○: Δt_1 = 300-80°C, ΔG_1 = 0.260 kg per cycle; □: Δt_2 = 310-210°C, ΔG_2 = 0.165 kg per cycle; △: Δt_3 = 270-145°C, ΔG_3 = 0.128 kg per cycle.

The results of the experiment are given in Fig. 2. From this it follows that the gas concentration in water of heated vessel 25 after 80, 130, and 300 heating–cooling cycles at mass transfers ΔG_1 = 0.260 kg/cycle (Δt_1 = 300-80°C), ΔG_2 = 0.165 kg/cycle (Δt_2 = 310-210°C), and ΔG_3 = 0.128 kg/cycle (Δt_3 = 270-145°C) attained, respectively, the value of the gas concentration in compensator 14, and after 130, 260, and 480 cycles these values were C_{hv_1} = 2200 normal cm³ N_2 in 1 kg H_2O compared with C_{co_1} = 1600 normal cm³ N_2 in 1 kg H_2O, C_{hv_2} = 2000 normal cm³ N_2 in 1 kg H_2O compared with C_{co_2} = 1400 normal cm³ N_2 in 1 kg H_2O, and C_{hv_3} = 1800 normal cm³ N_2 in 1 kg H_2O compared with C_{co_3} = 1200 normal cm³ N_2 in 1 kg H_2O.

As is deduced from the "C–P" diagram in [1], concentration C = 2000 normal cm³ N_2 in 1 kg H_2O appears to be the saturation figure at 310°C and 12.0 MPa pressure.

On the basis of the above it is possible to make the following deductions. An experimental study has been carried out on gas transfer from a gaseous volume compensator to a vessel, filled with water and periodically heated then cooled, having parameters typical of the primary circuit coolant in the NSSS of a water-moderated, water-cooled power reactor.

Never before has it been proved by experiment that the working gas concentration in a periodically heated then cooled primary circuit coolant can be higher than the gas concentration in the water in the compensators.

Obviously, during the operation of the NSSS of a water-moderated, water-cooled power reactor, circumstances exist in which the working gas concentration in the volume compensator in the primary circuit coolant system may be higher than in the water in the volume compensators.

LITERATURE CITED

1. Yu. A. Kalaida, Yu. D. Katkov, A. P. Lastochkin, et al., "Nitrogen solubility in water," At. Energ., 48, No. 2, 91-94 (1980).
2. P. V. Bychkov and A. I. Kasperovich, "Gas liberation in the primary circuit of a water-moderated, water-cooled power reactor with gaseous volume compensators," At. Energ., 28, No. 2, 145 (1970).
3. V. V. Gerasimov, A. I. Kasperovich, and O. I. Martynova, Water Characteristics of Atomic Power Stations [in Russian], Atomizdat, Moscow (1976), p. 398.
4. A. I. Kasperovich, P. V. Bychkov, and V. K. Shiryaev, "Gas transfer and gas liberation in the primary circuit of a water-moderated, water-cooled power reactor," At. Energ., 36, No. 5, 387-389 (1974).

DIFFERENTIAL CROSS SECTIONS FOR THE INELASTIC SCATTERING OF 14-MeV NEUTRONS BY NIOBIUM

A. A. Lychagin, G. V. Kotel'nikova,
B. V. Devkin, V. A. Vinogradov,
A. N. Mironov, and O. A. Sal'nikov

UDC 539.173.4

The differential and integral cross sections for the inelastic scattering of neutrons by niobium were measured by the time-of-flight method on a spectrometer at the KG-0.3 accelerator. The flux of primary neutrons was obtained from the $^{3}T(d, n)^{4}He$ reaction. A detailed description of the spectrometer, the electronics, and the measurement procedure is given in [1, 2].

The spectra of neutrons inelastically scattered by niobium were measured with 2.4- and 7-m flight paths (the distance in the latter case is given for 90°). In measurements with the 2.4-m flight path the threshold was 0.1 MeV and the resolving time was 1.3 nsec/m; with the 7-m flight path the threshold was 0.5 MeV and the resolving time was less than 0.65 nsec/m. This enabled us to describe both the low- and high-energy parts of the spectra satisfactorily. The scatterers were hollow cylinders 45 mm long with an outside diameter of 45 mm; the inside diameter was 35 mm for the 2.4-m flight path, and 15 mm for the 7-m flight path. In both cases the correction for multiple scattering was calculated by the Monte Carlo method, using the program given in [3]. The principal neutron detector was an NE-218 liquid scintillator with a KhR-2041 photomultiplier. An n–γ compensating circuit [4] was used for noise and γ suppression. The neutron counting efficiency was determined by comparing the ^{252}Cf spontaneous fission neutron spectra measured with the detector in question with the Maxwell distribution having a temperature of 1.42 MeV.

The neutron flux incident on the sample was monitored by the scintillation detector (the spectrum of the neutrons emitted from the target, the time-of-flight method) and by a long counter. The absolute flux was obtained by calibrating both monitors by the method of activation of aluminum foils [2]. Thus, it was possible to obtain the scattering cross section in absolute units. In addition, the absolute values of the scattering cross section were determined by using the method of standard specimens. By taking a polyethylene specimen 1 cm in diameter and 5 cm high as a standard it was possible to obtain the (n, p) scattering cross section for hydrogen and the (n, n') scattering cross section for carbon with the nucleus excited to the 4.43 MeV level, which are known with sufficient accuracy. Each of the three methods of normalization was accurate to ~5%, and gave results differing by no more than 3% from one another.

The measurements made with the 2.4-m flight path were corrected for the effect on the monitors of the position of the sample and the relative position of the principal detector and the monitors. Since the measurements extended over a long period, particularly with the 7-m flight path, the stability of the parameters of the measuring apparatus is very important. Special measurements showed that the integral count of the principal detector of radioactive sources varied by no more than 2.5%, and the long counter by no more than 1.5% in the course of a week. The efficiency was measured at the beginning, in the middle, and at the end of the week. The average value of the efficiency over the time of the cycle of measurements was used in the processing. The differential nonlinearity did not exceed 0.1%. In the measurements with the 2.4-m flight path the scattering angle was varied by rotating the detector about the axis of the sample. For the 7-m flight path the detector was kept fixed behind a 1.4-m-thick concrete wall, and the scattering angle was varied by displacing the sample along a line coincident with the axis of the detector and collimator and lying in the same plane, which is also the axis of the deuteron beam. In this case the distance from the target to the sample, the flight path, and the angle of emission of neutrons from the target varied from angle to angle. In processing the data a correction factor was introduced into the energy spectra to take account of these changes.

Translated from Atomnaya Énergiya, Vol. 58, No. 2, pp. 131-132, February, 1985. Original article submitted March 16, 1984.

 0038-531X/85/5802-0152$09.50

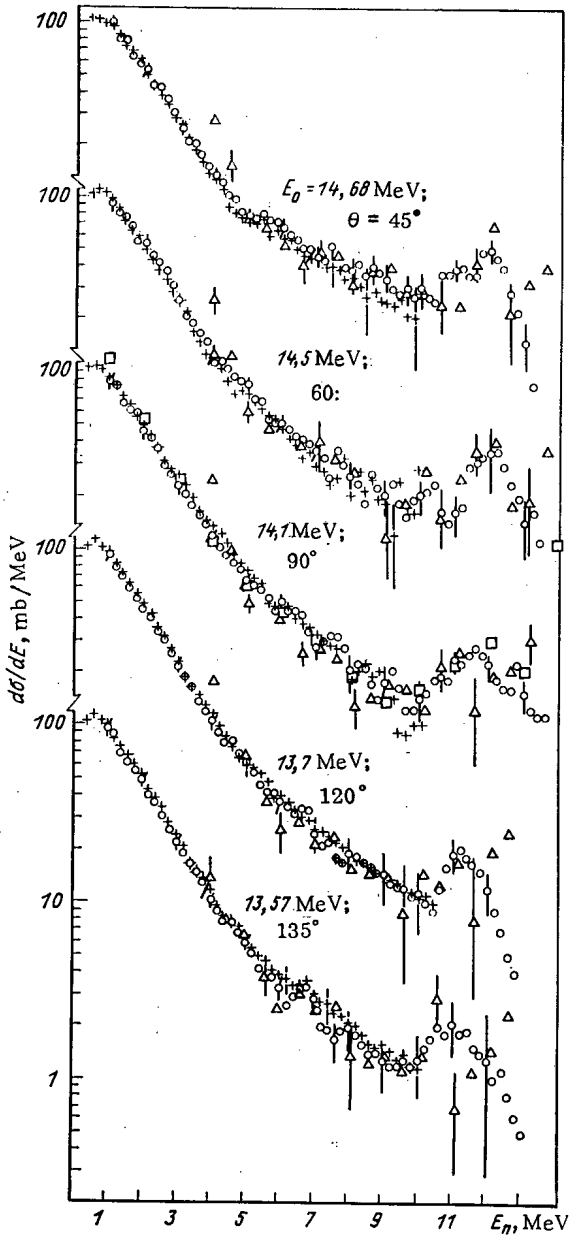

Fig. 1. Differential cross sections for the inelastic scattering of neutrons by ^{93}Nb: ō, +) our results for flight paths of 7 and 2.4 m, respectively; Δ, □) values from [6, 7], respectively.

At the same time, in this geometry the initial neutron energy varies from 14.62 MeV for 45° to 13.57 MeV for 135°. A comparison of the spectra obtained for the same angles but different flight paths, and consequently different initial energies, shows that in the range from 1 to 7-8 MeV the spectra agree within the limits of experimental error (Fig. 1). This enabled us to combine the results of the measurements with both flight paths to obtain the integral spectrum, on the one hand, with a low threshold (0.1 MeV), which is particularly important in the low-energy part of the spectrum for obtaining a more accurate value of the cross section and the neutron spectrum from the (n, 2n) reaction, and, on the other hand, with the high resolution in the high-energy part of the spectrum, which is necessary for more precise account of the contribution of the elastic interaction. In the intermediate part the combination of the spectra increased the statistical accuracy.

The integral spectrum and its analysis are given in [5]. The differential cross sections are given in the present article in the form of graphs of the angular distributions for each of the flight paths individually (Fig. 1). The values of the differential cross sections from [6, 7] are also plotted in Fig. 1. Comparison shows that the results agree for energies up to

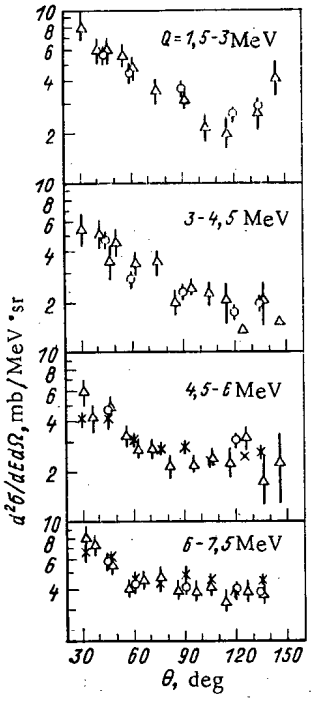

Fig. 2. Double differential cross sections for the inelastic scattering of neutrons by ^{93}Nb for four ranges of excitation energy: o, ×) our values for flight paths of 7 and 2.4 m, respectively; Δ) values from [6].

10 MeV. The greater divergence at energies above 10 MeV is apparently a result of the fact that in the spectrum in [6, 7] the peak of elastically scattered neutrons is not separated from neutrons which passed through the shield without interaction. The differential cross sections integrated over the ranges of excitation energy indicated on the graph are shown in Fig. 2. The values of the cross sections and the energies of the scattered neutrons are given in the center of mass system, but the angle and initial energy are in the laboratory system. Both the statistical and systematic errors are included in Figs. 1 and 2; a complete error analysis is given in [2]. The numerical data for all angles will be transmitted to the Center for Nuclear Data.

LITERATURE CITED

1. V. B. Anufrienko, B. V. Devkin, V. G. Demenkov, et al., "Universal fast neutron time-of-flight spectrometer," Vapr. At. Nauki i Tekh., Ser. Reaktorostr., 5(19), 34 (1977).
2. A. A. Lychagin, B. V. Devkin, V. A. Vinogradov, et al., "Measurement of spectra of inelastically scattered neutrons using a time-of-flight spectrometer with a 7-m flight path," Preprint FÉI-1406, Obninsk (1983).
3. V. I. Popov and G. V. Kotel'nikova, "Monte Carlo method of calculating the multiple scattering correction for inelastically scattered neutron spectra," Yad. Konstanty, No. 16, Atomizdat, Moscow (1974), p. 113.
4. N. N. Shchadin, "Devices for identifying particles by the shape of the signal from radiation detectors," Vapr. At. Nauki Tekh., Ser. Reaktorostr., 5 (19), 22 (1977).
5. A. A. Lychagin, V. A. Vinogradov, O. T. Grudzevich, et al., "Measurement and analysis of the spectrum of neutrons emitted by niobium when bombarded with 14-MeV neutrons," Preprin FÉI-1385, Obninsk (1983).
6. J. Kammerdiener, "Neutron spectra emitted by ^{239}Pu, ^{238}U, ^{235}U, Pb, Nb, Ni, Al, and C irradiated by 14-MeV neutrons," UCRL-51232 (1972).
7. A. Takahashi, J. Yamamoto, T. Murakami, et al., "Double differential neutron emission cross sections, numerical tables, and figures," OKTAVIAN Report A-83-01, Osaka Univ. (1983), p. 117.

INFLUENCE OF ACTIVATOR CONCENTRATION ON THE DOSIMETRIC PROPERTIES OF RADIOPHOTOLUMINESCENT GLASSES

N. Z. Andreeva, N. N. Vil'chinskaya,
A. V. Dmitryuk, A. S. Perminov,
G. T. Petrovskii, and O. Ch. Savvina

UDC 666.11.0

Despite the extensive use of radiophotoluminescent glasses for personal monitoring and intensive research in this area [1], at present no theory of radiophotoluminescence (RPL) is sufficiently complete to permit a purposeful prediction of the optimum composition of glasses, including the concentration of the activator, silver [2]. This work is devoted to the study of how the silver concentration affects the dosimetric properties of RPL glasses, with a view to possibly reducing its influence.

For our exposition it is desirable to determine some concepts used below. As the main dosimetric properties of RPL glass we consider the dose dependence of the radiophotoluminescence intensity $I = I(D)$, where I is the RPL intensity and D is the dose, and the RPL kinetics $I = I(t)$, where t is the time after the cessation of bombardment of the glass with ionizing radiation.* The indicated dependences $I = I(D, t)$ make it possible to determine some dosimetric characteristics of glasses employed in practice. Such characteristics are the sensitivity S of the glass, the operating range, the predose luminescence I_0, the "maturing" time t_m, and the fading f [3]. From the dose dependence we find the sensitivity $S = \partial I/\partial D$ of the glass to ionizing radiation, the operating range determined from the condition $S = \text{const}$, and the predose (initial, background) luminescence I_0. The predose luminescence of the unirradiated glass is characterized by the dose D_0 with which the glass should be irradiated for the luminescence intensity to double after the irradiation [4]. We note that the sensitivity is a relative quantity which is given in relation to a standard radiophotoluminescent glass.

The kinetics of RPL makes it possible to find the maturing time t_m, which is determined from the condition $\partial I/\partial t = 0$ for $t = t_m$, and the fading $f = (1/I_{max})(\partial I/\partial t) < 0$, where I_{max} is the maximum value of the RPL intensity. Thus, the RPL kinetics and the dose dependence carry exhaustive information about the dosimetric properties of RPL glasses since some auxiliary dosimetric characteristics, e.g., the weak dependence of the sensitivity of the glass on the energy of the ionizing radiation or the given sensitivity to thermal neutrons, are determined mainly by the composition of the glassy matrix and depend only insignificantly on the activator concentration.

The luminescent characteristics (luminescence intensity and spectrum) of the glasses were measured on a slightly modified SDL-1 spectrofluorometer. The differences consisted in the use of an FÉU-79 photomultiplier as the detector and an MDR-2 monochromator to separate the necessary spectral region of excitation. A DRSh-250 lamp with a stabilized light flux was used as the source of exciting light. When studying the RPL kinetics and the dose dependences we excited radiophotoluminescence with 365-nm ultraviolet radiation. Since preliminary experiments showed that photochemical degradation of the RPL centers can occur under the indicated excitation conditions and this effect depends on the exposure, we subsequently selected conditions that eliminated the obliteration of dosimetric information by the exciting light. In particular, during the kinetic measurements on the SDL-1 an electromechanical shutter synchronized with the tape transport of the recorder was used to modulate the exciting light, thus permitting automatic discrete measurement of the RPL intensity. The measuring time at each point in this case was 5 sec. In parallel the RPL intensity was recorded for a dose greater than 10^{-2} Gy by a fluorometer designed for integrated measurements of the luminescence intensity over the spectrum (for wavelengths longer than 600 nm). The basic scheme of the measurements (steady-state excitation conditions, wavelength of the exciting light)

*This definition of the kinetics is specific to RPL glasses and differs from that adopted in the spectroscopy of activated glasses and crystals.

Translated from Atomnaya Énergiya, Vol. 58, No. 2, pp. 132-135, February, 1985. Original article submitted March 26, 1984.

0038-531X/85/5802-0155$09.50

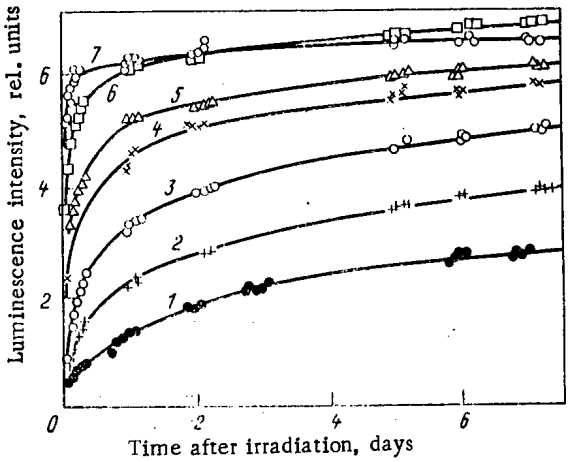

Fig. 1. Dependence of the RPL intensity on the time after irradiation for lithium aluminophosphate glasses of variable activator concentration, mole% Ag_2O: 1) 0.2; 2) 0.3; 3) 0.4; 4) 0.6; 5) 0.7; 6) 1; 7) 1.5.

was approximately the same in both cases considered but the details differed considerably. The RPL intensity was measured on the SDL-1 in a narrow spectral region (about 3 nm) at a wavelength of 600 nm, corresponding to the maximum of the luminescence spectrum. On the condition that the RPL spectrum is constant (which, as shown by control experiments, is satisfied for both the kinetic and dose dependences) the two methods of measurement give similar results. In measurements of an RPL intensity that corresponds to a dose of less than 10^{-2} Gy, we must take into account all possible causes of a decrease in the measurement accuracy owing to stray luminescence of organic impurities on the surface of the glass. The influence of the stray luminescence can be decreased by using excitation of only part of the specimen and not the entire bulk as well as by thoroughly cleaning the surface of the specimens. In the measurements on the SDL-1 the luminescing volume was 4 × 4 × 2 mm while the dimensions of the specimen were 10 × 10 × 4 mm.

To study the influence of the temperature on the dosimetric properties of RPL glasses we used a quick-response heater with a programmed thermoregulator. The temperature of the specimens was monitored with a Chromel–Alumel thermocouple and the accuracy with which the temperature of the specimen was fixed was ±5°C with a gradient not exceeding 1°C/mm. The specimens were irradiated with ^{60}Co γ rays in a line source at room temperature. The exposure dose rate varied within the limits from $0.49 \cdot 10^{-6}$ to $17.9 \cdot 10^{-6}$ A/kg. The exposure dose was calculated on the basis of certified measurements of the exposure dose rate carried out at the D. I. Mendeleev All-Union Scientific-Research Institute of Metrology. The main error in the dose rate at a 95% confidence coefficient did not exceed 7%. As the object of our investigation we chose lithium aluminophosphate glasses of variable composition with a fixed silver oxide content of 0.43 mole%.

We consider the results pertaining to lithium aluminophosphate glasses. Figure 1 shows the RPL kinetics of glasses of a variable activator concentration for an isodose irradiation of 5 Gy. The dependences presented here are not in themselves original since, as is well known, a decrease in the activator concentration leads to a longer maturing time [3]. It is seen from their example, however, that the main dosimetric characteristic of RPL glasses, viz., sensitivity, is not determined in the case under consideration because it is a function of time that does not lend itself to analytic description owing to the indeterminacy of its asymptotic form. Measurement of the sensitivity at any chosen time, therefore, does not permit comparison of glasses of different compositions since at a fixed average concentration of the activator its local concentration may differ considerably from that given by the composition because of segregation of activators in the glasses [6]. Thus, the choice of experimental conditions that eliminate the dependence of the sensitivity on time is important for the study of how the activator concentration affects the sensitivity of RPL glasses.

It is known that stabilization of the characteristics of RPL glasses is attained by heating them [3]. To determine the heat-treatment conditions we studied the kinetics of RPL glasses with an Ag_2O content of 0.2 mole% in the temperature range 300–450°K. When studying

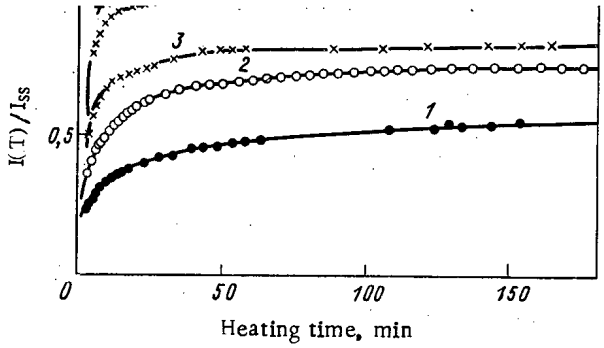

Fig. 2. Dependence of the RPL intensity on the heating time at a temperature (in °C) of 1) 53, 2) 78, 3) 98, and 4) 120. Lithium aluminophosphate glasses containing 0.2 mole% Ag_2O.

the temperature dependences of RPL intensity one must allow for the fact that in the general case they are due to two processes: thermal quenching of the luminescence and the variation of the concentration of RPL centers [7]. The first process, unlike the second, is reversible and in the glasses studied does not depend on the activator concentration. The irreversibility of the process of maturing of RPL centers manifests itself in the hysteresis of the RPL intensity in heating–cooling cycles. When a steady-state value of the concentration of RPL centers has been reached, the temperature dependence of the RPL intensity is due only to the thermal quenching of the luminescence, and the absence of hysteresis of the RPL intensity during heating and cooling of the specimen can serve as the criterion for the completion of the ripening.

Having experimentally determined the thermal quenching law $\eta(T)$, we can pass from the isothermal kinetics $I(t, T)$ of the RPL intensity to the isothermal kinetics of the concentration of RPL centers; the latter kinetics is proportional to $I(t, T)\cdot\eta(T)^{-1}$. These results for various temperatures are given in Fig. 2. Comparison of the data presented in Figs. 1 and 2 leads to the conclusion that the activator concentration and the temperature have a similar influence on the concentration of RPL centers, i.e., the steady-state value of the RPL center concentration, which determines the limiting sensitivity of the glasses, does not depend on the silver concentration within wide limits. A direct experiment, whose results are presented in Fig. 3, supports this conclusion. From the data presented above it follows that when the silver oxide content is higher than 0.2 mole% the sensitivity of the glasses practically does not depend on the concentration, and the function of the silver in the indicated range of concentrations reduces to one of controlling the maturing time. The search for promising compositions of radiophotoluminescent glasses, therefore, should be carried out primarily with respect to the indicated parameter, using a low activator concentration.

Using the example of lithium aluminophosphate glasses with a fixed activator concentration of 0.43 mole%, we managed to show that the kinetics of RPL is controlled by the ratio Na_2O/CaO. These results are presented in Fig. 4. The complete similarity of the data given in Figs. 1 and 4 allow the influence of the composition on the RPL kinetics to be explained as the result of a change in the local concentration of silver ions as a consequence of segregation of the activator. Further detailing of this model is still difficult today because of insufficient studies of the glasses under discussion.

Thus, the investigations have shown that when the activator concentration in the glasses decreases within certain limits, the sensitivity of the glasses does not decrease and the maturing time can be minimized by the choice of the composition of the glass or by heating of the specimens before the measurements. The results can be explained on the basis of the RPL center model presented in [5], according to which the radiophotoluminescence of silver-activated glasses is due to Ag_2^+ molecular ions that are formed as a result of the successive reactions

$$Ag^+ + e + Ag^+ \rightarrow Ag^0 + Ag^+ \rightarrow Ag_2^+.$$

In the process of radiation reduction of the silver, PO_3^{2-} electron-capture centers serve as an electron source, and the effectiveness of the protector properties of the ions of variable valence in the glasses studied is, as shown in [5, 8], so high that a silver oxide concentration of 10^{-1} mole% is sufficient for completely emptying the reservoir of electrons

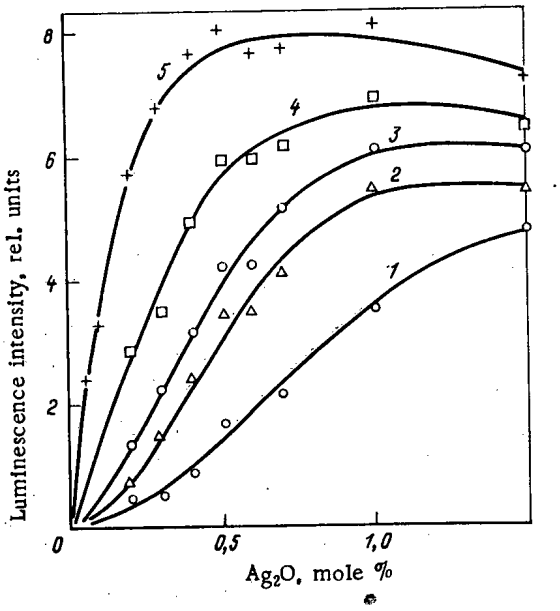

Fig. 3. Dependence of the RPL intensity on the activator concentration for lithium aluminophosphate glasses at different times after irradiation: 1) 1 h, 2) 7 h, 3) 1 day, 4) 8 days, 5) 8 days; annealing at 100°C for 1 h.

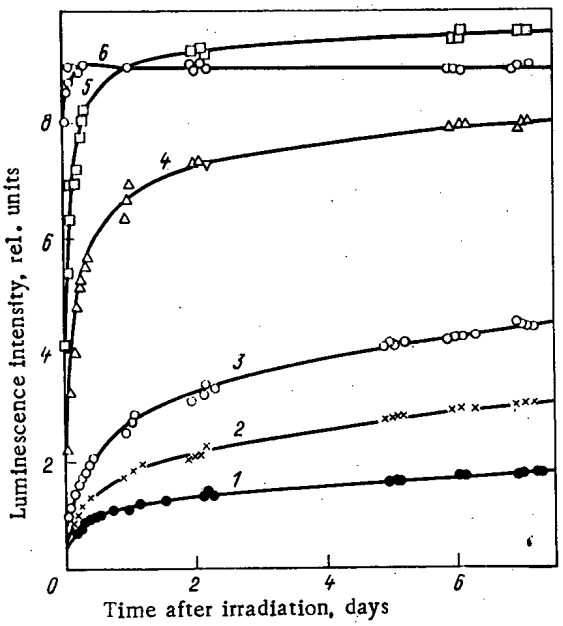

Fig. 4. Dependence of the RPL luminescence on the time after irradiation for lithium aluminophosphate glasses for the Na_2O/CaO ratios of 1) 0.4, 2) 0.75, 3) 1, 4) 1.3, 5) 1.8, and 6) 6.

expended on the reduction of the activator. A further increase in the activator concentration thus does not lead to a higher concentration of radiation-reduced silver. The observed concentration dependence of the rate of RPL center formation is, in our opinion, associated with the second stage of the indicated reaction and not with the first stage.

It must be pointed out that a decrease in the activator concentration has the consequence of not only saving silver but also improving the quality of the glass in the part of low-dose measurement. Insufficient attention is paid to this. It can be shown that the subdose indications of the unirradiated detectors are the factor that restricts the lower limit of the measured dose in any method of solid-state dosimetry (absorption, thermoluminescence, radio-

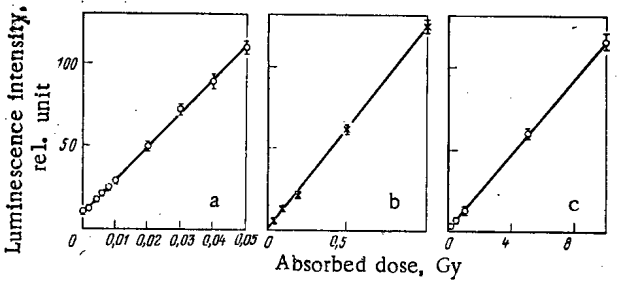

Fig. 5. Dose dependences for sodium calcium aluminophosphate glasses in the dose range $0-5\cdot10^{-2}$ (a), 0-1 (b), 0-10 Gy (c).

photoluminescence methods). The subdose luminescence of radiophotoluminescent glasses is due to several causes, including the luminescence of the reduced forms of the silver that always occurs in the glasses in accordance with the mass action law. A lowering of the silver content in the glasses, while the reduction–oxidation conditions remain constant, leads to a decrease in the concentration of all valence forms, including lower forms, and thus to a decrease in the predose luminescence. Using glasses with a low silver content, we managed to bring the predose luminescence to $3\cdot10^{-3}$-$4\cdot10^{3}$ Gy, which is illustrated by the dose dependence for sodium calcium aluminophosphate glasses with an Ag_2O content of 0.43 mole% (Fig. 5). The maturing time in the case of sodium calcium aluminophosphate glasses does not exceed 2 h and no fading is observed a month after irradiation. We note that the attained level of predose luminescence is close to the parameters of the best glasses of foreign firms [9] when the measurements are based on similar principles.

The results obtained permit the conclusion that glasses developed can be used to solve personal monitoring problems [10].

LITERATURE CITED

1. K. Becker and A. Scharmann, Einführung in die Festkörperdosimetrie, Thiemig, Munich (1975).
2. A. V. Dmitryuk and N. F. Orlov, Abstracts of Fifth All-Union Symposium "Optical and Spectral Properties of Glasses" [in Russian], Riga (1982), p. 119.
3. K. Becker, At. Energy Rev., 5, No. 1, 43 (1967).
4. H. Käs, A. May, and A. Scharmann, Glastechn. Ber., 45, No. 5, 182 (1972).
5. N. N. Vil'chinskaya et al., Fiz. Tverd. Tela (Leningrad), 26, No. 3, 825 (1984).
6. A. V. Dmitryuk, L. V. Maksimov, and G. O. Karapetyan, Zh. Prikl. Spektrosk., 22, No. 1, 153 (1975).
7. J. Barthe, D. Blanc, and G. Portal, J. Luminesc., 18/19, Part 1, 396 (1979).
8. N. N. Vil'chinskaya et al., Dokl. Akad. Nauk SSSR, 274, No. 5, 1117 (1984).
9. K. Becker et al., in: Proceedings Fourth International Conference on Luminescence Dosimetry, Cracow, Poland (1974), p. 441.
10. Radiation Safety Standards NRB-76 and Basic Sanitary Regulations of Work with Radioactive Materials and Other Sources of Ionizing Radiations OSP-72/80 [in Russian], Énergoizdat, Moscow (1981).

INFLUENCE OF THE ANISOTROPY OF ELASTIC SCATTERING ON NEUTRON MODERATING PARAMETERS

V. V. Kulik

UDC 539.125.52.550.832.5

The neutron characteristics of moderating media, such as the moderation length, asymptotic relaxation length, probability of avoiding resonant relaxation, etc. [1-4], are expressed in terms of the moderating parameters: $\bar{\xi}$ and $\bar{\xi}^2$ — the mean decrement and mean-square decrement of the energy per collision, $\bar{\mu}_L$ and $\bar{\mu}^2_L$ — the mean cosine and mean-square cosine of the scattering angle in the laboratory coordinate system (L-system), and $\overline{\xi\mu}_L$ — mean product of ξ and μ_L. The averaging is carried out over the angular distribution of the neutrons in the center-of-mass coordinate system (C-system).

It is known [2, 3] that starting from a certain energy the angular distribution of elastically scattering neutrons becomes anisotropic in the C-system. It is convenient to present it in the form of a series expansion in Legendre polynomials,

$$p(\mu_C E, A) = \sum_{n=0}^{\infty} \frac{2n+1}{2} f_n(E, A) P_n(\mu_C), \tag{1}$$

where $p(\mu_C, E. A)$ is a function, normalized to unity, of the angular distribution of neutrons of energy E elastically scattered on a nucleus A, $f_n(E, A)$ are the coefficients of the expansion (usually determined from the experimental dependences of p on the cosine μ_C of the scattering angle in the C-system), and $P_n(\mu_C)$ are Legendre polynomials.

The primary neutron parameters considered are linked directly to an elementary interaction act of a neutron with a nucleus and are defined as

$$\bar{\alpha}(E, A) = \int_{-1}^{1} \alpha(\mu_C, A)\, p(\mu_C, E, A)\, d\mu_C, \tag{2}$$

where $\bar{\alpha}(E, A)$ stands for any of the parameters $\bar{\xi}$, $1 - \bar{\mu}_L$, $-\overline{\xi\mu}_L$, $\bar{\xi}^2$, and $1 - \bar{\mu}^2_L$, while $\alpha(\mu_C, A)$ are the corresponding unaveraged quantities. Substituting the expansion (1) into expression (2), we have

$$\bar{\alpha}(E, A) = \sum_{n=0}^{\infty} B_n^{\alpha}(A) f_n(E, A), \tag{3}$$

where

$$B_n^{\alpha}(A) = \frac{2n+1}{2} \int_{-1}^{1} \alpha(\mu_C, A) P_n(\mu_C)\, d\mu_C. \tag{4}$$

Using the relation between ξ and μ_C and between μ_L and μ_C in the L- and C-systems [2, 3]

$$\xi = \ln[(1+1/A)^2 (1+2\mu_C/A+1/A^2)^{-1}], \tag{5a}$$

$$\mu_L = (\mu_C + 1/A)(1+2\mu_C/A+1/A^2)^{-\frac{1}{2}} \tag{5b}$$

and substituting the corresponding combination of ξ and μ_L in Eq. (4) and then integrating, we can get the coefficients B^{α}_n in explicit form.

With increasing n, however, this method leads to cumbersome formulas that are inconvient for analysis and computations, with the exception of the expression for $\bar{\mu}_L$ [5]. In the expressions obtained in this work for $\bar{\xi}$, $\bar{\xi}^2/2$, and $(3\bar{\mu}^2_L - 1)/2$ the order of anisotropy is limited to n = 2. Such a number of terms taken into account is not always sufficient for a correct description of the anisotropy. Moreover, as noted in [6] on the example of the calculation

Translated from Atomnaya Énergiya, Vol. 58, No. 2, pp. 135-137, February, 1985. Original article submitted April 27, 1984.

 0038-531X/85/5802-0160$09.50

TABLE 1. Coefficients C_n^{α} to within Terms of $(1/A^n)$

$\bar{\alpha}$	$n=1$	$n=2$	$n=3$	$n=4$
$\bar{\xi}$	$1+2/(3A)-4/(45A^2)$	$2/(3A)+4/(9A^2)$	$8/(15A^2)$	0
$1-\bar{\mu}_L$	$1+2/(3A)-7/(45A^2)$	$2/(3A)+4/(9A^2)$	$3/(5A^2)$	0
$-\overline{\xi\mu}_L$	$3+18/(5A)+4/A^2$	$2+6/A+279/(35A^2)$	$12/(5A)+33/(5A^2)$	$92/(35A^2)$
$\bar{\xi}^2$	$3/2+9/(10A)-1/(10A^2)$	$1/2+3/(2A)+47/(70A^2)$	$3/(5A)+7/(5A^2)$	$22/(35A^2)$
$1-\bar{\mu}_L^2$	$6/(5A)$	$-1+48/(35A^2)$	$-6/(5A)$	$-48/(35A^2)$

of the parameters $\bar{\xi}$ and $\gamma = \bar{\xi}^2/2\bar{\xi}$, anisotropy of $\bar{\xi}$ is determined primarily by f_1, while γ is affected significantly (through $\bar{\xi}^2$) by both f_1 and f_2, i.e., the order of anisotropy necessary for the calculation of different parameters may be different.

If instead of the exact relations (5) we use their representations in the form

$$\alpha(\mu_c, A) = \sum_{i=0}^{N} a_i^{\alpha}(A)\,\mu_C^i;\ a_i^{\alpha}(A) = \sum_k \beta_{ik}^{\alpha}/A^k,\ A>1, \tag{6}$$

then by substituting the expression (6) first into Eq. (4) and then into Eq. (3), we can easily get the sought parameters $\bar{\alpha}(E, A)$ in any approximation $k > 0$, neglecting terms of order $1/A^k$ in comparison with unity. In this case the order n of anisotropy is uniquely related to the chosen approximation k for each parameter $\bar{\alpha}$.

The parameters obtained in this way can be written conveniently in the form

$$\bar{\alpha}(E, A) = \bar{\alpha}_0(A)\left[1+\sum_{n=1}^{N(k)}(-1)^n C_n^{\alpha}(A)\,f_n(E, A)\right], \tag{7}$$

where $\bar{\alpha}_0(A) \equiv B_0^{\alpha}(A)$ is the isotropic part and $C_n^{\alpha}(A) = B_n^{\alpha}(A)/B_0^{\alpha}(A)$ are coefficients presented in the form of a power series in 1/A. These coefficients have the following properties:

$$\sum_{n=1}^{N}(-1)^n C_n^{\alpha}(A) = -1,\ C_n^{\alpha} > 0\ (\text{except } C_n^{(1-\bar{\mu}_L^2)} \text{ for } n \geqslant 2);$$

$$C_n^{\alpha}(A) \sim \frac{1}{A^{n-1}},\quad n=1, 2, \ldots,\ \bar{\alpha} = \bar{\xi},\ 1-\bar{\mu}_L;$$

$$C_n^{\alpha}(A) \sim \frac{1}{A^{n-2}},\ n=2, 3, \ldots,\ \bar{\alpha} = -\overline{\xi\mu}_L,\ \bar{\xi}^2,\ 1-\bar{\mu}_L^2.$$

For practical purposes when A > 10 it is usually sufficient to confine ourselves to the representation of the primary neutron parameters to within terms of the order of $1/A^3$, i.e., the third approximation (k = 3). The coefficients C_n^{α} in this approximation are given in Table 1 while the isotropic component of the parameters under consideration has the form

$$\bar{\xi}_0 = \frac{2}{A}\left(1-\frac{2}{3A}+\frac{1}{3A^2}\right);\ 1-\bar{\mu}_{L0} = 1-\frac{2}{3A};\ 1-\bar{\mu}_{L0}^2 = \frac{2}{3}\left(1-\frac{1}{5A^2}\right);\ -(\overline{\xi\mu}_L)_0 = \frac{2}{3A}\left(1-\frac{2}{A}+\frac{4}{5A^2}\right);\ \bar{\xi}_0^2 = \frac{16}{3A^2}\left(1-\frac{1}{A}+\frac{4}{5A^2}\right).$$

Here A is the nuclear mass, expressed in units of neutron mass.

As an illustration, Table 2 presents the primary neutron parameters of ^{12}C. The coefficients f_n have been taken from the handbook [7] according to the data of the ENDF/B IV library. The first row of Table 2 gives the isotropic values. Comparison of the numerical results with the tables of the parameters $\bar{\xi}$, μ_L, and γ given in [7] indicates agreement between the corresponding values.

From formula (7), the properties and values of the coefficients C_n^{α} and f_n, as well as the data of Table 2 it follows that the influence of anisotropy in the C-system on the primary neutron parameters reduces to the following.

In a large part of the energy range considered (1 eV ≤ E ≤ 15 MeV) the parameters under study decrease in comparison with their isotropic values, mainly as a result of the predominant scattering of neutrons forward in the C-system ($f_1 \equiv \mu_C > 0$).

The number of preserved terms of the sum in formula (7) is determined by the chosen approximation k: for $k \geqslant 2$, N = k for $\alpha = \bar{\xi}$, $1-\bar{\mu}_L$ and N = k + 1 for $\bar{\alpha} = -\overline{\xi\mu}_L$, $\bar{\xi}^2$, $1-\bar{\mu}^2_L$.

TABLE 2. Primary Neutron Parameters of ^{12}C

E, MeV	$\bar{\xi}$	$1-\bar{\mu}_L$	$-\overline{\xi\mu}_L$	$\overline{\xi^2}$	$1-\overline{\mu_L^2}$
$1\cdot10^{-6}$	0,1591	0,9441	0,04689	0,03471	0,6657
1,05	0,1471	0,8728	0,03643	0,03092	0,6567
2,08	0,1608	0,9539	0,40140	0,04416	0,3526
3,08	0,1707	1,0252	0,08365	0,04323	0,5279
4,00	0,1560	0,9258	0,07538	0,03904	0,4778
6,05	0,1332	0,7912	0,03915	0,02904	0,5581
8,25	0,0543	0,3223	0,00132	0,00926	0,3147
10,96	0,0696	0,4131	0,01407	0,01342	0,3536
15,00	0,0729	0,4329	0,00693	0,01345	0,3921

In the first approximation (k = 1) the influence of the anisotropy can be assessed from the formulas

$$\bar{\xi}=\bar{\xi}_0(1-f_1);\ 1-\bar{\mu}_L=(1-\bar{\mu}_{L0})(1-f_1);\ 1-\overline{\mu_L^2}=(1-\overline{\mu_{L0}^2})(1-f_2);\ \overline{\xi\mu}_L=(\overline{\xi\mu}_L)_0(1-3f_1+2f_2);$$

$$\overline{\xi^2}=\overline{\xi_0^2}(1-3f_1/2+f_2/2).$$

The deviation of the parameters $\bar{\xi}$ and $1-\bar{\mu}_L$ from their isotropic values is determined mainly by the coefficient f_1, of parameter $1-\bar{\mu}^2_L$ by f_2, and of parameters $\overline{\xi^2}$ and $\xi\mu_L$ by f_1 and f_2.

LITERATURE CITED

1. V. P. Kochergin and V. V. Orlov, At. Energ., 6, No. 1, 34 (1959).
2. A. W. Weinberg and E. Wigner, Physical Theory of Neutron Chain Reactors, Univ. of Chicago Press (1958).
3. S. M. Feinberg, S. B. Shikhov, and V. B. Troyanskii, Theory of Nuclear Reactors [in Russian], Vol. 1, Atomizdat, Moscow (1978).
4. I. A. Kozachok and V. V. Kulik, At. Energ., 53, No. 5, 328 (1982).
5. E. Pritchard and T. Ahrens, Nucl. Sci. Eng., 22, No. 2, 248 (1965).
6. W. Stasey, Nucl. Sci. Eng., 44, No. 2, 194 (1971).
7. Yu. A. Medvedev, B. M. Stepanov, and G. Ya. Trukhanov, Nuclear-Physical Constants of the Interaction of Neutrons with Constituent Elements of the Atmosphere and the Earth's Core [in Russian], Énergoizdat, Moscow (1981).

MEASUREMENT OF THE RATIO OF THE CROSS SECTIONS FOR FISSIONING OF ^{237}Np AND ^{235}U BY NEUTRONS WITH ENERGIES IN THE RANGE 4-11 MeV

A. A. Goverdovskii, A. K. Gordyushin,
B. D. Kuz'minov, V. F. Mitrofanov,
A. I. Sergachev, S. M. Solov'ev,
and G. M. Stepchenkova

UDC 539.173

^{237}Np nuclei are an intermediate link in the chain of formation of ^{236}Pu and ^{238}Pu in a fast reactor. Predicting the accumulation of ^{237}Np is part of the general problem of calculating the nuclide composition of spent fuel and requires reliable nuclear data determining this process. In particular, the required error in the determination of the fission cross section of ^{237}Np nuclei is equal to 1-5% for neutron energies ranging from threshold to 20 MeV [1]. However, with the existence of quite extensive data on σ^7_f the disagreements in the results obtained by different authors for both the energy dependence and the absolute values [2-11] significantly exceed the assigned measurement errors (1-3%).

This paper concerns the measurement of the ratio of the cross sections for fissioning of ^{237}Np and ^{235}U by neutrons with energies in the range 4.5-10.7 MeV by the method of pulsed synchronization on an electric charge-exchange ÉGP-10M generator at the Physico-Energy Institute.

The neutron source was the reaction D(d, n)^{3}He in a gaseous deuterium target, filled up to a pressure of $1.2 \cdot 10^5$ Pa, with an input window consisting of molybdenum foil with a thickness of 8.2 ± 0.2 mg/cm^2. A platinum disk 0.2 mm thick was fastened to the bottom. The average deuterium current was equal to 1.5 μA. The neutron spectrum from the target consisted of a single line E_n, whose width depended on the dispersion of the ionization losses and the average angular spread of the deuterons in the input window and in the gas as well as on the solid angle subtended by the fissioning samples. As the deuteron energy was increased, the group of background neutrons, associated with the break-up of the deuterons on the structural materials of the gaseous target and the saturation of the platinum foil by deuterium, increased. For energies $E_{do} > 5$ MeV, the background from the reaction D(d, np)D is distinctly manifested. The background neutron group had a continuous spectrum with an average energy of ~3 MeV and an intensity comparable with the intensity of the single line already in the experimental range $E_n > 8.5$ MeV.

A double ionization chamber, filled with methane up to a pressure of $\sim 1.8 \cdot 10^5$ Pa, was used as a detector for the fission fragments. The intensity of the field in the working volume of the chamber was equal to 2.3 kV/cm and the distance between the electrodes was 4 mm. It was possible to discriminate α particle pulses by height while preserving 99.5% of the pulses from the fission fragments of ^{237}Np (for thin samples) and 99.8% of the pulses for ^{235}U.

In this work, we use targets consisting of fissioning materials, which in turn consisted of thin layers (0.1-0.5 mg/cm^2) of uranium and neptunium oxides deposited on aluminum substrates 0.1 mm thick. The characteristics of the targets are shown in Table 1. The target 2 contained the following impurities: 0.52% ^{241}Am and 0.43% ^{239}Pu. The targets 3-8 were fabricated from materials with an isotopic purity of 99.9%. The thickness nonuniformity of the targets was 10%. The ratios of the uranium and neptunium masses in the samples of mixtures 3-8 were determined to within 1%. The uranium and neptunium targets were fastened with substrates to the ionization detector, with the help of a special holder, one to another perpendicularly to the neutron flux. To eliminate any effect of the finite distance between the samples on the final result, we performed the measurements with two opposite orientations of the assembly with respect to the gaseous target.

To measure the energy dependence of the ratio of the cross sections for fissioning of ^{237}Np and ^{235}U by fast neutrons and simultaneously determine the contribution of different

Translated from Atomnaya Énergiya, Vol. 58, No. 2, pp. 137-139, February, 1985. Original article submitted July 30, 1984.

0038-431X/85/5802-0163$09.50

TABLE 1. Characteristics of Targets and Results of Normalizing Measurements

Target number	Nuclide content, %		Normalizing values of the cross-section ratios with neutron energies in MeV				R_T^{-1}	Target thickness μg/cm²
	^{235}U	^{237}Np	6,55	6,95	7,34	7,75		
1	99,992							410; 256
2		99,05						460
3	3,46	96,54	1,320	1,260	1,190	1,175	35,82±0,40	300
4	4,40	95,60	1,328	1,242	1,230	1,200	24,20±0,25	300
5	6,50	93,50	1,312	1,272	1,226	1,189	18,52±0,14	300
6	18,26	81,74	1,310	1,250	1,232	1,209	12,65±0,11	306
7	24,65	75,35	1,300	1,262	1,180	1,221	10,32±0,10	100
8	34,75	65,25	1,335	1,270	1,174	1,176	7,635±0,079	98
9*	5,19	94,81	1,330	1,286	1,209	1,195		204
Average			1,319±0,016	1,263±0,015	1,206±0,015	1,195±0,014		

*Target 9 is a mixture of ^{238}U and ^{235}U.

components of the above-described neutron background, we used a time spectrometer based on the EGP-10M accelerator operating in the pulsed mode with the ionic current interrupted at a frequency of 5 MHz and a burst duration of 1 nsec. The total temporal resolution (instrumental width of the line at half height) was equal to 2.5-3 nsec, which enabled reliable separation of the useful events from the background events on a flight baseline of 0.7 m.

The monitoring channel of the spectrometer was constructed based on a scintillation detector, located 2.5 m from the target, and was used to align the bunching system of the accelerator and to monitor the state of the gaseous target. The operation of the spectrometrical channel was constantly monitored with the help of a ^{252}Cf source in the coincidence mode (of γ fission fragments).

We measured the ratios of the fission cross sections of ^{237}Np and ^{235}U in two stages. At the first stage we carefully studied the energy dependence with the help of isotopically pure targets 1 and 2 and at the second stage we normalized this dependence to the reference values obtained with the help of targets 3-9 by the method of isotopic impurities. The ratio of the fission cross sections can be represented in the form

$$\frac{\sigma_f^7}{\sigma_f^5} = \eta_i\left(\frac{R_i}{R_{Ti}}\prod_j K_j - 1\right), \quad (1)$$

where η_i is the ratio of the number of uranium nuclei to the number of neptunium nuclei in the i-th sample; R_i and R_{Ti} are the ratio of the counting rate of fission fragments in the i-th (from the mixture) and uranium samples produced by fast and moderated (thermal) neutrons; and K_j are the different corrections.

The isotopic weighting of targets 3-8 (the determination of R_{Ti}) with respect to target 1 was determined in a neutron flux with an initial neutron energy of 400 keV, moderated by a layer of polyethylene 20 cm thick. The data on the fission cross section of ^{237}Np obtained within the last 20 years indicate the presence of a measurable fissioning of this nucleus by neutrons with energies even lower than 10 keV [2, 12], which can distort the values of R_{Ti} with low concentrations of ^{235}U in the mixtures. In this work, in order to elucidate the effect of the indicated factor and to obtain an unbiased value of R_{Ti}, we used six samples with the ^{235}U impurity varying from 3 to 35%. The results of the isotopic weighting and the corresponding ratios of the fission cross sections of ^{237}Np and ^{235}U are presented in Table 1. Table 1 also shows the measurements of the cross section of ^{237}Np, obtained by multiplying the ratios $\sigma_f(^{237}Np)/\sigma_f(^{238}U)$ and $\sigma_f(^{238}U)/\sigma_f(^{235}U)$ measured sequentially on targets 1, 4, and 9. Within the limits of measurement error the latter values are in agreement with the previously obtained ones [13].

The average values of the ratios of the fission cross sections of ^{237}Np and ^{235}U in Table 1 are assigned errors which include the spread in the data in the series, the error in the isotropic composition (1%), and the error in the determination of the ratios of the efficiency of detection of ^{237}Np and ^{235}U fissioning events (0.4%).

TABLE 2. Results of Measurements of σ_f^7/σ_f^5

E_n, MeV	ΔE_n, keV	$\delta_{f}^{7}/\sigma_f^5$	δ_{ran}, %	δ_{total}, %	E_n, MeV	ΔE_n, keV	σ_f^7/σ_f^5	δ_{ran}, %	δ_{total}, %
4,44	150	1,363	1,00	1,37	8,12	68	1,169	1,00	1,37
4,97	130	1,420	0,92	1,32	8,31	66	1,172	1,12	1,48
5,21	123	1,416	0,94	1,33	8,50	64	1,159	0,89	1,30
5,44	120	1,449	1,05	1,41	8,66	63	1,154	0,90	1,33
5,66	116	1,458	1,07	1,43	8,82	62	1,163	0,78	1,25
5,88	109	1,481	0,93	1,32	9,01	60	1,145	0,86	1,34
6,11	102	1,434	0,89	1,30	9,18	59	1,142	0,99	1,42
6,14	102	1,409	1,11	1,46	9,35	58	1,126	0,90	1,34
6,35	98	1,361	1,07	1,43	9,51	56	1,127	1,08	1,49
6,38	96	1,365	0,95	1,34	9,65	55	1,123	1,00	1,42
6,55 *	92	1,319	0,45	1,21	9,82	54	1,129	1,10	1,50
6,75	88	1,262	1,16	1,50	9,96	53	1,120	1,12	1,55
6,95 *	84	1,263	0,48	1,19	10,11	53	1,115	1,00	1,47
7,15	81	1,213	1,10	1,45	10,22	52	1,125	0,90	1,40
7,34 *	78	1,206	0,83	1,24	10,36	52	1,132	1,05	1,50
7,53	75	1,198	1,21	1,53	10,49	50	1,120	1,15	1,57
7,75 *	73	1,195	0,54	1,17	10,69	50	1,127	1,20	1,61
7,94	70	1,172	1,08	1,43					

*Normalizing points.

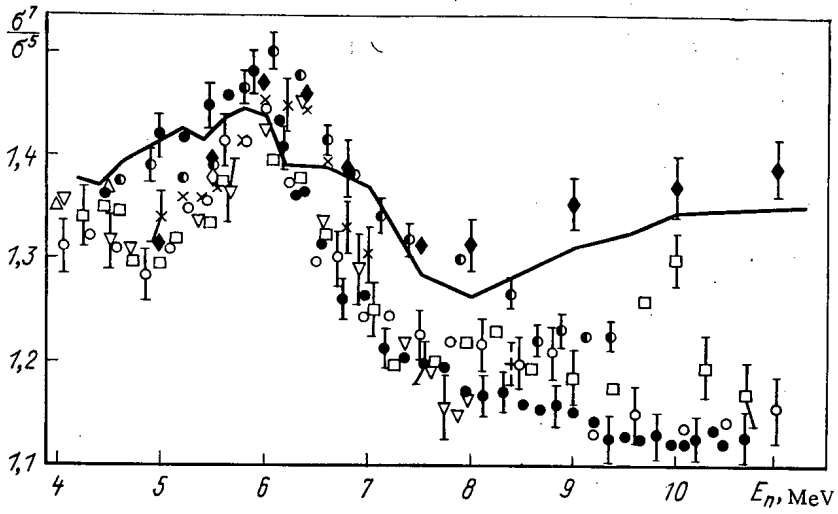

Fig. 1. Energy dependence of the ratio of the fission cross sections for ^{237}Np and ^{235}U nuclei: ●) this work; ○) [2], ◐) [3], □) [5], ▽) [6], ◇) [7]; +) [8], ×) [9], ◆) [10], △) [11], ——) [14].

The set of normalized coefficients (error 1.5-1.8%) obtained after normalization was analyzed as a set of independent quantities. The error in the normalizing coefficient of the energy dependence of σ_f^7/σ_f^5 determined in this manner was equal to 0.85%.

In analyzing the experimental data, we took into account a number of factors which can distort the measurements. In particular, we calculated the effect of the background formed by the neutrons scattered by the target holder, ionization detector, and the substrates of the layers using the Monte Carlo method. The corresponding correction did not exceed 0.04% in the entire range of neutron energies studied.

The correction for fissioning of peripheral nuclides in target 2 was determined from the data in [14] and was equal to 0.11-0.30% for $E_n \geq 10$ MeV.

The correction for total stopping of some of the fission fragments in the layers was determined analogously to [15] taking into account the angular distributions of the fragments [16] and was equal to 0.06-0.12%. With alternate irradiation of the target assembly by fast and slow neutrons, the correction with the values of E_n selected for normalization is determined by the difference between the angular distributions of the fragments and the isotopic distribution for the homogeneous mixture of uranium and neptunium. When homogeneity

is destroyed, the difference in the effective depth at which the ^{235}U and ^{237}Np nuclei lie begins to play the main role. To elucidate the degree of nonhomogeneity of the mixtures used in the experiments, we studied the targets with the help of a surface-barrier silicon detector. We irradiated the targets alternately with fast and slow neutrons with different orientations of the targets relative to the detector. The difference in the effective depth at which the ^{235}U and ^{237}Np nuclei lay was determined from the relative shift in the energy distributions of the fission fragments and was equal to about 20%, and the correction was equal to 0.12 and 0.4% for the thin (0.1 mg/cm^2) and thick (0.3 mg/cm^2) samples, respectively.

The total error in the measurements consisted of several components: the random error: varying from 0.8 to 1.1%; the error in the determination of the ratios of the detection efficiencies: from 0.3 to 0.6%; the normalization errors (0.85%) and corrections (<0.1%); errors in the discrimination of background events in the temporal spectra for $E_n > 8$ MeV: from 0.10 to 0.45%.

The measurements of the ratio of the cross sections for fissioning of ^{237}Np and ^{235}U by neutrons with energies in the range 4.44-10.69 MeV are presented in Table 2. The data obtained in this work are compared with the results obtained by others in Fig. 1.

LITERATURE CITED

1. WRENDA 83/84, World Request List for Nuclear Data Section, IAEA (1983).
2. J. Behrens, J. Browne, and J. Walden, Nucl. Sci. Eng., 80, No. 3, 393 (1982).
3. J. Meadows, Nucl. Sci. Eng., 85, No. 3, 271 (1983).
4. R. Jiacoletti, W. Brown, and H. Olson, Nucl. Sci. Eng., 48, 412 (1972).
5. A. Carlson and B. Patric, in: Proceedings of the International Conference on Nuclear Cross Sections for Technology, Knoxville, Tennessee, 22-26 October, 1979, NBS Special Publication 594, U. S. National Bureau of Standards (1980), p. 971.
6. H. Schmitt and R. Murray, Phys. Rev., 116, 1575 (1959).
7. P. White and G. Warner, J. Nucl. Energy, 21, 671 (1967).
8. R. Arlt et al., Jahresbericht 1981, ZFK-488, S. 20 (1982).
9. V. M. Kupriyanov, B. I. Fursov, V. I. Ivanov, and G. N. Smirenkin, "Measurement of the ratios of fission cross sections $^{237}Np/^{239}Pu$ and $^{241}Am/^{239}Pu$ for neutron energies in the range 0.13-7.0 MeV," At. Energ., 45, No. 6, 440-442 (1978).
10. V. M. Pankratov, "Cross sections of fissioning of ^{232}Th, ^{233}U, ^{235}U, ^{237}Np, ^{238}U nuclei by neutrons with energies in the range 5-37 MeV," At. Energ., 14, No. 2, 177-184 (1963).
11. W. Stein, R. Smith, and J. Grundl, in: Proceedings of the International Conference on Neutron Cross Section Technology, Washington, 22-24 March, U.S. AEC (1966), Vol. 2, p. 623.
12. W. Davey, Nucl. Sci. Eng., 26, 146 (1966).
13. A. A. Goverdovskii, A. K. Gordyushin, B. D. Kuz'minov, et al., "Measurement of the ratio of the fission cross sections of ^{238}U and ^{235}U nuclei for neutrons with energies in the range 5.4-10.4 MeV," At. Energ., 56, No. 3, 162-164 (1984).
14. ENDF/B-5, 3rd Edition, Brookhaven National Laboratory (1979), ^{237}Np (MAT-1337), ^{235}U (MAT-1395).
15. G. Carlson, Nucl. Methods, 119, 97 (1974).
16. J. Simmons and R. Henkel, Phys. Rev., 120, 198 (1960).

YIELDS OF LONG-LIVED RADIONUCLIDES IN THE IRRADIATION OF Be, C, Mg, Si, AND Sc BY CHARGED PARTICLES

I. O. Konstantinov, P. P. Dmitriev, and V. I. Bolotskikh

UDC 539.172.8

Physical and chemical processes, as a rule, are monitored by the method of radioindicators according to the long-lived radionuclides ($T_{1/2}$ > 2 days). They are particularly important for the investigation of prolonged processes of migration of substances and damage of the surface of the products. The most widespread method of inducing radioactivity consists in irradiation with accelerated charged particles [1]. The most important characteristic of the activation process of materials is the yield of the radionuclide for a thick target [2], i.e., the physical constant used also in other applied problems, in particular in the production of radionuclides in activation analysis, etc.

Part of the chemical elements that are the most abundant in the composition of structural materials have already been studied from this point of view [3, 4]. In the present experiments, conducted on the cyclotron of the Physico-Power Institute [5], measured and systematized data are presented about the yields of long-lived radionuclides formed by the irradi-

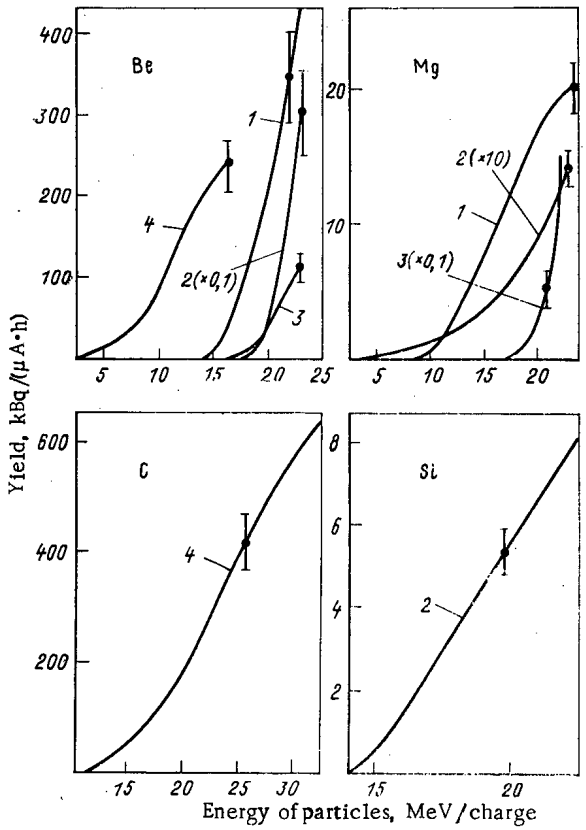

Fig. 1. Dependence of the yield of ^{7}Be from beryllium and carbon, and ^{22}Na from magnesium and silicon, on the energy of the protons (1), deuterons (2), α-particles (3), and ^{3}He ions (4).

Translated from Atomnaya Énergiya, Vol. 58, No. 2, pp. 140-143, February, 1985. Original article submitted July 30, 1984.

0038-531X/85/5802-0167$09.50

TABLE 1. Yields of Radionuclides for Maximum Energy of the Bombarding Particles

Nuclear reaction of formation	Particle energy, MeV	Yield, kBq/μA·h	Literature reference
$^{9}Be(p, t)^{7}Be$	22,4±0,2 22,4 23,0	406±49 390 800	* [7] [8]
$^{9}Be(d, tn)^{7}Be$	22,8±0,2 22,4	30±4 25	* [7]
$^{9}Be(\alpha, \alpha 2n)^{7}Be$	45,2±0,5 43,0	111±15 85	* [7]
$^{9}Be(^{3}He, \alpha n)^{7}Be$	32,1±0,5	237±31	*
$^{25}Mg(p, \alpha)^{22}Na$ $^{26}Mg(p, \alpha n)^{22}Na$	22,4±0,2 22 22 20,8 22	20±2 18,5 18,9 23,7 14,8	* [9] [10] [11] [12]
$^{24}Mg(d, \alpha)^{22}Na$ $^{25}Mg(d, \alpha n)^{22}Na$	22,8±0,2 20 20 25 16,1 15 15 14 14	141±15 122 93 118 53 74 56 115 37	* [9] [13] [14] [15] [16] [17] [18] [19]
$^{24}Mg(\alpha, \alpha pn)^{22}Na$	45,2±0,5 35,8	1,52±0,16 0,02	* [20]
$^{12}C(^{3}He, 2\alpha)^{7}Be$	32,1±0,5 30 27,5 24	620±80 450 470 320	* [21] [22] [23]
$^{28}Si(d, 2\alpha)^{22}Na$	22,3±0,2	7,8±0,8	*
$^{45}Sc(p, pn)^{44m}Sc$	22,3±0,2 22 22	$(43,7\pm5,8)\,10^{3}$ $37\cdot10^{3}$ $48\cdot10^{3}$	* [24] [25]
$^{45}Sc(d, t)^{44m}Sc$	22,8±0,2	$(5,52\pm0,65)\,10^{3}$	*
$^{45}Sc(d, p)^{46}Sc$	22,8±0,2	$(1,85\pm0,22)\,10^{3}$	*
$^{45}Sc(\alpha, n)^{48}V$	43,7±0,5 41,5 40	$(1,46\pm0,16)\,10^{3}$ $0,83\cdot10^{3}$ $1,67\cdot10^{3}$	* [26] [27]
$^{45}Sc(\alpha, \alpha n)^{44m}Sc$	43,7±0,5 40	$(5,4\pm0,7)\,10^{3}$ $5,3\cdot10^{3}$	* [27]
$^{45}Sc(\alpha, 2pn)^{46}Sc$	43,7±0,5 40	(74±10) 58	* [27]
$^{45}Sc(\alpha, 2pn)^{46}Sc$	43,7±0,5 40	$(0,79\pm0,16)\,10^{3}$ 1,0	* [27]
$^{45}Sc(^{3}He, \alpha)^{44m}Sc$	32,1±0,5 31	222±30 160	* [28]
$^{45}Sc(^{3}He, 2p)^{46}Sc$	32,1±0,5	34±4	*

Note. An asterisk denotes data of present paper.

tion of Be, C, Mg, Si, and Sc with accelerated ions of isotopes of hydrogen and helium. The literature data frequently are contradictory, incomplete, and, in certain cases, lacking.

The sample targets were disks with a diameter of 10 × (1-2) mm; silicon was used both as a pure semiconductor and in the form of a quartz plate; stacks of carbon and magnesium foils with a thickness of ~50 μm also were assembled. Irradiation was conducted in cassettes in the extracted beam of the cyclotron; it amounted to 1-2 μA·h and was measured by integration of the current.

A semiconductor γ-spectrometer was used for radiometry of the irradiated samples, with a Ge(Li)-detector with a volume of ~40 cm^3, and an NTA-1024 multichannel analyzer. The spectrometer was calibrated by means of the OSGI γ-emitter. The decay schemes of the radionuclides were chosen in accordance with the handbook [6].

Table 1 shows data about the yields for the maximum particle energy and also the results of integration of the excitation and yield functions according to the literature data. The first column of the table shows only the most preferable nuclear reaction channels with the stated energy.

The yields of radionuclides are given in Table 2 and also in Figs. 1 and 2 (in kBq/μA·h), obtained on samples irradiated with a different particle energy, in certain cases through stacks of foils, and also by the successive removal of layers from the samples irradiated with maximum particle energy.

The removal of layers was effected both by a mechanical method (for Be, C, Si, and SiO_2) on a special lapping machine, using different pastes, and by chemical etching (for Mo and Sc). The energy of irradiation of the samples was varied by the installation of stopping foils. The error of the majority of the data obtained amounts to 12-18%. For clarity, the error is given in Figs. 1 and 2 on each curve for only one experimental point.

TABLE 2

E_p, MeV	^{9}Be (p, t) ^{7}Be
22,8±0,2	406±49
21,8±0,2	342±41
20,4±0,3	266±32
18,7±0,3	167±20
17,2±0,4	78±9
15,7±0,4	22±3
15,0±0,4	2,0±0,4

$E_{^3He}$, MeV	^{9}Be (^{3}He, αn) ^{7}Be
32,1±0,5	237±31
27,6±0,6	201±26
24,0±0,7	153±20
20,2±0,8	96±12
16,2±0,9	37±5
10,5±1,2	4,1±0,5
5,8±1,6	1,1±0,2

E_d, MeV	^{9}Be (d, tn) ^{7}Be
23,0±0,2	30±4
22,4±0,2	25±3
21,0±0,3	12±2
19,7±0,3	3,3±0,5
17,9±0,3	0,10±0,03

E_α, MeV	^{9}Be (α, $\alpha 2n$) ^{7}Be
45,2±0,5	111±15
43,0±0,5	85±11
41,0±0,6	57±7
37,5±0,6	17±3
35,0±0,7	7±1
32,2±0,7	0,7±0,2

E_p, MeV	Mg + p → ^{22}Na
22,4±0,2	20,0±2,0
21,5±0,2	18,9±1,9
20,0±0,3	17,0±1,8
18,2±0,3	14,6±1,5
16,1±0,4	8,9±1,0
13,9±0,4	6,5±0,8
11,5±0,5	2,2±0,3
9,0±0,6	0,20±0,05

E_d, MeV	Mg + d → ^{22}Na
22,8±0,2	141±15
21,6±0,2	116±12
20,1±0,2	93±10
18,4±0,3	68±7
16,5±0,4	50±5
14,4±0,4	33±4
12,1±0,5	22±3
9,6±0,6	12±2
6,9±0,9	5,9±0,8
3,9±1,4	1,1±0,2

E_α, MeV	Mg + α → ^{22}Na
45,3±0,5	1,52±0,16
43,7±0,6	0,96±0,10
42,1±0,6	0,56±0,06
39,8±0,7	0,26±0,04
36,5±0,7	0,07±0,02

$E_{^3He}$, MeV	^{12}C (^{3}He, 2α) ^{7}Be
32,1±0,5	620±80
32,1±0,5	616±80
30,7±0,5	592±77
29,1±0,6	553±72
28,3±0,6	518±67
27,3±0,6	500±65
26,0±0,7	437±57
24,6±0,7	377±49
23,9±0,7	370±48
22,6±0,8	300±39
20,9±0,8	230±30
19,2±0,8	185±24
17,8±0,9	144±19
16,0±0,9	100±13

E_d, MeV	^{28}Si (d, 2α) ^{22}Na
22,3±0,2	7,8±0,8
22,1±0,2	8,1±0,8
21,2±0,2	6,8±0,8
20,2±0,2	5,6±0,6
20,0±0,2	5,6±0,6
19,3±0,3	4,8±0,5
19,2±0,3	4,8±0,5
18,5±0,3	4,1±0,4
18,1±0,3	3,7±0,4
17,6±0,3	3,0±0,3
17,4±0,3	3,0±0,3
16,8±0,4	1,9±0,2
16,5±0,4	2,2±0,3
14,8±0,4	0,7±0,2

$E_{^3He}$, MeV	^{12}C (^{3}He, 2α) ^{7}Be
15,0±1,0	56±7
14,0±1,0	37±5
12,1±1,1	11±2

E_d, MeV	^{28}Si (d, 2α) ^{22}Na
14,5±0,4	1,1±0,2

E_p, MeV	^{45}Sc(p, pn) ^{44m}Sc ×10^3
22,3±0,2	43,7±5,8
21,6±0,2	40,7±5,4
21,0±0,2	30,3±4,0
18,4±0,3	16,7±2,2
16,5±0,4	8,5±1,1
14,4±0,4	3,3±0,5
12,1±0,5	0,7±0,1
11,4±0,5	0,40±0,08

E_d, MeV	^{45}Sc (d, t) ^{44m}Sc ×10^3
23,0±0,2	5,52±0,65
22,4±0,2	5,55±0,65
21,0±0,2	5,37±0,63
19,7±0,3	5,25±0,63
17,9±0,3	5,10±0,61
15,7±0,4	4,70±0,60
13,2±0,4	4,00±0,50
10,4±0,5	2,96±0,37
7,3±0,7	1,48±0,20
3,9±1,0	0,19±0,04

E_d, MeV	^{45}Sc (d, p) ^{46}Sc ×10^3
23,0±0,2	1,85±0,22
22,4±0,2	1,78±0,21
21,0±0,2	1,78±0,21
19,7±0,3	1,70±0,20
17,9±0,3	1,59±0,20
15,7±0,4	1,41±0,20
13,2±0,4	1,18±0,16
10,4±0,5	0,81±0,12
7,3±0,7	0,41±0,07
3,9±1,0	0,007±0,002

E_α, MeV	^{45}Sc (α, n) ^{48}V ×10^3
43,7±0,5	1,46±0,16
41,5±0,5	1,44±0,16
37,9±0,6	1,43±0,16
35,3±0,7	1,41±0,16
29,4±0,8	1,37±0,16
22,4±1,0	1,20±0,14
17,0±1,2	0,86±0,10
12,9±1,4	0,45±0,08
6,9±1,8	0,020±0,006

E_α, MeV	^{45}Sc (α, αn) ^{44m}Sc ×10^3
43,7±0,5	5,4±0,7
41,5±0,5	4,9±0,6
37,9±0,6	3,8±0,5
35,3±0,7	3,0±0,4
29,4±0,8	0,40±0,06
22,4±1,0	0,07±0,02

E_α, MeV	^{45}Sc (α, 2pn) ^{45}Sc
43,7±0,5	74±10
41,5±0,5	59±8
37,9±0,6	30±4
35,3±0,7	15±2
29,4±0,8	7,5±1

E_α, MeV	^{45}Sc (α, 2p) ^{47}Sc ×10^3
43,7±0,5	0,79±0,16
41,5±0,5	0,74±0,15
37,9±0,6	0,61±0,12
35,3±0,7	0,48±0,10
29,4±0,8	0,20±0,04
22,4±1,0	0,07±0,02

$E_{^3He}$, MeV	^{45}Sc (^{3}He, α) ^{44m}Sc
32,1±0,5	222±30
28,3±0,6	196±30
23,9±0,7	160±22
19,2±0,8	110±15
14,0±1,0	5±1

$E_{^3He}$, MeV	^{45}Sc (^{3}He, 2p) ^{46}Sc
32,1±0,5	34±4
28,3±0,6	29±4
23,9±0,7	22±3
19,2±0,8	17,1
14,0±1,0	2,6±0,6

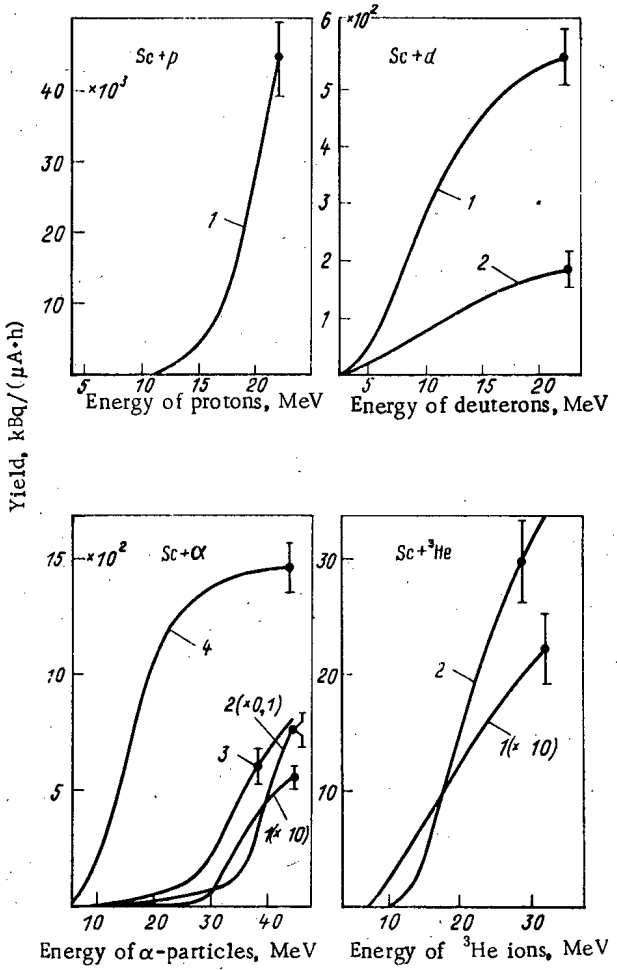

Fig. 2. Dependence of the yield of ^{44m}Sc (1), ^{46}Sc (2), ^{47}Sc (3), and ^{48}V (4) from scandium on the particle energy.

The authors thank the staff of the Physico-Power Institute cyclotron for cooperation in carrying out the irradiation and L. V. Ognev for participation in processing the measurement results.

LITERATURE CITED

1. V. S. Arkhipov, I. N. Garbar, I. O. Konstantinov, and I. A. Pavlov, Method of Surface Activation in Industry [in Russian], Atomizdat, Moscow (1975).
2. N. Krasnov, Int. J. Appl. Rad. Isotopes, 25, 222 (1974).
3. I. Konstantinov and N. Krasnov, J. Radioanal. Chem., 8, 357 (1971).
4. I. O. Konstantinov, V. V. Malukhin, N. N. Krasnov, and A. D. Karpin, "Activation of molybdenum and tungsten in the cyclotron," At. Energ., 44, No. 2, 183-185 (1978).
5. N. N. Krasnov et al., in: Proceedings of the Physico-Power Institute [in Russian], Atomizdat, Moscow (1974), p. 399.
6. N. G. Gusev and P. P. Dmitriev, Quantum Emission of Radioactive Nuclides [in Russian], Atomizdat, Moscow (1977).
7. P. P. Dmitriev, N. N. Krasnov, G. A. Molin, and M. V. Panarin, "Yields of ^{7}Be by the irradiation of lithium and boron by protons and deuterons, and beryllium by protons, deuterons and α-particles," At. Energ., 31, No. 2, 157-159 (1971).
8. B. Cohen and T. Handley, Phys. Rev., 93, No. 3, 514 (1954).
9. N. N. Krasnov and P. P. Dmitriev, "Yields of nuclear reactions in the production of ^{22}Na in the cyclotron," At. Energ., 21, No. 5, 400-402 (1966).

10. B. Cohen, H. Reynolds, and A. Zucker, Phys. Rev., 96, No. 6, 1617 (1954).
11. G. Glason, I. Gruverman, and J. Need, Int. J. Appl. Rad. Isotopes, 13, 223 (1962).
12. J. Martin et al., Nucleonics, 13, No. 3, 283 (1955).
13. M. Z. Maksimov, in: Proceedings of a Conference on the Production and Application of Isotopes [in Russian], Izd. Akad. Nauk SSSR, Moscow (1957), p. 31.
14. H. Moeken, "Production of radioisotopes with charged particles," Dissertation, Amsterdam (1957).
15. H. Röhm et al., J. Inorg. Nucl. Chem., 31, No. 11, 3345 (1969).
16. I. Gruverman and P. Kruger, Int. J. Appl. Rad. Isotopes, 5, 21 (1959).
17. K. Chackett, G. Chackett, and W. Hardy, Nucl. Instrum. Methods, 14, No. 2, 215 (1961).
18. N. A. Vlasov, S. P. Kalinin, A. A. Olgoblin, et al., "Excitation curves of the reactions $^{24}Mg(d, \alpha)^{22}Na$, $^{54}Fe(d, \alpha)^{52}Mn$, $^{54}Fe(d, n)^{55}Co$, and $^{66}Zn(d, 2n)^{66}Ga$," At. Energ., 2, No. 2, 169-171 (1957).
19. W. Garrison and K. Hamilton, Chem. Rev., 49, 237 (1951).
20. R. Lindsay and R. Carr, Phys. Rev., 118, No. 5, 1293 (1960).
21. T. Mikumo et al., Phys. Lett., 23, No. 10, 586 (1966).
22. J. England and B. Reece, Nucl. Phys., 72, No. 2, 449 (1965).
23. D. Cochran and J. Knight, Phys. Rev., 128, No. 3, 1281 (1962).
24. T. McGee, C. Rao, G. Saha, and L. Vaffe, Nucl. Phys., A150, 11 (1970).
25. J. Meadows and R. Holt, Phys. Rev., 83, No. 6, 1257 (1951).
26. P. P. Dmitriev, I. O. Konstantinov, and N. N. Krasnov, "Yields of ^{48}V in nuclear reactions in the cyclotron," At. Energ., 29, No. 3, 205-206 (1970).
27. K. Chen and J. Miller, Phys. Rev., 134, 1269 (1964).
28. C. Riley, Phys. Rev., C1, 1776 (1970).

ENERGY DEPENDENCES OF THE SCATTERING CROSS SECTIONS OF FAST NEUTRONS BY ^{50}Cr AND ^{54}Cr NUCLEI

I. A. Korzh, V. A. Mishchenko,
M. V. Pasechnik, and N. M. Pravdivyi

UDC 539.172.4

Chromium has great significance as an important component of the construction materials of nuclear facilities, which causes fairly high interest in it among investigators and requires rather reliable and accurate systematic data on its interaction cross sections with neutrons having a reactor spectrum. However, most of the attention has been concentrated on the experimental investigation and theoretical analysis of the interaction of neutrons with chromium of natural isotopic composition and with its principal isotope — ^{52}Cr (~84% of the composition).

Far less attention has been paid to the other isotopes of chromium, in particular, ^{50}Cr and ^{54}Cr. Meanwhile, investigation of the interaction of neutrons with it undoubtedly contributes to clarification of the role of various scattering mechanisms and refinement of the areas of applicability of theoretical models of the interaction of neutrons with nuclei which are used for analysis of experimental data on cross sections and for prediction of cross sections in energy regions in which there are no experimental data.

Therefore, in addition to the analysis already done of the total cross sections, the cross sections of elastic and inelastic scattering of fast neutrons, and the average cosines of the elastic scattering angle for the ^{52}Cr nucleus [1], we have analyzed the existing experimental data (ours and that of other authors) and the model calculations and estimates for the cross sections of elastic and inelastic scattering of neutrons in the 0.5-0.9 MeV range upon excitation of the two lowest levels of the ^{50}Cr and ^{54}Cr nuclei.

The energy dependences of the integrated cross sections of elastic scattering of neutrons obtained by us from the measured differential cross sections for the isotopes ^{50}Cr and ^{54}Cr [2] are given in Fig. 1.

Translated from Atomnaya Énergiya, Vol. 58, No. 2, pp. 143-145, February, 1985. Original article submitted August 3, 1984.

0038-531X/85/5802-0171$09.50

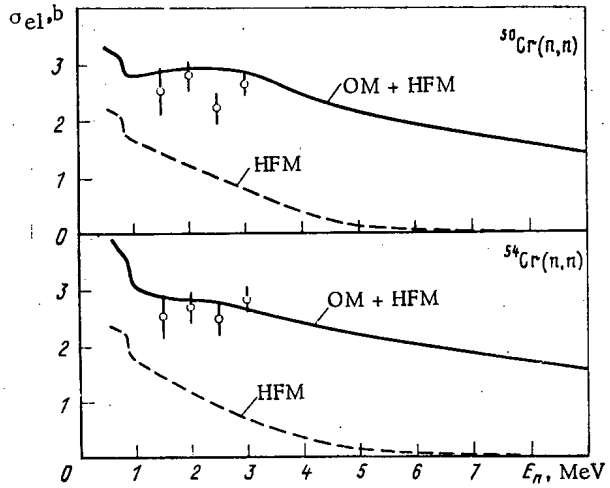

Fig. 1. Energy dependences of the integrated cross sections of elastic scattering of neutrons in the 0.5-9.0 MeV energy range by ^{50}Cr and ^{54}Cr nuclei: ○) experimental cross sections of [2]; ——) calculations by the optical model (OM) and the statistical model (HFM); ---) calculations by the statistical model.

There is relatively little experimental data on the inelastic scattering cross sections of neutrons upon excitation of the first 2^+-levels of ^{50}Cr and ^{54}Cr nuclei [2-5]; the majority of the points are obtained by the (n, n'γ) method [3, 4], whose reliability drops noticeably as the number of open levels increases. Only our results at an energy of 1.5, 2.0, 2.5, and 3.0 MeV [2] and one point at an energy of 2.9 MeV [5] have been obtained by the direct (n, n') method by means of integration of the measured differential cross sections. For the second levels the cross sections have been measured only at an energy of 3.0 MeV [2]. This experimental information is given in Fig. 2.

The results of the recent ENDF/B-V estimate [6] and the preliminary CND-2 estimate [7] are also shown in Fig. 2. It is difficult with the rather noticeable discrepancies between the sets of data obtained in measurements by various methods to make a reliable estimate. However, the estimate in ENDF/B-V in the energy region up to 4 MeV from the data of only one experimental paper [3], completely ignoring the other experimental data, seems unsound.

We have calculated the scattering cross sections within the framework of the approach described in [1] using the optical model (OM) with a spherical potential and a set of average potential parameters obtained previously [8] and using the statistical models of Hauser and Feshbach (HF) [9] and Hauser, Feshbach, and Moldauer (HFM) [10]. The cross sections of direct inelastic scattering were calculated by the method of coupled channels on the assumption of a vibrational nature of the levels and strong coupling of only the first excited level with the ground state [11]. The characteristics of known discrete levels from [12] and the level density parameters from [13] were used in the calculations by the statistical model. The values of the coupling parameter β_2 were taken equal in the calculations by coupled channels (CC) to the values of the quadrupole deformation parameter obtained from data on Coulomb excitation of the first 2^+-levels [14]: $\beta_2 = 0.30$ for ^{50}Cr and $\beta_2 = 0.27$ for ^{54}Cr. For ^{54}Cr the cross sections of direct inelastic scattering are calculated also for $\beta_2 = 0.23$, which is obtained in [15] (CC*). The results of these calculations are also given in Figs. 1 and 2. It is evident from the figures that within the framework of the optico-statistical approach one can describe sufficiently well both the elastic scattering cross sections of neutrons and the inelastic scattering cross sections of neutrons obtained by the (n, n') method.

In the energy region up to 3.0 MeV the experimental data on inelastic cross sections are contradictory; therefore, our calculations assist in selection of the orientation in making the estimate. There are no experimental data at a neutron energy above 4 MeV, in connection with which estimative cross sections are obtained in this energy region by extrapolation of calculations from the region in which there are experimental data and the theoretical calculations are in agreement with them. In this region it is rather difficult to determine objec-

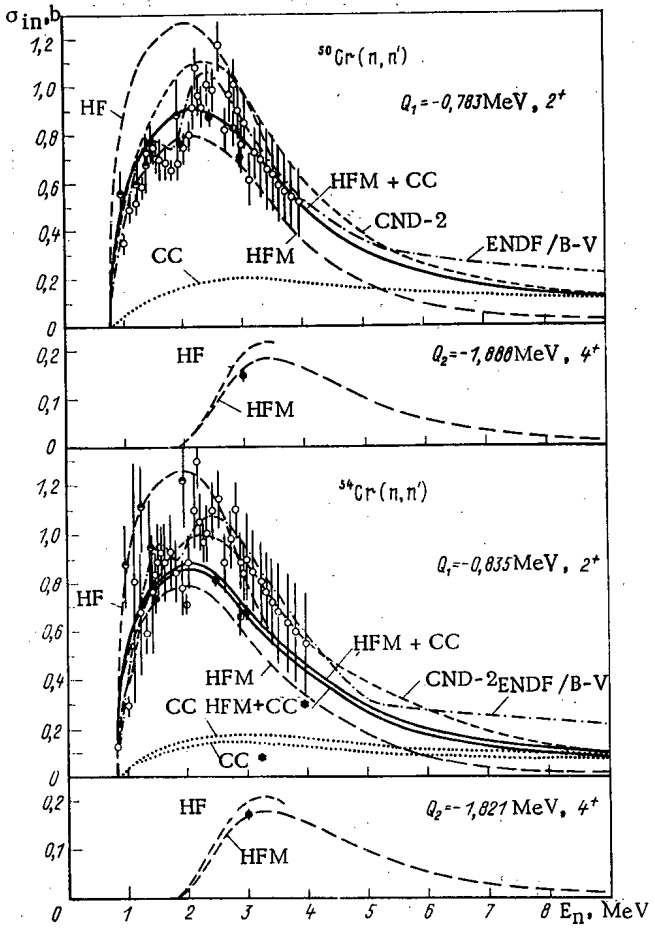

Fig. 2. Energy dependences of the inelastic scattering cross sections of neutrons with energy from the threshold to 9.0 MeV upon excitation of the two lowest levels of ^{50}Cr and ^{54}Cr nuclei. The experimental cross sections are as follows: ●) [2]; ◓) [3]; ○) [4]; and ◐) [5]. The curves give the results of calculations by the statistical model without taking into account fluctuations of the width of the levels (the HF model) and with them taken into account (the HFM model) and by the method of coupled channels CC and CC* (in the CC* method the values of β_2 are taken from [15]), as well as data of the ENDF/B-V and CND-2 estimates.

tively the degree of reliability of this or the other estimate. On the basis of a test of a good model description of the experimental data for the ^{52}Cr nucleus [1], which exist up to a neutron energy of ~8.5 MeV, one can say that the results of our calculation probably reflect better than the others the energy dependence of the scattering cross sections.

Thus, the analysis performed permits asserting that although the experimental data in the energy region above 4 MeV would noticeably improve the reliability of estimative cross sections for the ^{50}Cr and ^{54}Cr nuclei under investigation, one can rather reliably estimate scattering cross sections on the basis of model calculations. The results of our analysis have been taken into account by the Center on Nuclear Data (CND) in the creation of a recent version of estimative cross sections for chromium and its isotopes [16].

The authors are grateful to A. B. Klepatskii, V. P. Lunev, and E. Sh. Sukhovitskii for help in performing the theoretical calculations.

LITERATURE CITED

1. I. A. Korzh, V. A. Mishchenko, M. V. Pasechnik, and N. M. Pravdivyi, "Interaction cross sections of fast neutrons with chromium and its isotopes," At. Energ., 57, No. 5, 262-266 (1984).

2. I. A. Korzh et al., in: Neutron Physics. Data of the 3rd All-Union Conference, Kiev, 1975 [in Russian], Part 4, Moscow (1976), p. 220; Yad. Fiz., 26, No. 6, 1151 (1977).
3. D. Van Patter et al., Phys. Rev., 128, No. 3, 1246 (1962).
4. P. Karatzas et al., Nucl. Sci. Eng., 67, No. 1, 37 (1978).
5. M. B. Fedorov and T. I. Yakovenko, in: Neutron Physics. Data of the 2nd All-Union Conference, Kiev, 1973 [in Russian], Part 3, Obninsk (1974), p. 56.
6. A. Prince and T. Burrows, "Evaluation of natural chromium neutron cross sections for ENDF/B-V," Brookhaven National Laboratory, Upton, NY (1979), 86 p.
7. V. V. Vozyakov et al., Vopr. At. Nauki Tekh., Ser. Yad. Konstanty, No. 48, 44 (1982).
8. M. V. Pasechnik, I. A. Korzh, and I. E. Kashuba, in: Neutron Physics. Data of the 1st All-Union Conference, Kiev, 1971 [in Russian], Part 1, Kiev (1972), p. 253.
9. W. Hauser and H. Feshbach, Phys. Rev., 87, No. 2, 366 (1952).
10. P. Moldauer, Phys. Rev., 129, No. 2, 754 (1963); B135, No. 3, 642 (1964); B136, No. 4, 947 (1964).
11. A. V. Ignatyuk, V. P. Lunev, and V. S. Shorin, Vopr. At. Nauki Tekh., Ser. Yad. Konstanty, No. 13, 59 (1974).
12. S. Lederer and V. Shirley, Table of Isotopes, 7th ed., New York (1978), 1600 p.
13. W. Dilg et al., Nucl. Phys., A127, No. 2, 269 (1973).
14. P. Stelson and L. Grodzins, Nucl. Data, A1, No. 1, 21 (1965).
15. A. B. Yushkov, in: Data of the 2nd Conference of Young Scientists of the Kaz. SSR Academy of Sciences, Alma-Ata, 1970 [in Russian], Vol. 2, Alma-Ata (1971), p. 56.
16. T. S. Belanova et al., in: Neutron Physics. Data of the 6th All-Union Conference, Kiev, 1983 [in Russian], Vol. 3, Moscow (1984), p. 54.

NEUTRON YIELD IN HIGH-ENERGY DEUTERON-NUCLEAR REACTIONS

V. S. Barashenkov, L. G. Levchuk,
Zh. Zh. Musul'manbekov, A. N. Sosnin,
and S. Yu. Shmakov

UDC 539.172.84

The neutron yield and the heat released in a large, practically infinite uranium target under bombardment by 1-2-GeV deuterons were calculated in [1] by the Monte Carlo method. Since the data presented are given in many studies, it is interesting to refine them by using a more accurate technique for calculating the interaction of the flux of fast particles with matter (see [2]) and by describing more accurately the interaction of the hadrons and the deuterons with the nuclei [3, 4].

Deuteron–nuclear collisions can be calculated with the help of the model of intranuclear cascades, generalized to the case of interactions of two nuclei. For energies ranging up to several GeV, the cascade model agrees well with experiments on the interaction of particles and nuclei with hadrons.*

Table 1 presents the computed data for 1- and 2-GeV protons and deuterons interacting with the target studied in [1].† The contributions of different processes are shown separately.

Compared with the data in [1], the neutron yield obtained by bombardment with 1-GeV protons and deuterons decreased by 15 and 20%, respectively. This is attributable primarily to

*In particular, the deuteron cross sections calculated in this manner agree well with calculations using the optical model [5, 6], if the screening factor for the nucleon–nucleon interaction in the nucleus is chosen to be the same as in the case of the nucleon–nuclear collisions. The use of the cascade and optical models is at the present time the only method for obtaining information on deuteron–nuclear cross sections for energies in the range of tens and hundreds of MeV, where there are no experimental data.

†The target was 90 cm long, its diameter was equal to 120 cm, and the beam of particles hits an axial gap 26 cm deep; the target consists of metallic natural uranium.

Translated from Atomnaya Énergiya, Vol. 58, No. 2, pp. 145-146, February, 1985. Original article submitted August 13, 1984.

 0038-531X/85/5802-0174$09.50

TABLE 1. Characteristics of the Interaction of Protons and Deuterons with a Natural Uranium Target per Primary Particle (the random errors are equal to ~5%)

Characteristic	$E = 1$ GeV		$E = 2$ GeV	
	d	p	d	p
Number of captures in ^{238}U	90	82	187	181
Number of captures in ^{235}U	1,3	0,9	2,6	2,3
Leakage from the target	6,6	6,1	15,5	14,0
Total neutron yield	98	89	2,5	197
Number of fissionings of U nuclei for $E \geq 10.5$ MeV	5,8	5,4	11,8	11,6
Number of fissionings of ^{238}U with $E < 10.5$ MeV	15,3	14,5	33	33
Number of fissionings of ^{235}U with $E < 10.5$ MeV	5,5	4,2	11,4	10,2
Heat released, GeV	5,1	4,6	10,2	10,1
including:				
due to ionization losses	0,64	0,60	0,93	0,93
fissioning for $E \geq 10.5$ MeV	0,95	0,89	2,0	1,9
fissioning for $E < 10.5$ MeV	3,5	3,1	7,3	7,2

the decrease in the number of fissionings in the more accurate calculation. The heat released in the target decreased proportionately.

It is interesting that deuteron bombardment produces only 10% more neutrons than proton bombardment. This is much less than the value of 22% given in [1]. The disagreement with [1] is largely explained by the smaller cross sections for the interaction of deuterons with uranium nuclei, for whose calculation the wave function of the deuteron was used [7].

At E = 2 GeV the disagreement with the data in [1] is somewhat smaller: the neutron yields obtained with protons and deuterons decreased approximately by 10 and 15%. Their ratio was equal to $n(dU)/n(pU) = 1$.

LITERATURE CITED

1. V. S. Barashenkov, V. D. Toneev, and S. E. Chigrinov, "Electronuclear method for generating neutrons," At. Energ., 37, No. 6, 480-483 (1974).
2. V. S. Barashenkov and S. Yu. Shmakov, "Analysis of the neutron yield obtained by high-energy protons," At. Energ., 50, No. 2, 150-151 (1981).
3. V. S. Barashenkov and S. Yu. Shmakov, Report E2-12902, Joint Institute of Nuclear Research, Dubna (1979).
4. V. S. Barashenkov, Zh. Zh. Musul'manbekov, and S. Yu. Shmakov, Report R2-81-202, Joint Institute of Nuclear Research, Dubna (1981).
5. V. S. Barashenkov and V. D. Toneev, Interaction of High-Energy Particles and Nuclei with Nuclei [in Russian], Atomizdat, Moscow (1972).
6. N. S. Amelin et al., Report R2-81-366, Joint Institute of Nuclear Research, Dubna (1981).
7. L. Azhgirey, S. Rasin, A. Tarasov, and V. Uzhinsky, Report E2-12683, Joint Institute of Nuclear Research, Dubna (1979).

How To Comply With The New Copyright Law

Participation in the Copyright Clearance Center (CCC) assures you of legal photocopying at the moment of need.

Libraries everywhere have found the easy way to fill photocopy requests legally and instantly, without the need to seek permissions, from more than 3000 key publications in business, science, humanities, and social science. You can:

Fill requests for multiple copies, interlibrary loan (beyond the CONTU guidelines), and reserve desk without fear of copyright infringement.

Supply copies from CCC-registered publications simply and easily.

The Copyright Clearance Center is your one-stop place for on-the-spot clearance to photocopy for internal use.

Its flexible reporting system accepts photocopying reports and returns an itemized invoice. You send only one convenient payment. CCC distributes it to the many publishers whose works you need.

And, you need not keep any records, the CCC computer will do it for you. Register now with the CCC and you will never again have to decline a photocopy request or wonder about compliance with the law for any publication participating in the CCC.

To register or for more information, just contact:

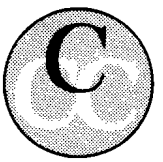

Copyright Clearance Center
21 Congress Street
Salem, Massachusetts 01970
(617) 744-3350

a not-for-profit corporation

NAME _____ TITLE _____

ORGANIZATION _____

ADDRESS _____

CITY _____ STATE _____ ZIP _____

COUNTRY _____ TELEPHONE _____

CHANGING YOUR ADDRESS?

In order to receive your journal without interruption, please complete this change of address notice and forward to the Publisher, 60 days in advance, if possible.

(Please Print)

Old Address:

name

address

city

state (or country) zip code

New Address

name

address

city

state (or country) zip code

date new address effective

name of journal

THE LANGUAGE OF SCIENCE
Plenum
PUBLISHING CORPORATION

233 Spring Street, New York, New York 10013

MEASUREMENT TECHNIQUES
Izmeritel'naya Tekhnika
Vol. 27, 1984 (12 issues) $520

MECHANICS OF COMPOSITE MATERIALS
Mekhanika Kompozitnykh Materialov
Vol. 20, 1984 (6 issues) $430

METAL SCIENCE AND HEAT TREATMENT
Metallovedenie i Termicheskaya Obrabotka Metallov
Vol. 26, 1984 (12 issues) $540

METALLURGIST
Metallurg
Vol. 28, 1984 (12 issues) $555

PROBLEMS OF INFORMATION TRANSMISSION
Problemy Peredachi Informatsii
Vol. 20, 1984 (4 issues) $420

PROGRAMMING AND COMPUTER SOFTWARE
Programmirovanie
Vol. 10, 1984 (6 issues) $175

PROTECTION OF METALS
Zashchita Metallov
Vol. 20, 1984 (6 issues) $480

RADIOPHYSICS AND QUANTUM ELECTRONICS
Izvestiya Vysshikh Uchebnykh Zavedenii, Radiofizika
Vol. 27, 1984 (12 issues) $520

REFRACTORIES
Ogneupory
Vol. 25, 1984 (12 issues) $480

SIBERIAN MATHEMATICAL JOURNAL
Sibirskii Matematicheskii Zhurnal
Vol. 25, 1984 (6 issues) $625

SOIL MECHANICS AND FOUNDATION ENGINEERING
Osnovaniya, Fundamenty i Mekhanika Gruntov
Vol. 21, 1984 (6 issues) $500

SOLAR SYSTEM RESEARCH
Astronomicheskii Vestnik
Vol. 18, 1984 (6 issues) $365

SOVIET APPLIED MECHANICS
Prikladnaya Mekhanika
Vol. 20, 1984 (12 issues) $520

SOVIET ATOMIC ENERGY
Atomnaya Energiya
Vols. 56-57, 1984 (12 issues) $560

SOVIET JOURNAL OF GLASS PHYSICS AND CHEMISTRY
Fizika i Khimiya Stekla
Vol. 10, 1984 (6 issues) $235

SOVIET JOURNAL OF NONDESTRUCTIVE TESTING
Defektoskopiya
Vol. 20, 1984 (12 issues) $615

SOVIET MATERIALS SCIENCE
Fiziko-khimicheskaya Mekhanika Materialov
Vol. 20, 1984 (6 issues) $445

SOVIET MICROELECTRONICS
Mikroelektronika
Vol. 13, 1984 (6 issues) $255

SOVIET MINING SCIENCE
Fiziko-tekhnicheskie Problemy Razrabotki Poleznykh Iskopaemykh
Vol. 20, 1984 (6 issues) $540

SOVIET PHYSICS JOURNAL
Izvestiya Vysshikh Uchebnykh Zavedenii, Fizika
Vol. 27, 1984 (12 issues) $520

SOVIET POWDER METALLURGY AND METAL CERAMICS
Poroshkovaya Metallurgiya
Vol. 23, 1984 (12 issues) $555

STRENGTH OF MATERIALS
Problemy Prochnosti
Vol. 16, 1984 (12 issues) $625

THEORETICAL AND MATHEMATICAL PHYSICS
Teoreticheskaya i Matematicheskaya Fizika
Vol. 58-61, 1984 (12 issues) $500

UKRAINIAN MATHEMATICAL JOURNAL
Ukrainskii Matematicheskii Zhurnal
Vol. 36, 1984 (6 issues) $500

Send for Your Free Examination Copy

Plenum Publishing Corporation, 233 Spring St., New York, N.Y. 10013
In United Kingdom: 88/90 Middlesex St., London E1 7EZ, England
Prices slightly higher outside the U.S. Prices subject to change without notice.

RUSSIAN JOURNALS IN THE PHYSICAL AND MATHEMATICAL SCIENCES

AVAILABLE IN ENGLISH TRANSLATION

ALGEBRA AND LOGIC
Algebra i Logika
Vol. 23, 1984 (6 issues) $360

ASTROPHYSICS
Astrofizika
Vol. 20, 1984 (4 issues) $420

AUTOMATION AND REMOTE CONTROL
Avtomatika i Telemekhanika
Vol. 45, 1984 (24 issues) $625

COMBUSTION, EXPLOSION, AND SHOCK WAVES
Fizika Goreniya i Vzryva
Vol. 20, 1984 (6 issues) $445

COSMIC RESEARCH
Kosmicheskie Issledovaniya
Vol. 22, 1984 (6 issues) $545

CYBERNETICS
Kibernetika
Vol. 20, 1984 (6 issues) $445

DIFFERENTIAL EQUATIONS
Differentsial'nye Uravneniya
Vol. 20, 1984 (12 issues) $505

DOKLADY BIOPHYSICS
Doklady Akademii Nauk SSSR
Vols. 274-279, 1984 (2 issues) $145

FLUID DYNAMICS
Izvestiya Akademii Nauk SSSR, Mekhanika Zhidkosti i Gaza
Vol. 19, 1984 (6 issues) $500

FUNCTIONAL ANALYSIS AND ITS APPLICATIONS
Funktsional'nyi Analiz i Ego Prilozheniya
Vol. 18, 1984 (4 issues) $410

GLASS AND CERAMICS
Steklo i Keramika
Vol. 41, 1984 (6 issues) $590

HIGH TEMPERATURE
Teplofizika Vysokikh Temperatur
Vol. 22, 1984 (6 issues) $520

HYDROTECHNICAL CONSTRUCTION
Gidrotekhnicheskoe Stroitel'stvo
Vol. 18, 1984 (12 issues) $385

INDUSTRIAL LABORATORY
Zavodskaya Laboratoriya
Vol. 50, 1984 (12 issues) $520

INSTRUMENTS AND EXPERIMENTAL TECHNIQUES
Pribory i Tekhnika Eksperimenta
Vol. 27, 1984 (12 issues) $590

JOURNAL OF APPLIED MECHANICS AND TECHNICAL PHYSICS
Zhurnal Prikladnoi Mekhaniki i Tekhnicheskoi Fiziki
Vol. 25, 1984 (6 issues) $540

JOURNAL OF APPLIED SPECTROSCOPY
Zhurnal Prikladnoi Spektroskopii
Vols. 40-41, 1984 (12 issues) $540

JOURNAL OF ENGINEERING PHYSICS
Inzhenerno-fizicheskii Zhurnal
Vols. 46-47, 1984 (12 issues) $540

JOURNAL OF SOVIET LASER RESEARCH
A translation of articles based on the best Soviet research in the field of lasers
Vol. 5, 1984 (6 issues) $180

JOURNAL OF SOVIET MATHEMATICS
A translation of Itogi Nauki i Tekhniki and *Zapiski Nauchnykh Seminarov Leningradskogo Otdeleniya Matematicheskogo Instituta im. V. A. Steklova AN SSSR*
Vols. 24-27, 1984 (24 issues) $1035

LITHOLOGY AND MINERAL RESOURCES
Litologiya i Poleznye Iskopaemye
Vol. 19, 1984 (6 issues) $540

LITHUANIAN MATHEMATICAL JOURNAL
Litovskii Matematicheskii Sbornik
Vol. 24, 1984 (4 issues) $255

MAGNETOHYDRODYNAMICS
Magnitnaya Gidrodinamika
Vol. 20, 1984 (4 issues) $415

MATHEMATICAL NOTES
Matematicheskie Zametki
Vols. 35-36, 1984 (12 issues) $520

continued on inside back cover

Declassified and Approved For Release 2013/03/11 : CIA-RDP10-02196R000300060002-4